Investigating the roles of *endoglin* in cardiovascular development, disease and repair

Ryan Oliver Snodgrass

Registration number: 180126040

A thesis submitted for the degree of Doctor of Philosophy

At the University of Sheffield

Department of Infection, Immunity and Cardiovascular Disease

Submitted: 11/03/2022

Table of Contents

Acknowledgements

Firstly, I would like to thank my supervisors Tim and Helen for the opportunity to perform this research under their guidance. Many thanks for their support, encouragement, and expertise which contributed both to this thesis and to my development as a scientist. I would like to thank Tim for always finding time to be dedicated supervisor alongside all his clinical and head of the department responsibilities. It was a privilege to work and study under his guidance. Many thanks to Helen for all the monthly meetings, they unquestionably reinforced my interest and understanding of TGFβ signalling and scientific research in general.

I would like to acknowledge Dr Arndt Siekmann and Dr Beth Roman for supplying of transgenic lines, protocols, and manuscript feedback. Thank you to Dr Caroline Pellet-Many for taking the time to train me in the zebrafish cryoinjury technique. I would like to thank all members of the Chico group, in particular Karen, Eli, and Karan their expertise and for keeping C10 a fun and interesting place to work and learn. Thank you to the Bateson Centre aquarium staff for their guidance on zebrafish experiments. Many thanks to the MRC DiMeN DTP for funding for this project, and providing valuable training courses which undoubtedly developed my research skills.

I would like to thank my mum and dad for their continuous support and understanding when undertaking my PhD and writing this thesis. Finally, I would like to thank my partner, Gabriella for her encouragement and seemingly never-ending patience. Thank you for everything.

Abstract

Objective: ENG or ALK1 heterozygous loss of function mutations lead to the human disease hereditary haemorrhagic telangiectasia. HHT is characterised by the development of arteriovenous malformations (AVMs). These form when arteries and veins directly connect without an intermediary capillary system. Large AVMs may occur in the lungs, liver and brain, leading to severe morbidity. There is growing evidence that targeting VEGFA signalling has a benefit in HHT. However, inhibiting VEGFA can have serious adverse effects.

Aims: Zebrafish embryos have a number of advantages for drug evaluation, including rapid cardiovascular development, ease of drug administration and transgenic models for imaging. VEGFA signalling is complex and has numerous downstream pathways. I therefore hypothesised that selectively targeting individual pathway(s) downstream of VEGFA may be beneficial in a previously-generated zebrafish genetic model of HHT caused by homozygous mutation of endoglin (*eng*^{mu130}). I first characterised the cardiovascular phenotype of *eng*^{mu130} embryos and adults in vascular territories not previously examined, including the cerebral vessels, skin, heart and retina. I then tested my hypothesis by treating zebrafish *eng*^{mu130} mutant and wildtype embryos with drugs that inhibit global VEGFA signalling or different pathways downstream of VEGFR2.

Results and conclusions: *eng* mutant embryos displayed a range of previously undescribed vascular defects, including an aneurysmal basilar artery (BA), while adult mutants developed skin AVMs, retinal vascular abnormalities, and cardiac enlargement. VEGF receptor tyrosine kinase inhibition prevented the vascular abnormalities in *eng* mutant embryos. Combined subtherapeutic TOR and MEK inhibition prevented the vascular abnormalities, confirming synergy between TOR and MEK/ERK signalling pathways. These results indicate the HHT-like phenotype in zebrafish *eng* mutants can be mitigated through modulation of VEGFA signalling, and suggest combined low dose MEK and TOR pathway inhibitors may represent a therapeutic strategy in HHT.

Publications and Preprints Arising

Snodgrass, R. O., Chico, T. J. A. and Arthur, H. M. (2021). "Hereditary Haemorrhagic Telangiectasia, an Inherited Vascular Disorder in Need of Improved Evidence-Based Pharmaceutical Interventions." Genes 12(2): 174.

Snodgrass, R. O., Plant, K., Kugler, C. K., Arthur, H. M. and Chico, T. J. A. (2021). "Synergistic TOR and ERK inhibition mitigates the hereditary haemorrhagic telangiectasia-like phenotype and excess *kugel* formation in endoglin mutant zebrafish." bioRxiv: https://doi.org/10.1101/2021.06.16.448717.

List of Figures

1. Introduction

2. Materials and methods

3. The role of endoglin in zebrafish cardiovascular development

4. The interaction between BMP9/BMP10 and VEGF signalling in zebrafish embryonic development

5. The role of *endoglin* in cardiac repair in zebrafish

6. Future work and conclusions

7. Appendices

List of Tables

Abbreviations

+/+ Wild type

+/- Heterozygous

-/- Homozygous

ALK Activin receptor-like kinase

aISV Arterial intersegmental Vessel

AVM Arteriovenous malformations

BA Basilar artery

BMP Bone morphogenetic protein

bpm Beats per minute

DA Dorsal aorta

DLAV Dorsal longitudinal anastomotic vessel

DNA Deoxyribonucleic acid

DOX Doxorubicin

dpf Days post fertilisation

dpi Days post Injury

EC Endothelial cell

eng Endoglin

HHT Hereditary haemorrhagic telangiectasia

HOHF High output heart failure

hpf Hours post fertilisation

fli1 Friend leukaemia integration 1 transcription factor

GFP Green fluorescence protein

ISV Intersegmental Vessel

kdrl Kinase insert domain receptor-like

KO Knockout

MIP Maximum intensity projection

MI Myocardial infarction

Nitric oxide (NO)

PAH Pulmonary arterial hypertension

PCV Posterior cardinal vein

PCR Polymerase chain reaction

Phosphorylated ERK (pERK)

RNA Ribonucleic acid

SBF-SEM Serial block face scanning electron microscopy

SMADs Small Mothers against decapentaplegic

SMC Smooth muscle cell

TALENs Transcription activator-like effector nuclease

TGF-β Transforming growth factor beta

T2DM type 2 diabetes mellitus

TM Transmembrane

VEGF Vascular endothelial growth factor

vISV Venous intersegmental Vessel

WT Wild type

1. Introduction

1.1 Background

Endoglin is a co-receptor predominately expressed on the cell surface of endothelial cells (ECs) where it is bound selectively by members of the TGF-β superfamily (Arthur, Ure et al. 2000). It has a particularly high binding affinity for bone morphogenetic protein (BMP)9 and BMP10. Endoglin is upregulated in actively proliferating endothelial cells, and regulates protective processes after myocardial infarction (MI), such as angiogenesis, inflammation, and wound repair (Arthur, Ure et al. 2000). The importance of endoglin in maintaining the normal vasculature in humans is highlighted by the link between endoglin mutations and the vascular disease hereditary haemorrhagic telangiectasia (HHT) (McAllister, Baldwin et al. 1995). There is therefore a need for a better understanding of endoglin's role in cardiovascular diseases such as MI and HHT. My project investigates the role of endoglin in vascular development and disease in a range of vascular territories using zebrafish models, and how this might be pharmacologically targeted therapeutically.

1.2 Vascular development & angiogenesis

The vascular system supplies cells with oxygen and nutrients to maintain homeostasis. Blood vessels need to be generated and maintained to perform these functions. Angiogenesis is a fundamental process involved in embryonic development and growth, as well as in adult tissue repair and disease (Risau 1997). When angiogenesis is dysregulated, it has a major impact on health. For example, solid tumour growth is dependent on the overstimulation of angiogenesis (Goel, Duda et al. 2011), whereas underproduction of blood vessels can cause hypoxia, resulting in tissue damage (Gimbrone and García-Cardeña 2016). It is therefore possible that inducing angiogenic mechanisms may provide treatments for patients suffering with cardiovascular diseases. For example, myocardial infarction (MI) is caused by the obstruction of blood vessels supplying blood to heart tissue (Murray, Barber et al. 2015). Recently, death rates from heart disease have decreased due to the success of current therapies to reopen the blocked vessel, but it is still the leading cause of death worldwide (Murray, Barber et al. 2015). Stimulating angiogenesis may help to re-establish blood flow following MI and therefore limit damage to the heart. There is therefore a pressing need to

understand the mechanisms that drive angiogenesis as it may be possible to develop drug targets that improve the prognosis of patients suffering with cardiovascular diseases such as myocardial infarction.

Vasculogenesis and angiogenesis are responsible for blood vessel development in vertebrates (Risau 1997). Vasculogenesis, the process of *de novo* blood vessel formation, occurs during embryonic development where blood vessels are formed from angioblastic precursors. Angiogenesis, the formation of new blood vessels from existing vessels, occurs via two main mechanisms; sprouting angiogenesis and non-sprouting (intussusceptive) angiogenesis (Burri, Hlushchuk and Djonov 2004). Sprouting angiogenesis is defined as a new blood vessel sprouting from pre-existing blood vessels. Stalk cells proliferate from pre-existing blood vessels to form a vascular sprout, headed by a tip cell. The vascular sprout subsequently matures to forms a lumen, which results in restoration of blood flow (Patel-Hett and D'Amore 2011). Intussusceptive angiogenesis takes place more rapidly as it does not rely on endothelial cell proliferation. In this case new blood vessels are created by splitting an existing blood vessel in two (Burri, Hlushchuk and Djonov 2004). Sprouting angiogenesis is the fundamental mechanism for blood vessel growth in vertebrates, but dysregulation of either sprouting or intussusceptive angiogenesis can result in disease.

1.3 TGF-β signalling

TGF-β signalling regulates a range of cellular processes, including cell growth, cell differentiation, and cell death (Cheifetz, Bellón et al. 1992). Dysregulation of TGF-β signalling in blood vessels can lead to a number of vascular pathologies (Govani and Shovlin 2009). The TGF-β family comprises over 40 structurally related growth factors, including TGF-βs, activins, and bone morphogenetic proteins (BMPs) (Gordon and Blobe 2008). TGF-β ligands bind directly to homodimeric complexes of TGF-β type I and II receptors with high affinity, and the Type II receptor subsequently phosphorylates the type I receptor, stimulating its activation (Wieser, Wrana and Massagué 1995). Activated TGF-β type I receptors recruit receptor regulated SMADs (homologues of the *Drosophila* protein, Mothers against decapentaplegic (MAD)) leading to a secondary phosphorylation event where R-SMAD accepts a phosphate group. Phosphorylated R-SMAD binds to SMAD 4 (co-SMAD) to form a SMAD complex that can shuttle into the nucleus where it regulates gene transcription **[Figure1.1]** (Schmierer and

Hill 2007). Multiple mechanisms are involved in regulating the TGF-β signalling pathway. For example, SMAD6 and SMAD7 target R-SMADS for degradation, resulting in a negative feedback loop (Govani and Shovlin 2009).

The TGF-β1 receptor on most cells is activin receptor-like kinase 5 (ALK5, also known as TGFBR1). Endothelial cells also express another receptor, activin receptor-like kinase 1 (ALK1, also known as ACVRL1). Endoglin is a transmembrane glycoprotein first characterised in the 1980s (Quackenbush and Letarte 1985). Endoglin interacts with both ALK1 and ALK5 type I receptors, but binds to ALK1 with much higher affinity (Brown, Zhao et al. 2005) **[Figure 1.1].** Endoglin is expressed in endothelial cells, mesenchymal cells and myofibroblasts of the heart, and regulates processes known to be protective after myocardial infarction such as angiogenesis (Gougos and Letarte 1990, Jonker and Arthur 2002).

BMP9 and BMP10 circulate in the blood and bind to ALK1 and Endoglin. Endoglin acts as a BMP9/BMP10 reservoir on the surface of ECs and induces ALK1 stimulated phosphorylation of SMAD1, 5 and 8. The R-SMAD/SMAD 4 complex subsequently stimulates gene expression of angiogenic factors, including IL1R1 and ID1 (Goumans, Valdimarsdottir et al. 2002). The precise function of endoglin in BMP9 signalling remains unclear. Originally, it was proposed that endothelial cells lacking endoglin do not proliferate because BMP9 signalling is decreased and TGF-β signalling is increased (Li, Sorensen et al. 1999). More recently, it was shown that endoglin knock out (*ENG*-KO) endothelial cells show increased proliferation *in vivo*, leading to arteriovenous malformations (AVMs) (Mahmoud, Allinson et al. 2010). This defective vascular phenotype suggests endoglin has an important role in maintaining angiogenesis and that endoglin may act as an angiogenic switch by balancing ALK1 and ALK5 signalling. It is therefore likely that endoglin plays a fundamental role in the balance of ALK1 and ALK5 signalling to regulate endothelial cell proliferation, and consequently a reduction in endoglin results in vascular pathologies such as AVM formation. For example, it was previously shown in a mouse model of HHT that endoglin loss of function results in defective endothelial cell migration against blood flow, which leads to retinal AVM formation (Jin, Muhl et al. 2017).

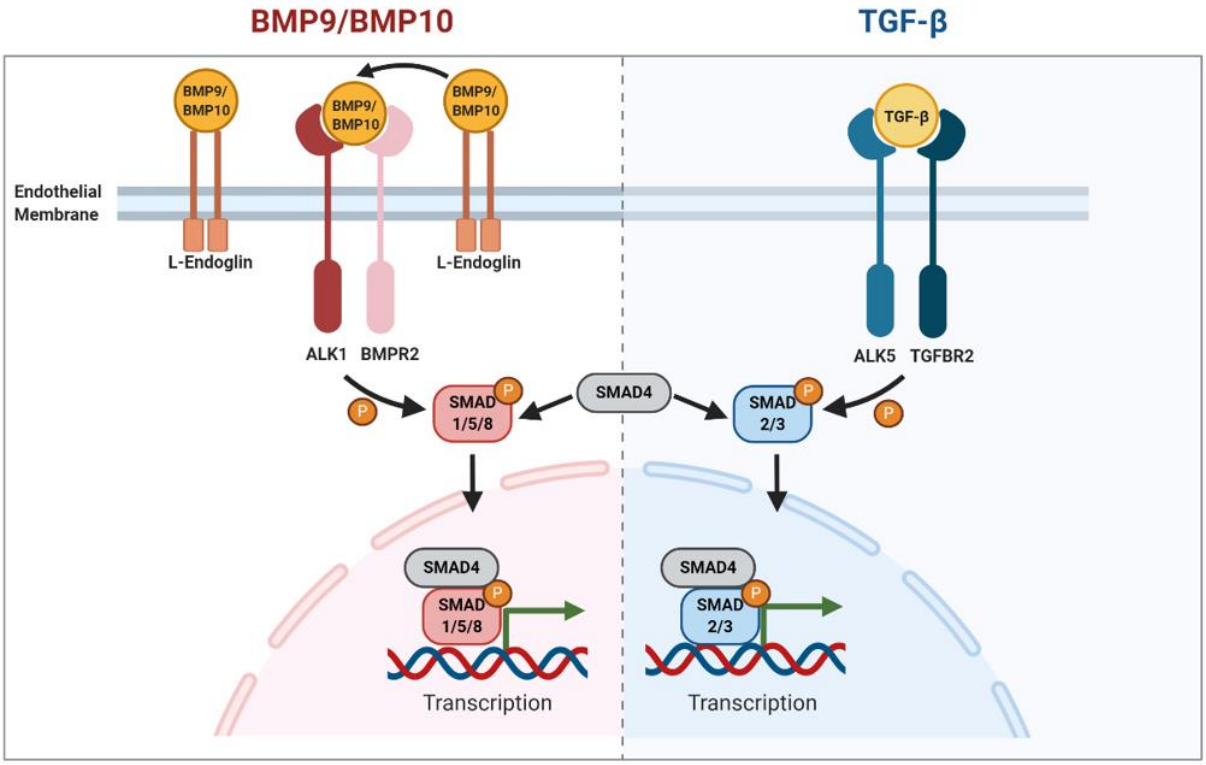

Figure 1.1 Schematic showing the predominant TGF-β signalling pathways in endothelial cells.

The TGF-β family includes TGF-βs and BMPs. Endoglin binds BMP-9/BMP-10 at the cell surface of endothelial cells where they signal via the BMPR2/ALK1 or ActRIIB/ALK1 receptor complex. Type 2 receptors such as BMPR2 and ActRIIB phosphorylates ALK1 in response to the binding of BMP-9 or BMP10. Activated ALK1 subsequently initiates intracellular signalling via catalysing the phosphorylation of SMAD 1/5/8. SMAD4 (Co-Smad) associates with pSMAD 1/5/8 to form a SMAD complex which subsequently shuttles to the nucleus where it regulates genes associated with endothelial cell proliferation and migration. However, TGFBR2/ALK5 stimulation results in the upregulation of genes that inhibit angiogenesis and cell proliferation. Figure created with BioRender (**https://biorender.com/**). Figure taken from Snodgrass *et al.*, 2021 (Copyright CC BY 4.0 license (open access)) (Snodgrass, Chico and Arthur 2021).

The precise roles of endoglin in the TGF-β signalling pathway remains unclear. For example, ALK5 and ALK1 stimulate phosphorylation of the same serine and threonine residues in endoglin (Ray, Lee, How and Blobe 2010), but it is unclear why endoglin interacts with both receptors even though they seemingly have contrasting functions. The literature suggests that endoglin haploinsufficiency results in an imbalance between the ALK1/ALK5 pathways resulting in vascular abnormalities such as AVMs. Furthermore, *in vitro* and *in vivo* studies show that endoglin promotes angiogenesis (Jonker and Arthur 2002), whereas BMP9 can act as an anti-angiogenic factor that plays a role in blood vessel quiescence (David, Mallet et al. 2008). BMP9 inhibits proliferation and migration of ECs via ALK1 signalling. Furthermore, BMP9 signalling was shown to inhibit expression of vascular endothelial growth factor (VEGF) (Shao, Lin, Yao and Boström 2009). In contrast, Suzuki and colleagues showed that BMP9 induces proliferation of ECs both *in vitro* and *in vivo* (Suzuki, Ohga et al. 2010). This discrepancy may be a result of ligand redundancy, as BMP10 has also been shown to bind to and consequently activate ALK1 (David, Mallet et al. 2008). The importance of the BMP9/10 signalling pathway in HHT is confirmed by evidence from combined loss of BMP9 and BMP10 activities in mouse models that recapitulate the vascular malformations typical of HHT (Ola, Dubrac et al. 2016, Ruiz, Zhao et al. 2016). The requirement for loss of both ligands to generate AVMs points to functional redundancy. However, BMP10, but not BMP9 plays the critical role in maintaining normal vascular architecture in zebrafish (Capasso, Li et al. 2020). Work in mice suggests some differences between BMP9 and BMP10 functions, where loss of BMP9 affects the lymphatic but not systemic vasculature (Levet, Ciais et al. 2013), and loss of BMP10 is embryonic lethal at E10.5 due to failure of heart development (Chen, Shi et al. 2004). More recently, Chen and colleagues developed specific antibodies against bone BMP9 or BMP10 and showed that the two proteins are functionally and physiologically equivalent ligands for ALK1 signalling during angiogenesis. Furthermore, timing of expression during vascular development directs the role of each ligand (Chen, Hao et al. 2013). Further investigations are required to interrogate the overlapping and different functions of BMP9 and BMP10.

1.4 The structure, expression and function of endoglin

Endoglin is a 633 amino acid (aa) protein configured as a disulphide bond-linked homodimer (Quackenbush and Letarte 1985). Human endoglin is encoded by the 14 exon *ENG* gene on chromosome 9q34, and pathogenic mutations in this gene are most commonly associated with hereditary haemorrhagic telangiectasia type 1 (HHT1) syndrome (McAllister, Baldwin et al. 1995). However, endoglin expression is also associated with other diseases including pulmonary arterial hypertension (PAH), pre-eclampsia, and several cancers (Levine, Lam et al. 2006, Girerd, Montani et al. 2010, Pérez-Gómez, Del Castillo et al. 2010).Endoglin protein has 3 domains: the large extracellular domain, followed by a hydrophobic transmembrane (TM) region and a short intracellular (IC) domain **[figure 1.2].** The extracellular domain consists of an N-terminal orphan region (OR) and a C-terminal region called the zona pellucida (ZP). The ZP domain contains a tripeptide arginine-glycine-aspartic acid (RGD) motif, which is a key recognition structure for integrin binding (Gougos and Letarte 1990). Endoglin lacks enzymatic motifs but contains several serine and threonine residues that can be phosphorylated by TGF-β receptor complexes (Pérez-Gómez, Del Castillo et al. 2010). The IC domain contains a PDZ-binding motif that modulates phosphorylation of neighbouring serine and threonine residues (Koleva, Conley et al. 2006). There are two distinct alternatively spliced isoforms of human endoglin, which differ in the length of the intracellular domain. These are long (L)-endoglin and short (S)-endoglin. L-endoglin has an IC domain consisting of 47 amino acid residues, whereas S-endoglin has only 14 residues **[figure 1.2 A].** The first 7 residues closest to the TM region are the same in both isoforms, but S-endoglin lacks the PDZ-binding motif, which is important for BMP signalling (Bellón, Corbí et al. 1993). L-endoglin is the predominant isoform expressed in endothelial cells, and the focus of most endoglin research concerning HHT. Saito and colleagues reported new insights into the 3D structure of endoglin. The endoglin-BMP9 complex was crystallised, revealing high-resolution structural information including how it interacts with BMP9 (Saito, Bokhove et al. 2017). The binding domain for BMP9 lies within a hydrophobic pocket of the orphan region **[figure 1.2 B]**, and therefore mutations that alter hydrophobicity of this region are likely to be pathogenic. Furthermore, this study suggested that endoglin accumulates BMP9 molecules on the endothelial cell surface, where they bind to ALK1 and are subsequently released from endoglin making them available for interactions with type II receptors, such as BMPRII and

ActRIIB (Saito, Bokhove et al. 2017). Lawera and colleagues provided further evidence for this by proving that soluble ENG (sENG) binds with BMP9 to form an sENG:BMP9 complex. Furthermore, they showed that the sENG:BMP9 complex facilitates BMP9 signalling by directing BMP9 to ALK1 at the endothelium via cell-surface ENG (Lawera, Tong et al. 2019).

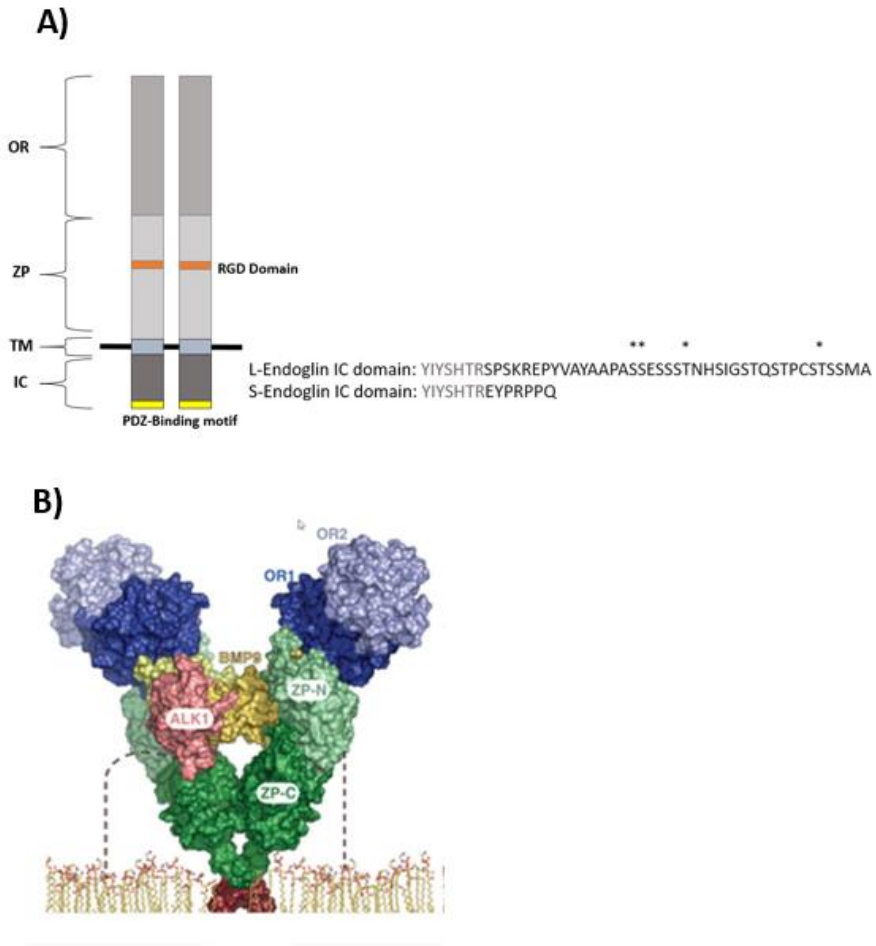

Figure 1.2 Human endoglin structure and isoforms.

A) Schematic representation of endoglin protein structure. Endoglin is expressed as a homodimer with a large extracellular domain, a transmembrane region (TM), and a small intracellular domain (IC). The extracellular domain consists of the orphan region (OR) and the zona pellucida (ZP), the latter contains a tripeptide RDG binding domain. Endoglin has two splice forms: long (L) endoglin and short (S) endoglin, which differ by their intracellular regions. L-endoglin is phosphorylated by ALK1 and ALK5 at residues indicated with an asterisk. Figure adapted from Pérez-Gómez *et al*., 2010 (Pérez-Gómez, Del Castillo et al. 2010). B) Model of the 3-D structure of the endoglin extracellular region in complex with BMP9 and ALK1. Model was taken from Saito *et al*., 2017 (CC BY-NC-ND license (open access)) (Saito, Bokhove et al. 2017).

These studies revealed some of the mechanisms that drive BMP9 signalling, which helps to further our understanding of the molecular basis of angiogenesis.

1.5 The role of endoglin in disease

Familial cardiovascular diseases are often caused by mutations in genes that are essential for regulating angiogenesis. For example, a reduction in ENG or ALK1 activity due to heterozygous loss of function mutations leads to the inherited human vascular disorder hereditary haemorrhagic telangiectasia (HHT) (McAllister, Grogg et al. 1994). HHT is a highly penetrant genetic disease, and most patients show symptoms in childhood. HHT is characterised by development of arteriovenous malformations (AVMs) (Dupuis-Girod, Ginon et al. 2012). Large AVMs may occur in the lungs, liver and brain, leading to severe morbidity. Smaller AVMs known as telangiectases are prevalent on the skin and mucosal lining of the nose, mouth and gastrointestinal tract and are prone to haemorrhaging, and thus manifestations of HHT include recurrent severe nosebleeds (epistaxis) and gastro intestinal bleeding (Govani and Shovlin 2009). Larger AVMs are more stable but can affect blood flow with serious consequences. For example, lung AVMs can lead to systemic hypoxia and liver AVMs increase risk of high output heart failure (Govani and Shovlin 2009) **[Figure 1.3]**.

HHT1 and HHT2, the most common types of HHT, are caused by mutations in endoglin and *ALK1*, respectively. More recently, mutations in *BMP9* (*GDF_2)* have also been linked to a HHT-like disease, with similar clinical manifestations (Wooderchak-Donahue, McDonald et al. 2013). Furthermore, *SMAD4 (MADH4)*, another gene in the BMP9 signalling pathway has been linked to HHT. *SMAD4* is mutated in a proportion of HHT patients with juvenile polyposis (JP) (Gallione, Repetto et al. 2004). These patients do not have mutations in endoglin or *ALK1*, and therefore it is classed as distinct syndrome called JP-HHT. Approximately 80% of HHT cases are caused by mutations in either *ENG* (endoglin) or *ACVRL* (ALK1), with a further 5% in *BMP9,* or *SMAD4* **[Figure 1.4].** HHT1 (*ENG*) and HHT2 (*ALK1*) patients differ by the frequency of AVMs in particular organs. For example, ALK1 mutations are more likely to cause heart problems due to hepatic AVMs, whereas *ENG* mutations are more commonly linked to pulmonary and brain AVMs (Ruiz, Zhao et al. 2016). It is unclear why these differences occur, but it suggests that ENG and ALK1 have distinct but overlapping

functions. Phenotypic variability in HHT patients also makes diagnosis and therapy challenging.

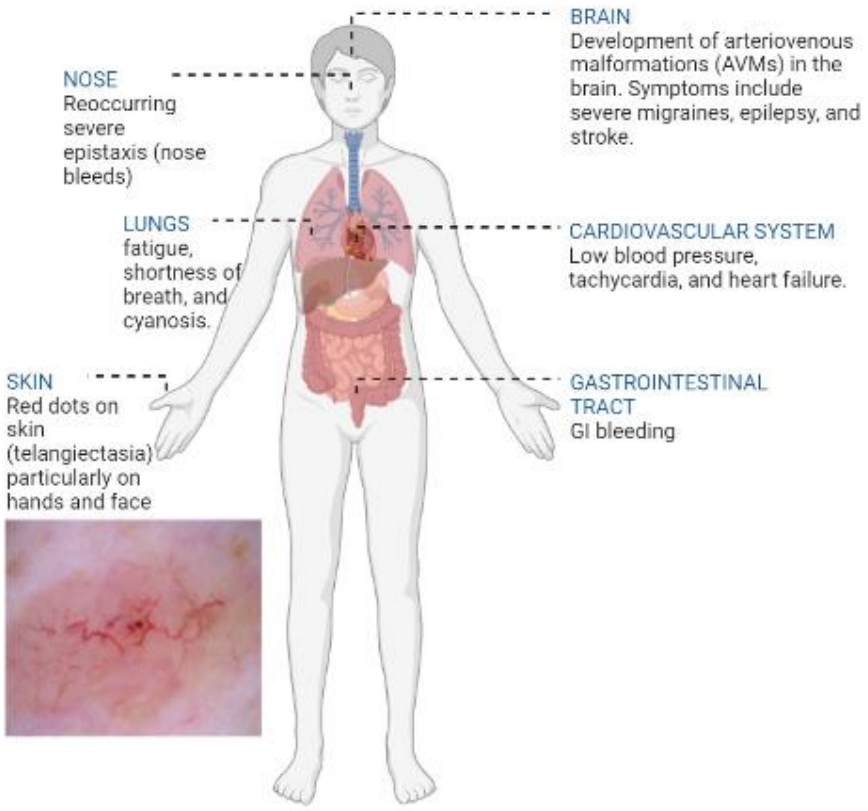

Figure 1.3 Hereditary haemorrhagic Telangiectasia (HHT) symptoms in humans.

HHT is characterised by development of arteriovenous malformations (AVMs). Large AVMs may occur in the brain, leading to severe morbidity. Smaller AVMs known as telangiectasia are prevalent on the skin and mucosal lining of the nose, mouth and gastrointestinal tract and are prone to haemorrhaging. Bottom left image shows an example of telangiectatic vessels (Copyright CC BY 4.0 license (open access)). Figure created with BioRender (https://biorender.com/).

The phenotype of each patient develops due to a mixture of genetics and environmental factors, and family members with the same mutation often display different clinical features. It is not yet clear why the vascular lesions in HHT are localised to specific organs and tissues. Nasal telangiectases and nosebleeds are the most highly penetrant feature affecting over 90% of young HHT adults. Dermal and GI telangiectases accrue later in adult life, whilst pulmonary and cerebral AVMs may be present from birth, usually reaching their final size by adult life (Shovlin 2010). The majority of the vascular architecture in HHT1/2 patients appears normal, supporting the conclusion that one wild type allele is sufficient for development, maintenance and function of the vast majority of the vasculature. Therefore, to explain the development of AVMs, it is possible a second "hit" is responsible. For example, inflammation resulting from infection or injury generates a proangiogenic stimulus that has been shown in preclinical models to be required for AVM formation (Tual-Chalot, Oh and Arthur 2015). Furthermore, organs that are frequently affected in HHT are all exposed to environmental and/or inflammatory insults. This is most obvious for the lung, skin, and GI tract. Snellings and colleagues provided further evidence for the second hit hypothesis with next-generation sequencing (NGS). They identified somatic mutations in 9 out of 19 telangiectasia in HHT patients, and confirmed that mutations in these malformations result in bi-allelic loss of *ENG or ALK1,* which is consistent with the second hit hypothesis (Snellings, Gallione et al. 2019). Although our understanding of the AVM formation has increased significantly over recent years, the underlying molecular and cellular mechanisms that drive AVM formation remain unclear, and further development of animal models is needed to better understand the molecular drivers and to screen new therapies for HHT patients.

BMP9 signalling is also involved in pulmonary arterial hypertension (PAH). PAH is a rare, potentially life-threatening vascular disease characterised by high blood pressure in the arteries of the lungs that eventually leads to right ventricular failure (Girerd, Montani et al. 2010). Symptoms of PAH include shortness of breath, lethargy, and tachycardia. The precise cause of PAH is currently unknown, but mutations in *BMPR2*, *ALK1*, and *ENG* have been linked to the development of PAH (Girerd, Montani et al. 2010). Vorselaars and colleagues provided further evidence that indicates PAH and HHT are linked. Echocardiography-based right ventricular systolic pressure was measured in approximately 300 HHT patients and 100

control patients. They found that the probability of developing PAH was 14% in HHT patients, compared with 4% in the control group (Vorselaars, Velthuis et al. 2017). HHT patients are at risk of developing PAH, and are screened for PAH when diagnosed with HHT. It is also possible that successful therapies for HHT may improve prognosis and quality of life in patients with PAH.

Pre-eclampsia is a systemic disorder characterised by hypertension and proteinuria in the third trimester of pregnancy. Pre-eclampsia affects the foetus and the mother and occurs in approximately 3% of pregnancies. Maternal implications include kidney failure, liver failure, and haematological dysfunction, whereas foetal implications include growth restriction and placental abruption. Pre-eclampsia is caused by an excess of placenta-derived VEGF receptor 1, but more recently endoglin has also been linked with this disease. A placental derived soluble form of endoglin protein, known as sENG is increased in the sera of pregnant women with pre-eclampsia (Leaños-Miranda et al. 2019 Levine, Lam et al. 2006). Furthermore, pre-eclampsia disease severity correlates with sENG concentration, and sENG concentration drops after delivery. Rodent studies showed that overexpression of soluble endoglin in pregnant rats induced the clinical manifestations of pre-eclampsia (Venkatesha, Toporsian et al. 2006). These findings have important diagnostic applications. For example, sENG levels increase approximately 2 months before the onset of pre-eclampsia, and therefore sENG levels can be used as a diagnostic marker to assess the risk of pre-eclampsia. This may be a tool to screen for pre-eclampsia and the resulting morbidity and mortality.

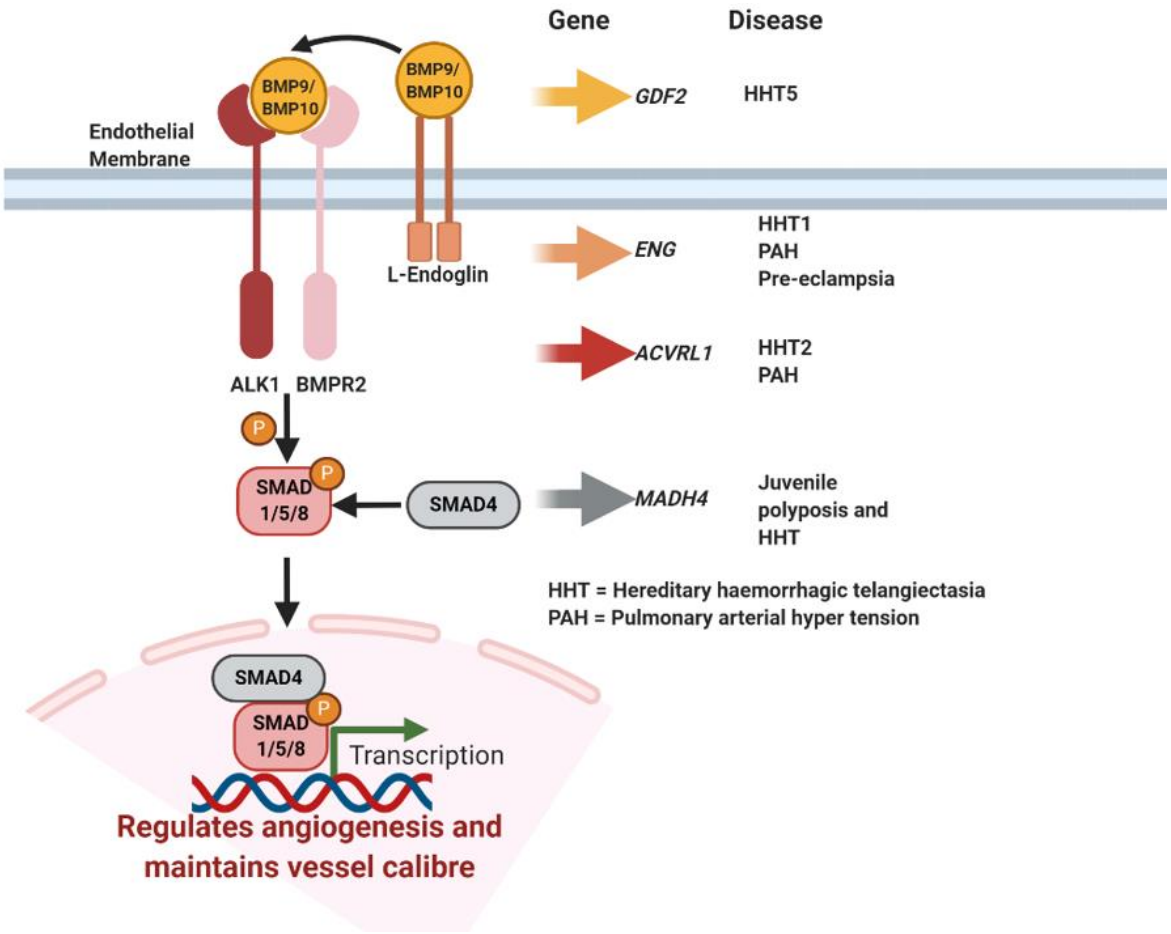

Figure 1.4 Hereditary haemorrhagic telangiectasia (HHT) is a rare autosomal dominant disorder caused by mutations in several genes in the BMP9/10 signalling pathway.

ENG, ACVRL1, GDF2 (*BMP9)*, and MADH4 (SMAD4) mutations lead to HHT1, HHT2, HHT5, and JP-HHT, respectively. Furthermore, endoglin is also linked with other cardiovascular diseases such as pulmonary arterial hypertension (PAH) and pre-eclampsia. Figure adapted from (McDonald et al. 2015, Snodgrass, Chico, et al., 2021).

1.6 Animal models of hereditary haemorrhagic telangiectasia

HHT is characterised by development of vascular abnormalities called AVMs, but the precise mechanisms leading to these vascular abnormities are not yet understood. There is therefore a need to develop robust animal models of HHT, with the aim of understanding these mechanisms that drive disease, and to screen possible therapeutic targets to treat these symptoms.

Various genetic mouse models have been developed to study the pathobiology of HHT (Tual-Chalot, Oh and Arthur 2015). Endoglin-null mice show embryonic lethality, and die by gestational day 11.5 due to blood vessel and heart defects (Li, Sorensen et al. 1999, Arthur, Ure et al. 2000). Blood vessels in endoglin mutant embryos are fragile and haemorrhage, and embryos are smaller than their wild type siblings. This phenotype is similar to ALK1 knockouts suggesting a link between endoglin and other BMP receptors during embryonic development (Urness, Sorensen and Li 2000). Furthermore, Ricard and colleagues produced a BMP9 knockout mouse model that displayed liver, kidney and lung problems. Enlarged vessels and haemorrhaging was observed in the liver of BMP9-null mice (Ricard, Ciais et al. 2012). However, only a small subset of patients with BMP9 mutations develop a HHT-like phenotype. This appeared to be due to redundancy between BMP9 and BMP10 for the HHT phenotype as either signalling molecule appears able to compensate for the other (Ricard, Ciais et al. 2012).

Heterozygous (*Eng*+/– and *Alk1*+/–) mice are genetically closer to the human HHT genotype (Bourdeau, Dumont and Letarte 1999). However, heterozygous models are challenging to study due to their very mild phenotype. Bourdeau and colleagues showed that *Eng*+/– mice develop to adulthood with normal survival. The mice do display features of HHT, including AVMs, telangiectasia, and nosebleeds (Bourdeau, Dumont and Letarte 1999, Torsney, Charlton et al. 2003), but these phenotypes are variable and mild compared to the inducible endothelial specific *Eng* KO and *Alk1* KO models (Mahmoud, Allinson et al. 2010, Tual-Chalot, Mahmoud et al. 2014). These models utilise Cre-lox technology to inactivate *Eng* or *Alk1* in time and specific tissue of choice providing a robust and reproducible model of HHT.

The zebrafish is a widely used model organism to study vascular development. Sugden and colleagues created the first *endoglin*-/- zebrafish model and reported that the endoglin locus

is conserved between human chromosome 9q33-34 and two paralogous loci on zebrafish chromosome 5 **[Figure 1.5]** (Sugden, Meissner et al. 2017). They subsequently demonstrated that *endoglin* mutants developed arteriovenous shunting between the dorsal aorta (DA) and the posterior cardinal vein (PCV). Additionally, they showed that *endoglin* mutant blood vessels have increased diameter – a key characteristic of AVM formation (Sugden, Meissner et al. 2017). This was not due to an increase in cell number, but a change in endothelial cell shape resulting in an increased blood flow through these major vessels and reduced flow through the smaller intersegmental vessels causing them to collapse. The larger arteries and veins prevented blood perfusion into the capillaries as blood flow was greatly increased. This may contribute to the development and enlargement of AVMs (Sugden, Meissner et al. 2017).

Loss of *ALK1* function leads to increased basilar artery (BA) diameter and AVMs in the embryonic cranial vasculature. This is due to accumulation of ECs resulting from reduced migration against blood flow (Corti, Young et al. 2011). Furthermore, *violet beauregarde* (*vbg*) mutants – a zebrafish mutant model for HHT2 caused by a loss function of the *alk1* gene, develop dilated cranial blood vessels, and die between 7 and 10 dpf (Roman, Pham et al. 2002). *bmp10* mutant zebrafish embryos also develop enlarged cranial vessels. They subsequently develop high cardiac output associated with dermal and hepatic vascular defects (Capasso, Li et al. 2020). Thus, ENG promotes BMP9/10/ ALK1 signalling to couple haemodynamic cues to enable EC migration against blood flow during development and remodelling of the vasculature.

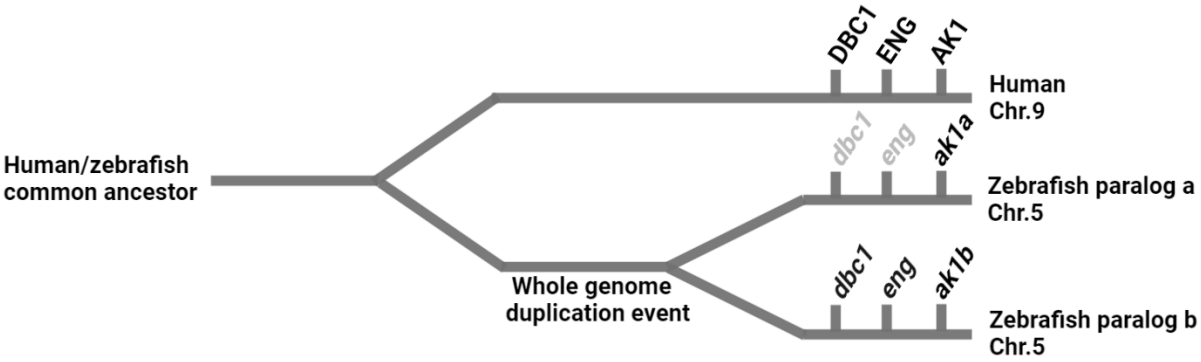

Figure 1.5 The endoglin locus showing genetic conservation between human chr.9 and zebrafish chr.5.

Two paralogous loci on zebrafish chromosome 5 contains: Deleted in bladder cancer 1 (dbc1), endoglin (eng), and adenylate kinase 1 (ak1) genes. Genes were duplicated during the zebrafish whole genome duplication event. Gene loss (shown in grey) on the paralogous chromosomes resulted in the current gene order. Figure adapted from (Sugden, Meissner et al. 2017).

1.7 The role of endoglin in cardiac repair

Revascularisation by angiogenesis after cardiac injury (such as myocardial infarction) is essential to restore cardiac function. For example, *de novo* coronary vessel growth provides oxygen to active cardiac cells in the injured area, and revascularisation is initiated immediately post-MI. Clear differences exist between regenerative models, and there are marked differences between angiogenesis in cardiac and non-cardiac tissues (Lupu, De Val and Smart 2020). The underlying mechanisms that drive revascularisation are complex and not fully understood.

A recent study evaluated the role of a range of vascular signalling pathways, including VEGF and BMP, in response to cardiac injury (Payne, Gunadasa-Rohling et al. 2019). This was done by analysing endothelial enhancer expression patterns in adult and neonatal mouse hearts. They showed that VEGFA is upregulated in adult mouse coronary ECs post-MI, but interestingly the downstream pathways of VEGFA are repressed. Furthermore, they showed that BMP signalling is present in the venous-derived vasculature post-MI in neonates, but it is not active post-MI in adult hearts (Payne, Gunadasa-Rohling et al. 2019). This suggests BMP signalling has a role in the development of the coronary vasculature, which contributes to revascularisation post-MI in neonates.

Van Laake and colleagues showed that endoglin is upregulated in the coronary vessels after MI Using immunohistochemical analysis of mouse and human hearts (van Laake, van den Driesche et al. 2006). Furthermore, endoglin haploinsufficiency results in defective cardiovascular repair, which resulted in lower cardiac function as measured by magnetic resonance imaging. Endoglin heterozygote knockout mice had a 50% reduction in LV function after 4 weeks post MI compared with wild-type controls (van Laake, van den Driesche et al. 2006). These vessel malformations were rescued by injection of mononuclear cells from healthy human donors.

Further work is needed to facilitate the identification of novel therapeutics to promote revascularisation of the infarcted heart. Knowledge of how these signalling mechanisms differ between the embryonic and adult heart may be critical to our understanding of vessel growth post-MI.

1.8 The role of BMP and VEGF in arterio-venous differentiation of endothelial cells

Arterio-venous differentiation is genetically programmed prior to the onset of blood flow. For example, Efnb2 is a specific marker for endothelial precursors cells that develop into arteries and Ephb4 is a marker that is specifically expressed on venous precursors (Neal, Nornes et al. 2019).

Previous zebrafish studies have demonstrated that BMP signalling has an essential role in venous vasculature identity and sprouting. They demonstrated that venous genes are transcriptionally activated by BMP signalling (Neal, Nornes et al. 2019). Disruption of TGF-β and BMP signalling in zebrafish results in abnormal vein formation and loss of the venous-specific gene *Ephb4*. Loss of *Ephb4* has no effect on arterial vasculature development. These results suggest that the venous development is the primary function for BMP signalling during embryogenesis (Neal, Nornes et al. 2019).

Sonic hedgehog (*shh*) is the critical inducer of arterial differentiation. *shh* knockdown in zebrafish by the inhibitor cyclopamine results in failure to establish the dorsal aorta, and loss of the arterial maker expression *efnb2a* (Lawson, Vogel and Weinstein 2002). Furthermore, microinjection of *shh* messenger RNA results in an upregulation of *efnb2a* and downregulation of venous markers in the posterior cardinal vein (Lawson, Vogel and Weinstein 2002). Lawson and colleagues also demonstrated that *shh* knockdown results in failure to express VEGF within the somites of the developing embryo. They went on to show that VEGF knockdown by morpholino microinjection results in reduced arterial differentiation, and conversely overexpression of VEGF in the *shh* knockdown model rescues the impaired *efnb2a* expression. These results therefore suggest VEGF signalling has a critical role in arterial differentiation (Lawson, Vogel and Weinstein 2002).

1.9 Zebrafish as a model to study human cardiovascular disease

Biomedical research has focussed on implementing the use of model organisms to study biological mechanisms that are conserved between humans and other vertebrates. Mice are the most common mammalian model used in biomedical research, including in the field of endoglin and BMP9/10 signalling (Tual-Chalot, Oh and Arthur 2015). These murine models have significant advantages, but also some limitations such as they are difficult to genetically manipulate, image *in vivo,* and expensive to maintain (Cassar, Adatto et al. 2020). The unique

characteristics of the zebrafish model address some of these limitations, and have thus provided a powerful model for studying development and disease (Lawrence 2016).

The zebrafish (*Danio rerio*) is a small freshwater fish that has many useful attributes to study cardiovascular disease *in vivo* (Lawrence 2016). They reach sexual maturity by 3-4 months, and have a lifespan up to approximately 5 years (Cassar, Adatto et al. 2020). Large numbers of these adults can be maintained relatively inexpensively, and females can produce up to 500 embryos per spawning session (Cassar, Adatto et al. 2020). It is therefore relatively simple and inexpensive to get large sample sizes for zebrafish embryo experiments. Embryos develop a highly conserved cardiovascular system by 24-26 hpf, including a beating heart and the development of major vessels (Isogai, Horiguchi and Weinstein 2001, Boselli, Freund and Vermot 2015). Furthermore, at this developmental stage, embryos are transparent, and develop *ex utero* making them ideal for imaging the cardiovascular system throughout development (Cassar, Adatto et al. 2020). This is in contrast to traditional mammalian models which generally require imaging of explanted tissue or *in vitro* cell lines, and thus this allows detailed study of the mechanisms involved in vascular development, including angiogenesis, vasculogenesis, and vascular remodelling.

The zebrafish is a powerful vertebrate model for studying vascular development. zebrafish have a closed circulatory system, and the molecular mechanisms that drive vessel formation are highly conserved in mammalian models (Isogai, Horiguchi and Weinstein 2001, Boselli, Freund and Vermot 2015). In zebrafish embryos, the first vessels form by vasculogenesis, in which precursor endothelial cells and angioblasts merge to form the dorsal aorta, cardinal vein, and primitive cranial vasculature (Roman, Pham et al. 2002). These primary vessels differentiate into arterial or venous vasculature as they develop. Subsequently, the primitive cranial vasculature matures, and a more complex vasculature bed develops via angiogenesis, and the recruitment of mural cells (Roman, Pham et al. 2002). This initial vasculature pattern observed in the zebrafish cranial vasculature bed is highly conserved with other developing mammalian models including humans (Isogai, Horiguchi and Weinstein 2001, Boselli, Freund and Vermot 2015).

The development of molecular and genetic techniques has increased the approaches possible using zebrafish. Zebrafish development *ex utero* allows rapid and effective genetic

manipulation (Cassar, Adatto et al. 2020). For example, morpholino antisense oligonucleotides are commonly used to inhibit gene expression. Morpholinos are designed to specifically bind to a gene of interest, which results in knockdown of gene function and therefore gene function can be simply assessed. Additionally, gene expression can be inhibited in specific tissues using CRISPR-Interference (CRISPRi) (Rossi, Kontarakis et al. 2015). Stable mutant lines are now easily achievable due to the development of genetic engineering techniques. Zinc finger nucleases (Kim, Cha and Chandrasegaran 1996), TALENs (Transcription activator-like effector nucleases) (Cermak, Doyle et al. 2011), and CRISPR-Cas9 (clustered regularly interspaced short palindromic repeats) (Ran, Hsu et al. 2013) can be used to specifically knockout a gene of interest. Furthermore, the zebrafish genome has been entirely sequenced (Howe, Clark et al. 2013). This study showed that 70% of human genes and 82% of human disease-causing genes have a zebrafish orthologue (Howe, Clark et al. 2013).

The developmental pathways regulating vascular development, including BMP9/10 (Sugden, Meissner et al. 2017), VEGF (Lawson, Vogel and Weinstein 2002) and Notch (Siekmann and Lawson 2007) are highly conserved between humans and zebrafish. Zebrafish can therefore provide a useful developmental model to uncover the molecular mechanisms regulating vascular disease. For example, zebrafish are a powerful model for *in vivo* screening of vascular genes. Previously, a zebrafish model for the functional screening of mechanoreceptors involved in flow-regulated endothelial cell apoptosis was developed (Serbanovic-Canic, de Luca et al. 2017). This model was then utilised to screen a panel of genes to identify four candidate regulators of apoptosis. Two of these genes, CDH13 and PERP, were subsequently validated with the use of human endothelial cells (Serbanovic-Canic, de Luca et al. 2017).

The production of transgenic cell specific zebrafish lines has enabled detailed visualisation of the vasculature throughout embryo development. For example, the endothelial specific promoters *fli1* and *kdrl* drives the expression of fluorescent proteins such as, enhanced green fluorescent protein (eGFP) or mCherry. This allows visualisation of all blood vessels throughout embryogenesis using fluorescent microscopy techniques such as confocal or light sheet fluorescence microscopy (LSFM). LSFM uses a thin sheet of light to excite fluorescent proteins within the focal plane of interest. This results in a stack of images in the z-plane that

can be viewed in 3d or processed to produce a 2d maximum intensity projection (MIP) (Stelzer, Strobl et al. 2021). LSFM has many advantages, such as increased resolution, high acquisition speed, and reduced phototoxicity. LSFM is therefore relatively non-invasive, making it ideal for *in vivo* experiments.

Zebrafish embryos are a very useful for studying drug screening (Tamplin, White et al. 2012, MacRae and Peterson 2015). Embryos are permeable and a wide range of drugs can be administered by simply dissolving the chemical in the E3 growth media. This along with the availability of transgenics, and their optical transparency allows simple visual assessment of the phenotypic changes and/or toxicity in response to drug treatments (MacRae and Peterson 2015). A range of small molecules discovered in zebrafish have gone onto clinical trials, including an inhibitor of BMP type 1 receptors, dorsomorphin (Yu, Deng et al. 2008). Dorsomorphin selectively blocks ALK2, ALK3 and ALK6 activity, and was used in clinical trials as a potential therapeutic to treat fibrodysplasia ossificans progressiva (FOP), which is a congenital disorder characterised by progressive muscle and connective tissue ossification (replacement with bone) (Yu, Hong et al. 2008, Cassar, Adatto et al. 2020). This highlights the ability to apply scientific discoveries in the zebrafish models to potentially treat human patients. The cardiovascular system is highly conserved between zebrafish and mammals. Previously zebrafish have been used as a model to study cardiovascular toxicity, and a range of cardiovascular diseases have been recapitulated in zebrafish (Santoro, Beltrame et al. 2019).

1.10 Zebrafish as a model to study cardiac repair

The zebrafish is a unique model organism to study mechanisms of cardiac repair. There are a range of cell-specific transgenic lines are available to image the heart *in vivo*. For example the *Tg(kdrl:EGFP)*^{y7} line allows visualisation of the endocardium of the zebrafish (Roman, Pham et al. 2002). Imaging of fluorescent hearts can be used to assess cardiac function, such as fractional shortening, chamber size, and heart rate (HR) (Liu, Asnani et al. 2014). Several mechanisms are essential to drive cardiac regeneration, including angiogenesis to provide adequate blood flow to the affected area (Kim, Wu et al. 2010). However, the molecular mechanisms of zebrafish heart regeneration remain poorly understood.

1.11 Ventricular amputation and cryoinjury models of heart regeneration

Several techniques have been developed to induce cardiac damage in zebrafish to model human myocardial infarction (MI). The adult zebrafish heart can fully regenerate after amputation of up to 20% of its ventricle. The injured area forms a fibrin clot, which is replaced by healthy muscle by 60 days post injury (dpi) (Poss, Wilson and Keating 2002). This is in contrast to mammals as cardiac damage results in a permanent fibrotic scar instead of the regeneration of functional cardiomyocytes (Laflamme and Murry 2011). Adult zebrafish sustain the ability to robustly proliferate cardiomyocytes, providing the ability to regenerate the myocardium after damage. During this process, angiogenesis is stimulated to revascularise the regenerating tissue (Kim, Wu et al. 2010).

Cryoinjury can also be used to induce cardiac damage (González-Rosa and Mercader 2012). Cryoinjury is a MI model, in which a metal probe is cooled in liquid nitrogen and pressed against the ventricle, resulting in freezing to the ventricle wall and thus injury to the cardiac tissue. This recapitulates mammalian MI more than resection as it achieves cardiac cell death in a localised region. Furthermore, the regenerative process relies on formation of a fibrotic scar similar to that formed in human MI (González-Rosa and Mercader 2012). Initially the injured cardiac tissue is replaced with scar tissue, which is completely replaced within two months in healthy zebrafish adults. The ability for zebrafish cardiomyocyte proliferation results in regression of the fibrotic scar over time as it replaced with healthy tissue (González-Rosa and Mercader 2012).

More recently, Bise and colleagues, investigated whether heart regeneration remains effective after multiple rounds of cryoinjury in the same adult zebrafish sample (Bise, Sallin, Pfefferli and Jaźwińska 2020). They assessed regeneration after two to six injuries interspaced by varying recovery periods, and found that regeneration efficiency decreased with the number of repeated cryoinjuries. All samples failed regenerate the fibrotic tissue by 6 successive cryoinjuries. This suggests that there is a limit to the ability for zebrafish to replace the fibrotic tissue with new cardiomyocytes (Bise, Sallin, Pfefferli and Jaźwińska 2020).

Relatively little is known about the molecular mechanism that drive zebrafish heart regeneration. Chablais and colleagues, showed that TGFβ signalling is involved in the regeneration process, using the cryoinjury model (Chablais and Jazwinska 2012). They

chemically Inhibited type I receptors using the *alk* inhibitor SB-431542, and showed complete prevention of heart regeneration (Chablais and Jazwinska 2012). Further work is needed to fully understand the molecular aspects regulating heart regeneration, with the aim of stimulating similar regeneration in human patients.

1.12 Zebrafish model of chemotherapy induced heart failure

Chemotherapy-induced heart failure is another technique used to induce cardiac damage in zebrafish embryos. Previously, it was shown that administration of chemotherapeutic drugs used in humans induces heart failure in embryonic zebrafish (Liu, Asnani et al. 2014). Doxorubicin (DOX) is an anthracycline used to treat a range of cancers including breast cancer and leukaemia. However, medical use of anthracyclines are limited by the risk of inducing cardiotoxicity, and cancer patients treated with anthracyclines have a significantly increased risk of developing heart failure. Liu and colleagues developed a doxorubicin-induced cardiomyopathy model in zebrafish and showed that zebrafish embryos exposed to 100µM of doxorubicin developed extensive pericardial oedema, reduced heart contractility and increased cardiomyocyte apoptosis. Therefore, the zebrafish model recapitulates several characteristics of chemotherapy-induced heart failure in humans, including increased apoptosis and reduced contractility.

1.13 Zebrafish models of diabetes mellitus

Diabetes mellitus (T2DM) is a metabolic condition characterised by chronic hyperglycaemia. Hyperglycaemia causes various vascular complications such as atherosclerotic disease, retinopathy and nephropathy (Paneni, Beckman, Creager and Cosentino 2013). Currently, there is no cure for T2DM, and treatment is limited to prevention or symptomatic care. Therefore, there is a clear need for robust models of t2DM to identify potential new therapeutics. T2DM has been modelled in variety of animals using a range of chemical and/or genetic techniques (Salehpour, Rezaei et al. 2021). As discussed in section 1.8 the majority of biomedical research is completed using murine models, but more recently zebrafish has emerged as the useful model to study diabetes (Salehpour, Rezaei et al. 2021).

There are a range of chemical and genetic approaches to model hyperglycaemia in zebrafish, but glucose exposure is common due to its relative simplicity and inexpensiveness. Gleeson and colleagues developed a method for inducing T2DM in zebrafish. Zebrafish were exposed

to 2% glucose for 30 days, and diabetes symptoms were observed, such as retinopathy and increased blood glucose (Gleeson, Connaughton and Arneson 2007). An additional embryonic zebrafish model for hyperglycaemia was reported (Jörgens, Stoll et al. 2015). Hyperglycaemia was induced by the addition of 55mM D-(+)-glucose in the E3 growth media, which increased methylglyoxal concentrations in zebrafish embryos. This resulted in the development of vessel malformations sprouting from the ISVs (Jörgens, Stoll et al. 2015). These vessel malformations resemble the AVMs that form in HHT.

1.14 Potential therapeutic strategies to treat hereditary haemorrhagic telangiectasia

Despite the huge developments in unravelling the molecular and cellular mechanisms behind angiogenesis, the current treatment options for cardiovascular diseases such as HHT remain limited to symptomatic care. The majority of therapeutic approaches in severe disease focus on surgical or interventional radiological procedures to cauterise bleeding telangiectases or occlude AVMs to reduce disease symptoms or risk of complications such as stroke. This is achieved by implantation of intravascular metal coils to occlude AVMs. However, access to symptomatic AVMs in the brain and liver is more challenging and higher risk.

CRISPR-Cas9 gene therapy has emerged as a powerful technique to edit the genome of a wide variety of organisms, potentially including humans. This enables precise modification of genetic sequences and gene expression (Ma, Marti-Gutierrez et al. 2017). Gene therapy includes the replacement of a mutated gene with a correct copy, the inactivation of a mutated gene, or the introduction of a new gene to restore protein function. HHT is caused by a defect in one allele of a single gene (either *ENG*, *ALK1 and* SMAD4), and thus may be a candidate for gene therapy. Therapy based on adeno-associated viruses (AAVs) can be implemented as these readily infect humans but are non-pathogenic. AAVs can insert recombinant DNA in specific tissues (Ma, Marti-Gutierrez et al. 2017). For example, AAV1 targets the developing vasculature, and could be used to treat HHT (Youjin and Jun 2009). The majority of HHT patients have mutations in endoglin (HHT1) or ALK1 (HHT2) genes, making these genes likely targets for gene therapy. However, gene therapy remains highly challenging and has only translated to clinical practice in a very small number of specific, severe, diseases. For most chronic diseases, long-term pharmacological treatments remain the mainstay of treatment.

Advances in understanding the molecular and cellular defects that drive HHT and the availability of reproducible preclinical models have driven further investigations to identify novel pharmaceutical strategies to prevent or ameliorate AVMs. Translation of these findings to the clinic depends on development of effective yet safe drugs. These efforts are summarised in Table 1.1 and Table 1.2. There is growing evidence that targeting VEGF signalling may benefit HHT patients. For example, targeting VEGF signalling has been shown to be effective in protecting against AVM formation in many animal models of HHT (Han, Choe et al. 2014, Jin, Muhl et al. 2017, Tual-Chalot, Garcia-Collado et al. 2020). A marked improvement of HHT disease symptoms was noted when the anti-VEGF antibody Bevacizumab was used to treat cancer in an HHT patient (Dupuis-Girod, Ginon et al. 2012). This led to the realisation that reducing VEGF activity may be beneficial in HHT and was followed by successful (nonrandomised) clinical trials showing improved cardiac function in HHT patients with hepatic VMs and reduced epistaxis (Dupuis-Girod, Ginon et al. 2012, Al-Samkari, Kasthuri et al. 2021) . A major caveat is that to be effective intravenous Bevacizumab is repeated over a substantial period, can incur significant side effects including hypertension, thrombosis, and impaired healing. Such treatment is also expensive.

1.15 Targeting vascular endothelial growth factor signalling to treat hereditary haemorrhagic telangiectasia

Angiogenesis is complex and driven by multiple signalling pathways. Understanding these will have significant implications for developing novel disease therapies. For example, anti-angiogenic therapies to treat cancer have been trialled by targeting the master regulator of angiogenesis, VEGF signalling (Yadav, Puri et al. 2015). However, most anti-angiogenic treatments have been unsuccessful, and patients often suffer severe side-effects such as nausea, vomiting and impaired wound healing. Furthermore, studies of cancer patients have highlighted the increased risk of serious adverse cardiovascular risk of targeting VEGF signalling (Totzeck, Mincu and Rassaf 2017). This suggests a greater understanding of the downstream signalling processes in angiogenesis is required.

Table 1. 1 Pharmacological treatment of HHT in humans

DRUG	TARGET	NUMBER OF PATIENTS	RESULT	REFERENCE
Bevacizumab (Avastin)	Anti-VEGFA antibody	24	Reduced epistaxis and improved cardiac function in liver VM patients with high-output heart failure	(Dupuis-Girod, Ginon et al. 2012)
Bevacizumab (Avastin)	Anti-VEGFA antibody	238	Reduced epistaxis	(Al-Samkari, Kasthuri et al. 2021)
Tacrolimus	Increased activation ALK1	24	Reduced epistaxis	(Dupuis-Girod, Fargeton et al. 2020)
Thalidomide	Increased PDGFB expression	7	Reduced epistaxis	(Lebrin, Srun et al. 2010)

Table 1. 2 Pharmacological treatment of HHT-like phenotypes in preclinical mouse models

DRUG	TARGET	MOUSE MODEL	RESULT	REFERENCE
Wortmannin	PI3K inhibitor	*Alk1-iKOe*	Reduced retinal AVMs	(Ola, Dubrac et al. 2016)
Nintedanib , Sirolimus	TKI , mTOR inhibitor	Neonatal antibody blockade of BMP9/10	Combination therapy reduced and reversed retinal AVMs	(Ruiz, Zhao et al. 2020)
SU5416	VEGFR2 inhibitor	*Eng-iKOe* neonate	Significant reduction in retinal AVM size	(Jin, Muhl et al. 2017)
Thalidomide	Increased PDGFB expression	*Eng+/−* Adult	reduced cerebral haemorrhage	(Lebrin, Srun et al. 2010)

Angiogenesis is highly regulated by VEGFA and its receptor VEGFR2 **[Figure 1.6].** For example, VEGFA controls endothelial cell migration, proliferation and survival. The critical importance of VEGFA is highlighted as heterozygous Vegfa mutant mice are embryonic lethal and die due to vascular defects (Carmeliet, Ferreira et al. 1996). VEGFA signalling is complex and drives numerous downstream pathways, opening the possibility that targeting more specific downstream pathways may be beneficial. However, it is not yet clear which pathway (or combination of pathways) is critical to target therapeutically.

It is clear there is crosstalk between the BMP9/BMP10 and VEGFA signalling pathways, but the precise mechanisms of how these interact is currently unclear. BMP9 signalling prevents inactivation of PTEN (Phosphatase and TENsin homologue), consequently inhibiting the activity of PI3K, a key component of the VEGFA signalling pathway (Ola, Dubrac et al. 2016, Jin, Muhl et al. 2017). Endoglin haploinsufficiency leads to overstimulation of PI3K signalling (Alsina-Sanchís, García-Ibáñez et al. 2018), triggering a variety of cellular responses including cell survival, cell metabolism, and cell permeability **[Figure 1.6]**. Furthermore, telangiectasia from HHT2 patients show increased PI3K pathway activity (Alsina-Sanchís, García-Ibáñez et al. 2018). Pharmacological PI3K (Alsina-Sanchís, García-Ibáñez et al. 2018) inhibition reduces incidence of mouse neonatal retinal AVMs following loss of endothelial Alk1, but only had a minor effect on AVMs in *Eng* mutant neonatal retinas (Ola, Dubrac et al. 2016, Jin, Muhl et al. 2017). As *Eng* mutants show increased phosphorylated (p)ERK activity in endothelial cells associated with AVMs (Tual-Chalot, Garcia-Collado et al. 2020), this may represent an alternative pathway to target downstream of VEGFA. Indeed, sporadic human cerebral AVMs also have an exaggerated pERK response (Nikolaev, Vetiska et al. 2018). In addition, targeting mTOR has a beneficial effect in a mouse neonatal retinal model caused by loss of BMP9/10 ligands (Ruiz, Zhao et al. 2020). Therefore, although it is clear that AVMs resulting from loss of endothelial *Eng* or *Alk1* genes is due to an abnormal vascular response to VEGFA, there is some debate as to which is the best pathway (or combination of pathways) downstream of VEGFA signalling to target.

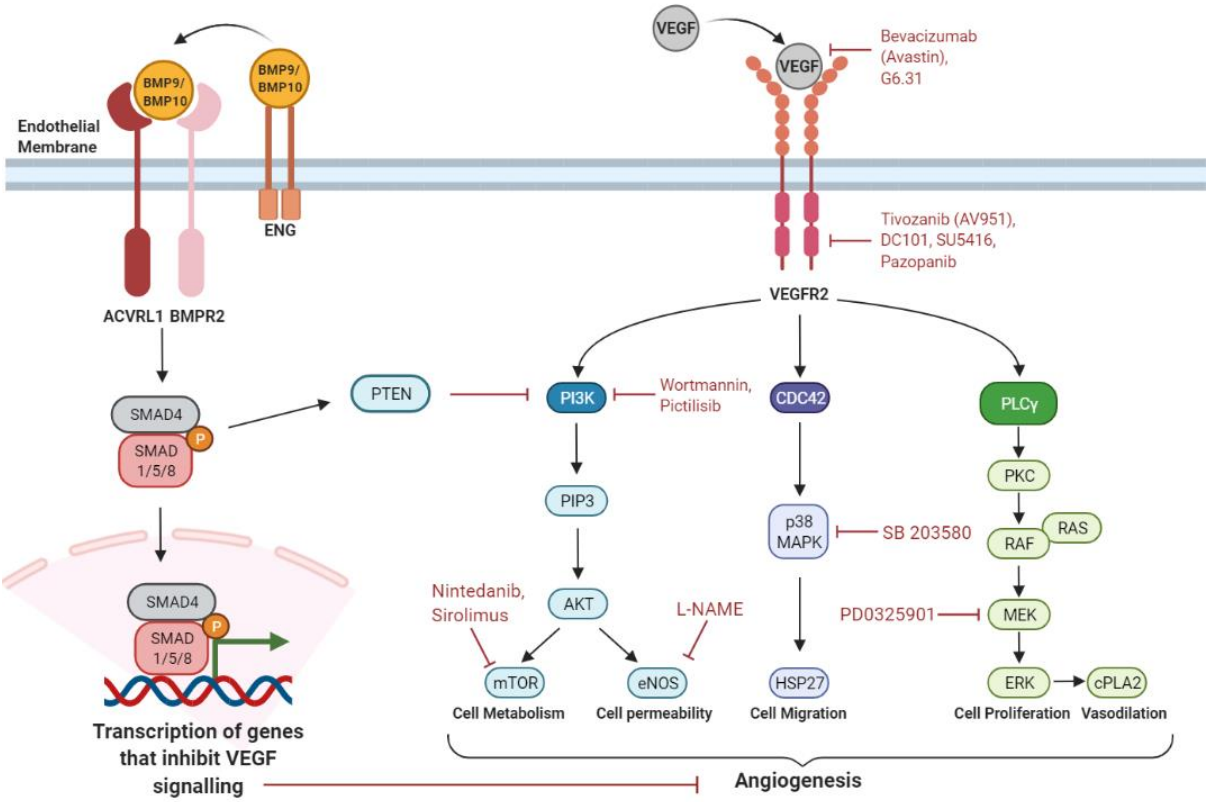

Figure 1.6 Summary of crosstalk between BMP9/10 and VEGF signalling pathways in endothelial cells.

BMP9 signalling prevents inactivation of PTEN, consequently inhibiting the activity of PI3K. Endoglin haploinsufficiency leads to the overstimulation of PI3K signalling, which triggers a variety of cellular responses, including cell survival, cell metabolism, and cell permeability. Dysregulating these cellular processes results in AVM formation. Figure created with BioRender (https://biorender.com/). Figure taken from Snodgrass *et al*., 2021 2021 (Copyright CC BY 4.0 license (open access)) (Snodgrass, Chico and Arthur 2021).

1.16 Summary

Since the discovery that endoglin haploinsufficiency causes HHT, interest in the roles of endoglin in other cardiovascular diseases has greatly increased. There is strong evidence to suggest that endoglin is involved in other cardiovascular diseases such as PAH and pre-eclampsia, but the treatment for these diseases is currently limited to symptomatic care. There is therefore a pressing need to understand the endoglin mediated mechanisms that drive angiogenesis, as it may be possible to develop drug targets that improve the prognosis of patients suffering with these cardiovascular diseases. The molecular mechanisms underlying the formation of AVMs are currently being unravelled using *in vivo* and *in vitro* models, but many questions remain unanswered regarding the pathogenesis of HHT. The zebrafish model allows real time imaging of the vasculature following endoglin loss of function. It therefore offers great promise to investigate the cellular and molecular events that lead to AVM formation. Furthermore, it is a useful model for drug screening to develop therapeutics that may help treat cardiovascular diseases such as HHT.

1.17 Aims and objectives

In this chapter, I have summarised the current literature related to my project, ranging from angiogenesis to using zebrafish as an animal model for studying cardiovascular disease. In addition, I have outlined current knowledge regarding endoglin and its relation to BMP9 and VEGF signalling, and discussed the unanswered questions related to this field and the potential impact of this thesis.

endoglin mutants displayed a significant increase in the diameter of the dorsal aorta (DA) and posterior cardinal vein (PCV). This is due to an increase in EC size and not increased EC number (Sugden, Meissner et al. 2017)**.** Increased flow through the enlarged major vessels in *eng*^{mu130} mutants leads to correspondingly reduced flow in ISVs, which leads to a delayed opening of their lumens (Sugden, Meissner et al. 2017). However, the role of endoglin in zebrafish cerebral vasculature, heart, and trunk vasculature after the developmental stage of 3 dpf is currently unknown. Furthermore, the adult *eng*^{mu130} mutant phenotype has not been described. There is evidence that endoglin mutants develop tortuous vessels in the brain that resemble AVMs (Sugden, Meissner et al. 2017), but how endoglin affects retinal vasculature development, heart development, and mortality is unknown.

I therefore hypothesise that:

1) *endoglin* is required for normal cardiovascular development in multiple vascular territories, including embryonic cranial and adult retinal vasculature.

2) *endoglin* mutant zebrafish are sensitised to VEGFA signalling and therefore modulation of VEGFA results in rescue of the mutant phenotype.

3) *endoglin* mutant zebrafish show increased sensitive to chemotherapy induced heart failure, and display defective cardiac repair and cardiac angiogenesis post injury.

The first aim of my thesis is therefore to further characterise the zebrafish model of HHT (adult and embryonic). Subsequently, I treat zebrafish *endoglin* mutant and control embryos with different drugs to block either global VEGF signalling or components of different pathways downstream of VEGFR2 to explore which is the most critical downstream pathway or combination of pathways to prevent development of the *endoglin* mutant phenotype. The final aim of my thesis is to characterise the role of *endoglin* in response to cardiovascular disease including cardiac damage and diabetes, although these studies were significantly curtailed by the effects of the pandemic (see COVID--19 mitigation statement). The overall goal of my work is to use the zebrafish model of HHT to better understand disease mechanisms to inform the development of improved therapies for both heart attack and HHT patients.

2. Materials and methods

2.1 Zebrafish husbandry

Animal experiments were performed at the University of Sheffield under Home Office project licences PPL 70/8588 and PP3256323. The *endoglin* mutant (*eng*^{mu130}) (Sugden, Meissner et al. 2017) was kindly provided by Dr Arndt Siekmann. *eng*^{mu130} lines were raised in *Tg(kdrl:Hsa.HRAS-mCherry)*^{s916} (Chi, Shaw et al. 2008), *Tg(kdrl:EGFP)*^{y7} (Roman, Pham et al. 2002), and Tg(fli1a:nEGFP)y7 (Roman, Pham et al. 2002) transgenic backgrounds, which label the EC membrane, endothelial cytoplasm respectively, and EC nuclei, respectively. Data from ALK1 mutants in a Tg(fli1a.ep:mRFP-CAAX)pt50 transgenic background was kindly provided by Dr Beth Roman (Corti, Young et al. 2011, Capasso, Li et al. 2020). Adult fish were housed in a recirculating aquarium with a 14-hour light / 10-hour dark cycle at 28.0±1^{o}C, pH 7.5, and oxygen saturation 80%.

2.1.1 *eng*^{mu130} Mutant zebrafish lines

The *eng*^{mu130} line consists of a 14-bp deletion in the coding sequence of exon 1, causing a frameshift mutation resulting in the premature truncation of the protein **[figure 2.1]**. The *eng*^{mu130} mutant line was outcrossed with *Tg(kdrl:EGFP)*, and heterozygous adults were raised.

2.1.2 Generation of zebrafish embryos

Clutches of embryos were generated by pair-mating individual male and female zebrafish. Zebrafish were placed into a holding tank separated by a divider. The following morning the divider was removed allowing the fish mate. To generate *eng*^{mu130} embryos, heterozygous adults were in-crossed by pair-mating to generate clutches of embryos of mixed wild type (wt), heterozygous (+/-), and homozygous (-/-) mutant siblings.

2.1.3 Handling of zebrafish embryos

Fertilised embryos were maintained in petri dishes containing approximately 50ml of E3 medium (5 mM NaCl, 0.17 mM KCl, 0.33 mM MgSO4, and 0.33 mM CaCl2 (sigma-Aldrich)) and Methylene blue (sigma-Aldrich). Up to 60 embryos per petri dish were incubated at 28°C. Petri dishes were examined each day and unhealthy/dead embryos were removed from the population. Upon completion of the experiment, zebrafish up to 5.2 days post fertilisation

(dpf) were culled in a bleach solution. Zebrafish above 5.2 days post fertilisation (dpf) are protected and were placed into tanks and maintained according to the home office project licence.

2.2 Genotyping

2.2.1 Genomic DNA extraction from zebrafish embryos

Anaesthetised embryos were individually placed in microcentrifuge tubes containing 25µl of 50mM NaOH (Sigma Aldrich). Samples were heated to 95°C for 10 minutes, and subsequently cooled to 10°C. The reaction was neutralised by addition of 0.5µl Tris-HCl pH9.5 (sigma Aldrich).

2.2.2 Genomic DNA extraction from adult zebrafish

Individual adult zebrafish were anaesthetised in 0.4% tricane (4g MS-222 (Sigma Aldrich)) in 1L dH_2O – adjusted to pH 7-7.5 using NaOH) diluted with aquarium water. A small section of the caudal fin was removed using a clean razor blade and placed in a microcentrifuge tube containing 25µl of 50mM NaOH. Samples were heated to 95°C for 10 minutes, and subsequently cooled to 10°C using a PCR machine. The reaction was neutralised by addition of 0.5 µl Tris-HCl pH9.5.

2.2.3 PCR amplification and restriction enzyme DNA digestion

Genomic DNA isolated from methods 2.2.1/2.2.2 was amplified using polymerase chain reaction (PCR) (MultiGene™ OptiMax Thermal Cycler). PCR Primers were used to amplify a 418bp fragment spanning the TALEN-binding site to identify WT and mutant zebrafish (table 2.1, 2.2 and 2.3). *Msp*1 restriction enzyme (New England Biolabs) was used to cleave the WT but not the *eng* mutant PCR product into 246bp + 172bp fragments **[Figure 2.2]** via incubation at 37°C for 20 minutes.

Figure 2.1 Transcription activator-like effector nuclease (TALEN) genome editing was used to disrupt the zebrafish *eng* gene.

TALEN binding site is highlighted in red, and the **bold** sequence is removed in the *eng*^{mu130} mutant allele. This results in a predicted loss of function due to a premature stop codon within exon 1. The Sanger sequencing chromatogram depicts sequencing data from PCR amplification with a forward primer specific to the *eng* gene.

Table 2.1 Oligonucleotide primers used for genotyping *endoglin* mutants

PCR FRAGMENT	NAME OF PRIMER	SEQUENCE 5' → 3'
endoglin	1	GCTGATTAGGGCTGCAAGA
	2	TGTTGTGGTAATTTTACAGTTGCT

Table 2.2 Reaction mixture for DNA amplification

REAGENT	VOLUME (µl)
5 ng DNA template	2
10 µM sense primer	1
10 µM anti-sense primer	1
2X Biomix Red	10
Distilled water	6
Total	20

Table 2.3 PCR conditions for DNA amplification

STEP	TEMPERATURE (°C)	TIME	NUMBER OF CYCLES
Initial denaturation	98	30 s	1
Denaturation	98	5 s	35
Annealing	58	30 s	35
Extension	72	10 min	35
Hold	37	N/A	1

Table 2.4 Reaction mixture for *Msp1* restriction enzyme digestion

REAGENT	VOLUME (µl)
PCR reaction	5
*Msp*1	0.5
Cutsmart buffer	1
MilliQ H_2O	3.5

2.2.4 Agarose gel electrophoresis

1.5% agarose gels were made by adding agarose powder (Bioline) to 1X TAE buffer (0.04M Tris-acetate (sigma Aldrich); 1mM EDTA (sigma Aldrich)). Ethidium bromide (Alfa-Aesar) was added to the melted agarose for visualisation of DNA bands. 10µl Samples were loaded alongside 4µl of 100bp hyperladder (Bioline). Gel electrophoresis was performed at 120V for 30 minutes to determine differences in fragment size for each sample. Gels were imaged using a UVdoc (UVtec). An example of a gel used for genotyping is shown in **[Figure 2.2]**.

2.2.5 Sequence analysis

PCR samples were sequenced by the core genome facility at the University of Sheffield to ensure the PCR genotyping is reliable. Sequencing data was analysed using ApE plasmid editor (http://jorgensen.biology.utah.edu/wayned/ape/).

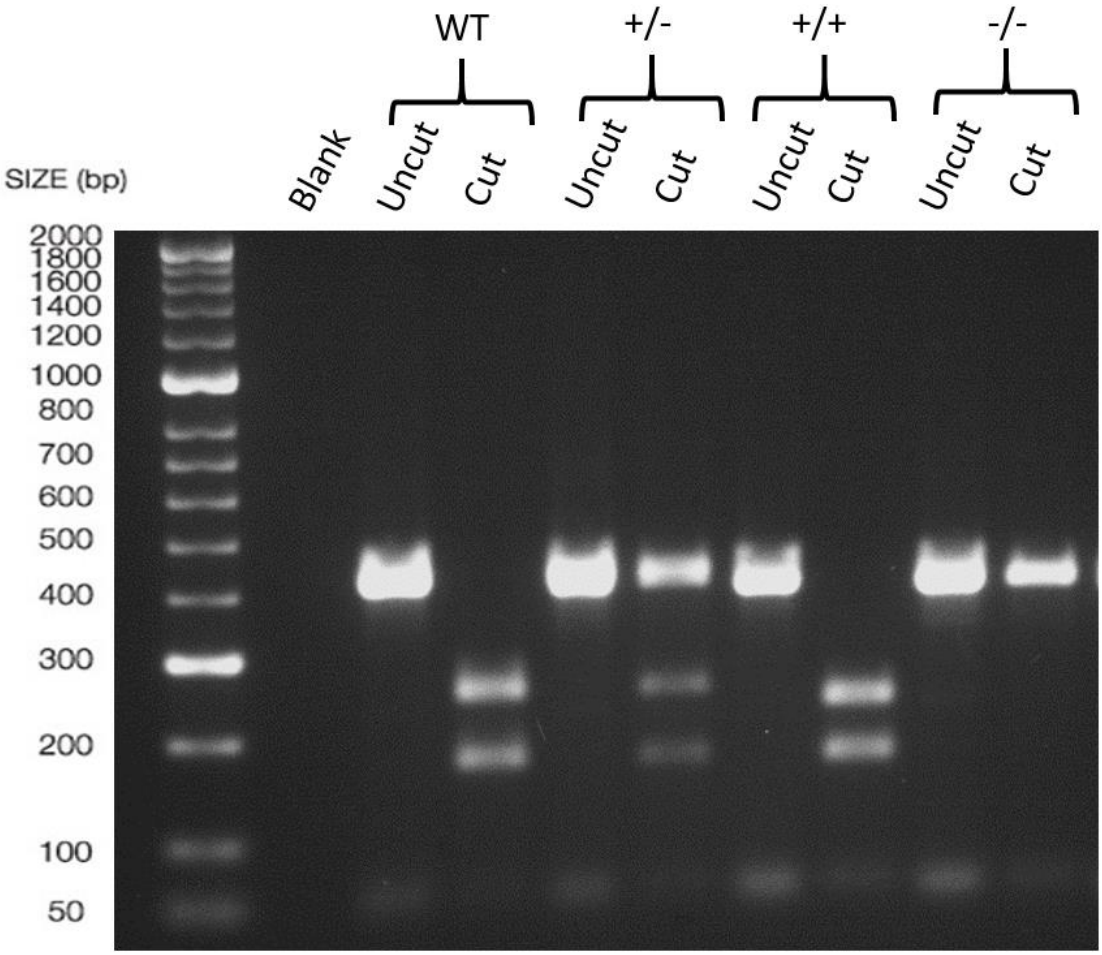

Figure 2.2 *Msp1* restriction enzyme analysis of the *endoglin* allele in the *eng*^{mu130} embryos.

Wild type, heterozygous and homozygous band sizes are indicated. WT wild type (control), +/+ wild type (experimental), +/- heterozygous mutants, -/- homozygous mutants. The *Msp*1 restriction enzyme site is preserved in the wild type *endoglin* allele (figure 2.1). *Msp*1 digestion yields fragments of 248bp and 173bp. In contrast, *Msp*1 does not digest the mutant allele, and therefore yields a single band of 408bp. Presence of all three bands indicates heterozygosity. The gel includes a blank (no gDNA), and positive wild type control to ensure genotyping is reliable.

2.3 Morphology of adult zebrafish hearts and retinae

Tg(kdrl:Hsa.HRAS-mCherry)^{s916} adult fish (5-6 months) were culled by a lethal dose of tricaine (MS-222). Freshly dissected hearts were fixed in 4% paraformaldehyde overnight at 4°C. Hearts were weighed, and imaged using a stereomicroscope (Olympus IX81). To prepare retinae, heads were fixed in 4% paraformaldehyde overnight at 4°C. Eyes were enucleated and retinae dissected, flat-mounted onto glass slides, and imaged using a fluorescent stereomicroscope (Axio zoom V.16). Number of capillary interconnections, optic artery diameter, and vessel branching was quantified as previously described (Wiggenhauser, Kohl et al. 2017).

2.4 Vascular imaging and quantification

2.4.1 Light-sheet microscopy

Zebrafish embryos were sorted for red and/or green fluorescence using a fluorescent stereomicroscope (Axio zoom V.16). The sorted zebrafish embryos were anaesthetised using 0.4% tricaine, and were subsequently mounted in 1% low melting point agarose (LMP) (Biolabs) within a 1mm diameter glass capillary. Samples were suspended in the chamber of a Zeiss Z1 lightsheet microscope filled with E3 medium at 28°C. Samples were excited with a lightsheet generated by 488nm and 561nm wavelength lasers, and the emitted signal collected by a LP560 filter. Image acquisition and processing was performed using ZEN Black software (Zeiss). Z-stacks of the trunk and head vasculature were obtained from 2-4dpf. Imaged embryos were retained for subsequent genotyping (2.2.1).

2.4.2 Quantifying blood vessel diameter and *kugel number*

Diameters of the dorsal aorta (DA) and posterior cardinal vein (PCV) were measured using Fiji image analysis software (Schindelin, Arganda-Carreras et al. 2012) at the midway point between 2 intersegmental blood vessels (ISVs) along the yolk extension, five points in total, to generate mean diameter per embryo as previously described (Sugden, Meissner et al. 2017). For ISV diameter, three measurements were made along three ISVs between the DA and dorsal longitudinal anastomotic vessel (DLAV) to calculate average ISV diameter for both arterial and venous ISVs. Diameter of the basilar artery (BA) was measured at three points

along the vessel, and mean diameter calculated for each embryo. *Kugeln* were identified and counted as previously described (Kugler, van Lessen et al. 2019).

2.4.3 Heart rate measurements

Individual embryos were observed under a brightfield stereomicroscope (Olympus IX81) before light-sheet imaging. The number of heartbeats were counted for 15 seconds, three times per embryo. The average value of these repeats was multiplied by four to give an estimate of heartbeat per minute (bpm). All heart rate experiments were done without the addition of tricaine anaesthetic.

2.4.4 Serial block face scanning electron microscopy (SBF-SEM)

5dpf zebrafish embryos were imaged using light-sheet microscopy (see 2.4.1), and subsequently fixed with glutaraldehyde (2% EM grade glutaraldehyde (Agar Scientific), 2% paraformaldehyde (VWR) and 0.1M sodium cacodylate buffer (Agar Scientific)) for 48 hours at room temperature (RT). Embryos were washed with 0.1M sodium cacodylate buffer 3 times for 5 minutes, and stored for transportation to EM Research Services at Newcastle University. All embryos were processed and imaged by Tracey Davey at Newcastle University in accordance with the previously described protocol (Cocks, Taggart, Rind and White 2018). Embryos were imaged using a Zeiss Sigma SEM (Zeiss), at a resolution of 12 nm. Data analysis was conducted using Microscopy Image Browser (MIB) (Belevich, Joensuu et al. 2016).

2.5 Morpholino injection

Heart contraction was inhibited by injection of *tnnt2a* morpholino (1.56 ng final concentration) (sequence 5'-CATGTTTGCTCT GATCTGACACGCA-3') (Sehnert, Huq et al. 2002, Sehnert and Stainier 2002). Control morpholino injections (5'-CCTCTTACCTCAGTTATTTATA-3') was performed at the same concentration as above. Embryos were injected at the one-cell stage using phenol red as an injection control.

2.6 Drug treatments

2.6.1 Drug treatments

All chemicals were dissolved in E3 medium and administered by immersion from 24 hours post fertilisation (hpf) to 48hpf. VEGF signalling was inhibited using 25nM Tivozanib (AV-951, AVEO pharmaceuticals), vehicle control groups were exposed to 0.0025% DMSO. TOR

signalling was inhibited using 2-2.5µM Rapamycin (Sigma-Aldrich), vehicle control groups were exposed to 0.2-1% DMSO. MEK signalling was inhibited using 7.5-10µM PD0325901 (Sigma-Aldrich), vehicle control groups were exposed to 0.75-1% DMSO. p38 MAPK signalling was inhibited by 25µM SB 203580 (Sigma-Aldrich), vehicle control groups were exposed to 1% DMSO. VEGF signalling was induced using 2.5µM GS4012 (Sigma-Aldrich), vehicle control groups were exposed to 1% DMSO. Notch signalling was inhibited using 50µM DAPT (Sigma-Aldrich), vehicle control groups were exposed to 1% DMSO. Nitric oxide synthase (NOS) inhibition was achieved by incubation with 1µM L-NAME (Sigma-Aldrich) diluted in E3 medium (table 2.5). For all drug treatment experiments, preliminary data was generated using doses ranging from undetectable concentrations to toxic concentrations to find potential doses that can rescue the endoglin phenotype (data not included).

Table 2.5 List of drug treatment used and their respective IC^{50} values

Inhibitor	Target	Doses	IC_{50}
AV951	VEGFR1/2/3	25nM, 50nM	0.21/0.16/0.24 nM
Rapamycin	mTOR	2µM, 2.5µM	0.1nM
PD0325901	MEK1/2	7.5µM, 10µM	0.33nM
L-NAME	NOS	1µM	70uM
SB203508	P38 MAPK	25µM	50nM

2.6.2 Zebrafish model for doxorubicin-induced heart failure

Doxorubicin hydrochloride (DOX) (Sigma-Aldrich) was dissolved in E3 in a stock solution (1mM), and stored at -20 in 400µl aliquots. Zebrafish embryos (1dpf) were placed into 48-well plates, each well containing two embryos in 200µl E3 containing 50-150µM DOX and 0.5% DMSO (Sigma-Aldrich) (Liu, Asnani et al. 2014). Zebrafish were examined every 24 hours, and dead embryos removed from the population. Zebrafish embryos were exposed to DOX for 48 hours and subsequently examined for signs of chemotherapy-induced heart failure.

2.6.3 Zebrafish model for glucose induced hyper proliferation

Zebrafish embryos (1hpf) were placed into 48-well plates, each well containing two embryos in 200µl E3 containing 55mM D-(+)-glucose (Sigma-Aldrich). Zebrafish were examined every 24 hours, and dead embryos removed from the population. Zebrafish embryos were exposed to glucose for 72 hours and subsequently examined for signs of glucose induced hyper proliferation as reported by (Jörgens, Stoll et al. 2015).

2.7 pERK immunostaining

Embryos were immunostained in accordance with the previosuly described protocol (Shin, Beane et al. 2016). 3dpf embryos were fixed with 4% PFA/PBS overnight at 4°C, and subsequently washed with 3% H_2O_2. Fixed embryos were washed with TBS/0.1% Tween20/0.1% Triton X-100 (TBSTwT) for 5 minutes and permeabilised with TBS/0.1% Tween20/1% Triton X-100 for 30 minutes on ice. Embryos were placed in 1% bovine serum albumin/10% goat serum blocking solution for 2 hours on ice. Embryos were incubated with 1:250 phospho-p44/42 MAPK (Thr202/Tyr204) XP rabbit monoclonal antibody overnight at 4°C. embryos were rinsed with maleic buffer (150 mM maleic acid/100 mM NaCl/0.05% Tween20, pH7.4), and blocked with blocking buffer for 2 hours. Embryos were incubated with 1:1000 goat anti-rabbit IgG-HRP overnight 4°C. Embryos were washed five times with maleic buffer for 30 minutes and incubated with 1:50 TSA Plus tyramide-Cy3 in 1× amplification diluent (Perkin Elmer). Finally, embryos were washed with TBSTwT, and imaged using light-sheet fluorescence microscopy.

2.8 Zebrafish cryoinjury

Zebrafish cardiac cryoinjury was performed in accordance with the previously described protocol (González-Rosa and Mercader 2012). Adult zebrafish (5-6 months old) were anaesthetised, and an incision was made to expose the heart. A copper probe (0.75 mm diameter), cooled in liquid nitrogen for 20 seconds, was pressed onto the ventricle for 5 seconds. Zebrafish were culled, and the heart dissected and placed in 0.1 M KCL to arrest heart in diastole. Hearts were subsequently fixed overnight in 4% PFA. After fixation, hearts were rinsed in PBS, dehydrated with ethanol, embedded and sectioned into 10 µm slices. Sections were stained with Acid Fuchsin Orange G (AFOG) staining.

2.9 Statistical analysis

2.9.1 Group size calculations

Power analysis was performed using *priori* to calculate group sizes for all adult zebrafish experiments based on an estimated effect size of 33% difference between group means, using an alpha of 0.05 and β value of 0.2.

2.9.2 Statistical analysis of normality and significance

All Statistical analysis was performed using GraphPad Prism 7, and statistical tests used to determine p-values between groups are indicated. All data were subjected to the D'Agustino and Pearson normality test before performing statistical analysis. All error bars display standard deviation (S.D). Each experiment was repeated three times, unless otherwise stated. P values are indicated as follows: *=<0.05, **=<0.01, ***=<0.001, ****=<0.0001.

3. The role of *endoglin* in zebrafish cardiovascular development

3.1 Introduction

The aim of this chapter is to characterise the role of *eng* in embryonic and adult cardiovascular development. Using an *eng*^{mu130} mutant zebrafish line in a *kdrl* fluorescence-tagged transgenic background to visualise endothelial cells with light sheet fluorescence microscopy, I establish the cardiovascular phenotype of *eng*^{mu130} embryonic and adult fish at developmental stages and in vascular territories not previously described.

Data from Sugden and colleagues showed that increases in blood flow during zebrafish embryonic development results in eventual vessel contraction. This is driven by endothelial shape changes, and *eng* is a key receptor that regulates this process. At 3dpf, the DA and PCV are approximately 30% larger in the homozygous mutants compared to wild types (Sugden, Meissner et al. 2017). The role of *eng* throughout further development, and during blood vessel formation in other vascular beds such as the zebrafish cranial vasculature, has not been described. Here I assess the role of *eng* in the development of the zebrafish trunk vasculature from 3dpf, as well as cranial vasculature and the heart throughout development. Furthermore, I characterise the adult *eng*^{mu130} mutant phenotype.

3.2 Characterisation of the adult cardiovasculature phenotype in *eng*^{mu130} mutants

Heterozygous adult *eng*^{mu130} mutants in a *Tg(Kdrl:eGFP)*^{s438} or T*g(kdrl:Hsa.HRAS-mCherry)*^{s916} background were in-crossed to generate clutches of embryos. Adults were fin clipped and genotyped at approximately 3 months, and subsequently separated into equal groups of wild-type and *eng*^{mu130} homozygous zebrafish.

Adult *eng*^{mu130} mutant zebrafish adults were smaller and weighed less than WT siblings [**Figure 3.1 A,C**]. However, hearts were significantly larger in *eng*^{mu130} mutants [**Figure 3.1 B,D**], similar to the phenotype observed in endothelial-specific *Eng* knockout adult mice (Tual-Chalot, Garcia-Collado et al. 2020). Given that skin vascular abnormalities are highly characteristic of human HHT patients, I examined *eng*^{mu130} mutants for similar cutaneous phenotypes. 71% (5/7) of adult *eng*^{mu130} zebrafish displayed cutaneous blood vessel abnormalities, which never occurred in WT (0/5) [**Figure 3.1 A**]. Extensive retinal vessel malformations in adult *eng*^{mu130} mutant zebrafish were observed [**Figure 3.1 E,G,H,I**], including increased capillary

interconnections, increased optic artery diameter, and increased vessel branching compared with WT.

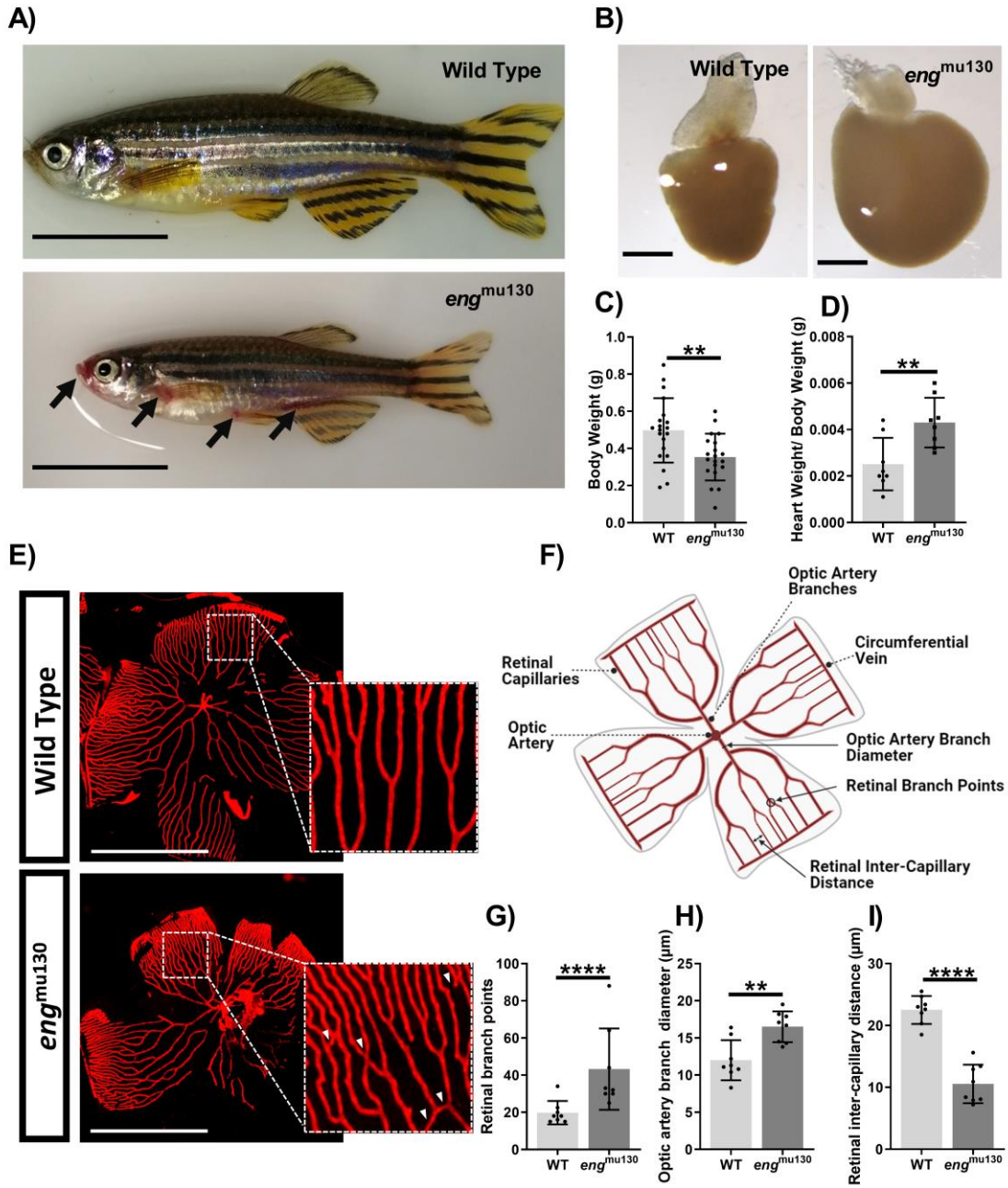

Figure 3.1 Adult *eng*^{mu130} fish display cutaneous and retinal vascular malformations similar to HHT and an enlarged heart at 5-6 months.

A) Adult 5-6 month old *eng*^{mu130} zebrafish display cutaneous vascular malformations (black arrows). Scale bar = 1cm. B) Representative *eng*^{mu130} and wild type (WT) sibling hearts (n=8/group). Scale bar = 500µm. C) Body weight of adult WT and *eng*^{mu130} zebrafish D) Heart weight/body weight of WT and *eng*^{mu130} zebrafish. E) Fluorescent micrographs of whole mount retinae from *Tg*(*kdrl:Hsa.HRAS-mCherry*)^{s916} zebrafish showing abnormal vessel communications in *eng*^{mu130} (white arrowheads). F) Schematic diagram of a 5-6 month old zebrafish retinal vasculature. Figure created with BioRender (https://biorender.com/). G) Number of retinal vascular branches in WT and *eng*^{mu130} homozygous siblings. H) Optic artery diameter in WT and *eng*^{mu130} homozygous siblings. I) Inter-capillary distance in WT and *eng*^{mu130} homozygous siblings. (Unpaired Student's t-test, 8-10 animals/group.) Figure from Snodgrass *et al.*, 2021 (Snodgrass, Arthur and Chico 2021).

3.3 Characterisation of embryonic trunk vasculature in *eng*^{mu130} mutants

Heterozygous adult *eng*^{mu130} mutants in a *Tg(Kdrl:eGFP)*^{s438} or T*g(kdrl:Hsa.HRAS-mCherry)*^{s916} background were in-crossed to generate clutches of WT, heterozygous and homozygous embryos. Light sheet microscopy (LSFM) was used to visualise trunk vasculature at 52, 76, and 100 hours post fertilisation (hpf). Image acquisition and subsequent analysis was performed blinded to genotype. Homozygous mutants displayed no obvious morphological differences during vascular development [**Figure 3.2**]. However, an increase in the diameter of the DA and PCV in the *eng*^{mu130} mutants was observed at all three time points [**Figure 3.3**].

At 3dpf, the DA and PCV were dilated by approximately 15% in homozygous mutants compared with wild type siblings. This is consistent with previously data **[Figure 3.3 C,D]** (Sugden, Meissner et al. 2017). Subsequent analysis of older embryos was performed to investigate if this change in vessel diameter is restored as the embryo develops. At 4dpf the DA and PCV are dilated by approximately 25%, suggesting the difference in vessel size is more substantial in older embryos **[Figure 3.2 C,D]**. Furthermore, these results show that the DA and PCV reduces in size during wild type embryo development, but this reduction in vessel size is absent in the *eng* mutants. This data confirms that *eng* plays an important role in maintaining vessel calibre in zebrafish embryos.

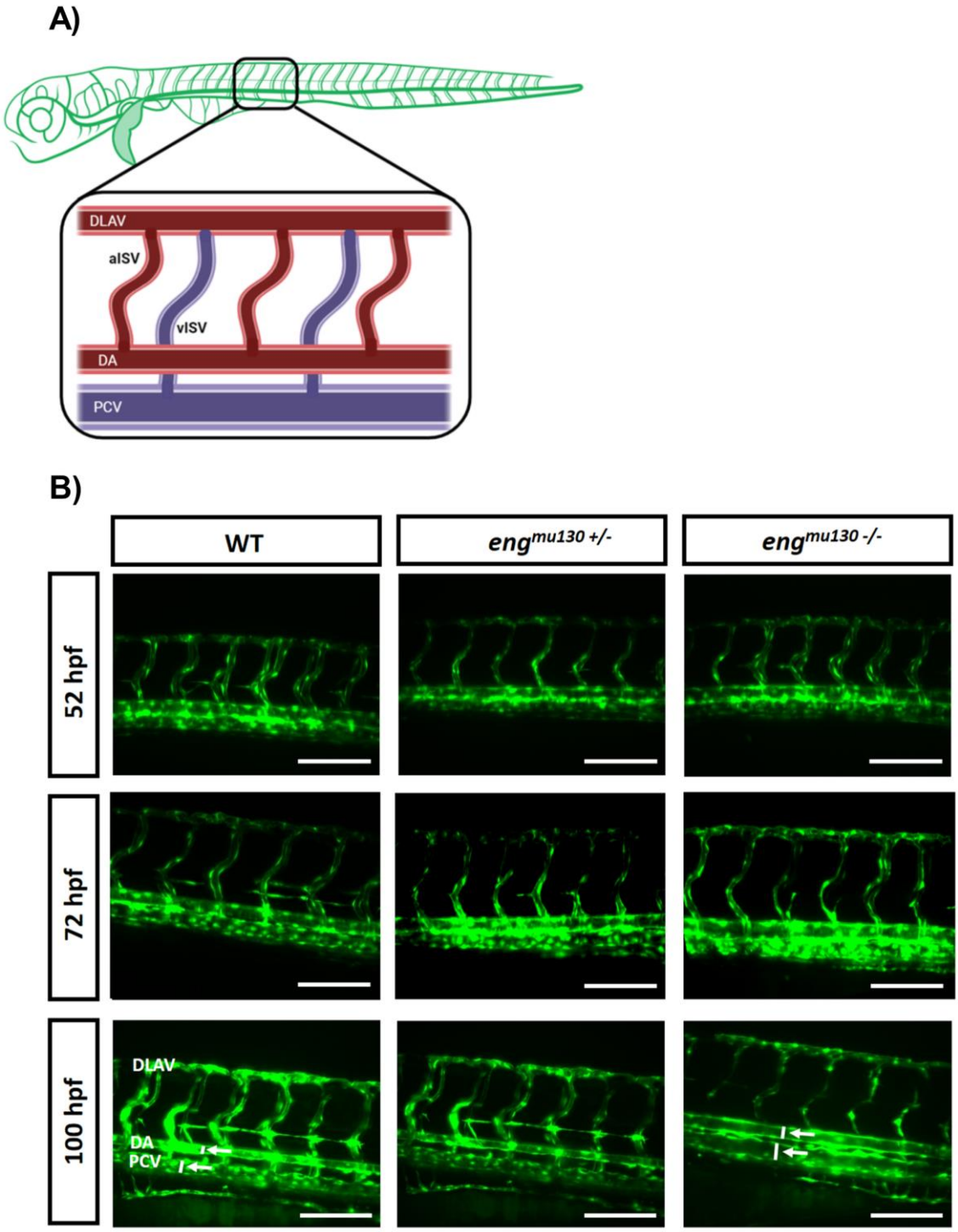

Figure 3.2 *eng*^{mu130} mutant embryos display increased aortic and cardinal vein diameters compared with wild type siblings at 2-4 dpf.

A) Schematic diagram of 3dpf zebrafish vasculature and the region of interest. Figure created with BioRender (https://biorender.com/). B) Representative images of trunk vasculature in *eng*mu130 wild type (WT), heterozygous (+/-) and homozygous (-/-) mutant siblings, 52-100hpf. An increase in Dorsal aorta (DA) and Posterior cardinal vein (PCV) dimeter is visible in the homozygous mutants compared to WT siblings at all-time points. Images displayed as maximum intensity projections (MIPs) of z-stacks acquired using LSFM. Scale bars = 100µm.

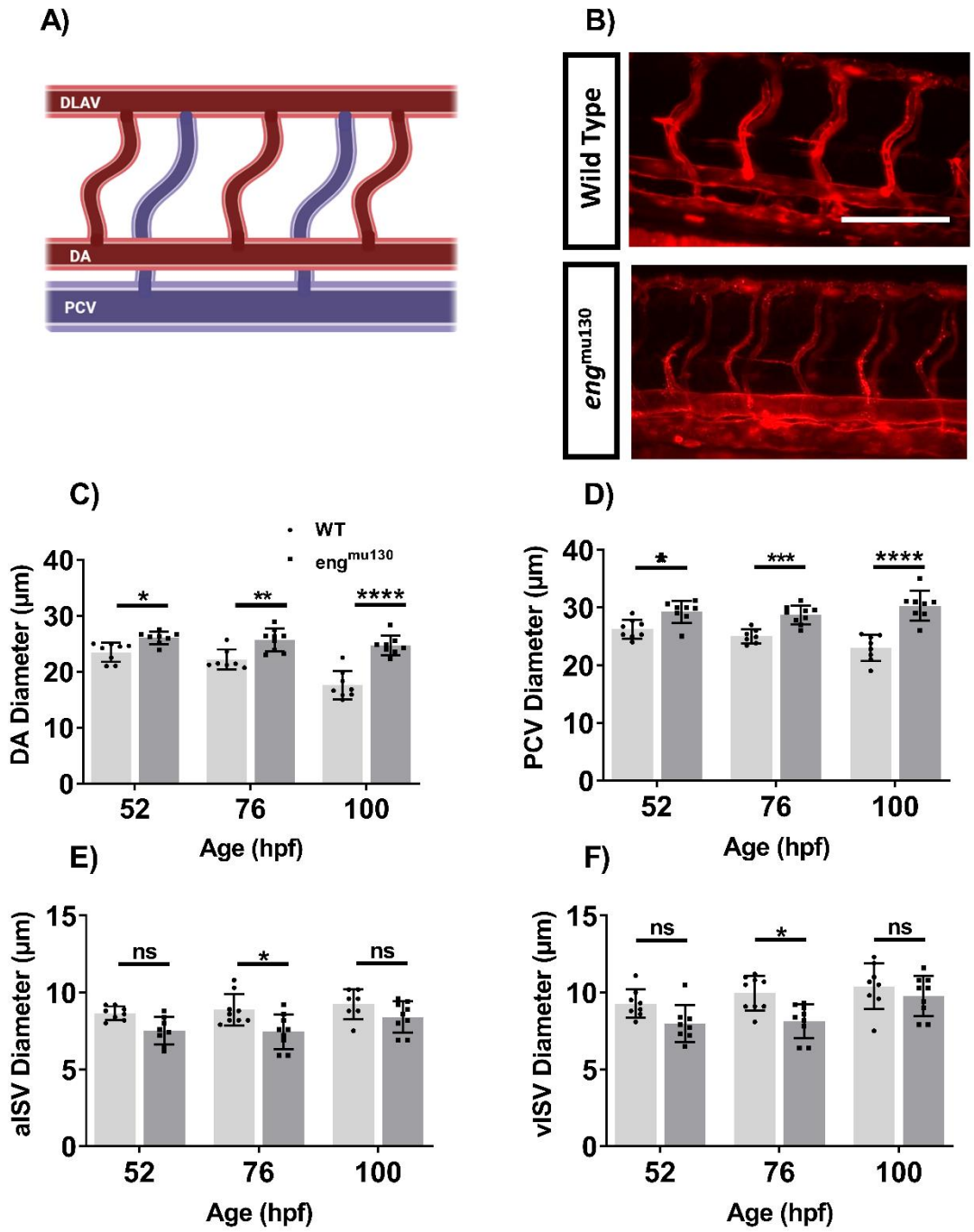

Figure 3.3 *eng*^{mu130} mutant embryos display increased diameters in the dorsal aorta and cardinal vein compared with control siblings at 2-4 dpf.

Schematic diagram of the region of interest. Figure created with BioRender (https://biorender.com/). B) Representative maximum intensity projection of *Tg(kdrl:Hsa.HRAS-mCherry)*^{s916} WT and *eng*^{mu130} trunk vasculature at 76hpf. Abbreviations: DA, dorsal aorta; PCV, posterior cardinal vein; aISV, arterial intersegmental vessel; vISV, venous intersegmental vessel. Scale bar = 100µm. C,D,E and F) Significantly enlarged diameters of DA and PCV in *eng*^{mu130} fish compared with WT siblings. aISV, and vISV are thinner in *eng*^{mu130} mutants at 76h, and partially normalise by 100h. (one-way ANOVA with Tukey post-hoc test. n = 8-10/group.) Figure taken from Snodgrass *et al*., 2021 (Snodgrass, Arthur and Chico 2021).

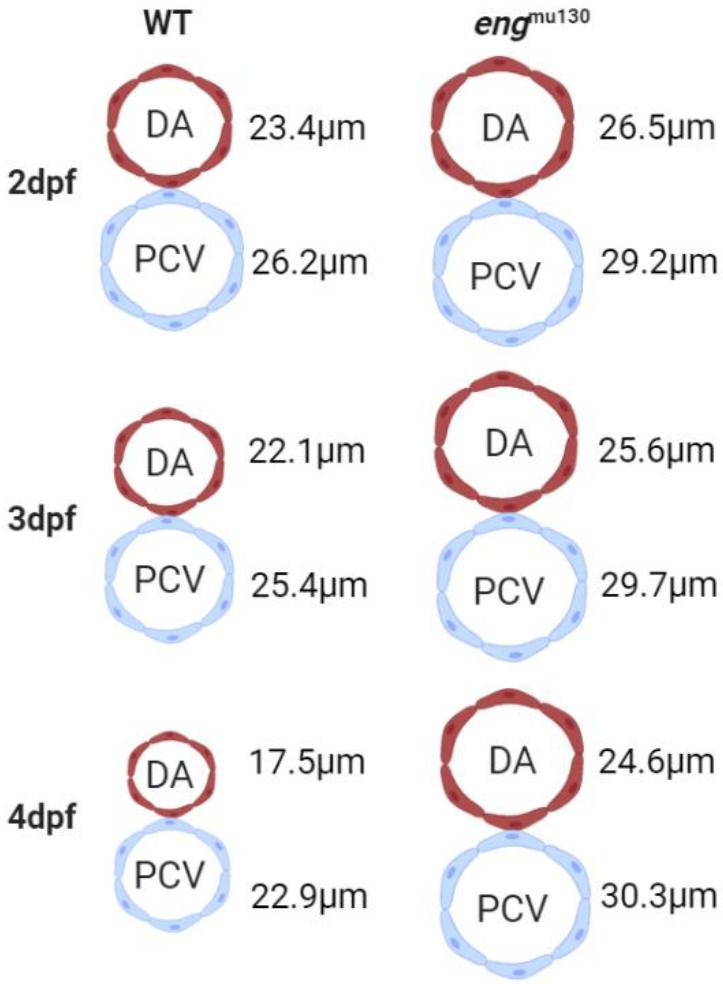

Figure 3.4 Schematic diagram summarising the vessel calibre changes observed in *eng*^{mu130} mutant embryos compared to WT siblings.

Abbreviations: DA, dorsal aorta; PCV, posterior cardinal vein; dpf, days post fertilisation. Note that in the WT the diameter of the DA and PCV reduces after 2dpf during maturation, but this fails to happen in the WT leading to significantly enlarged diameters of DA and PCV in *eng*^{mu130} fish compared with WT siblings. Note also that endothelial number is unchanged in Eng compared with WT, and diameter changes therefore involve a change in the endothelial cell footprint. Mean vessel diameters are shown for each group. Figure created with BioRender (**https://biorender.com/**).

I then set out to investigate if these diameter changes are a result of increased endothelial cell number. Previously it was reported that increased DA diameter is due to an increase in EC size and not increased EC number (Sugden, Meissner et al. 2017). I utilised the Tg(fli1a:nEGFP)y7 transgenic background to observe endothelial nuclei in the developing vasculature. EC number was quantified in the whole region of interest **[Figure 3.5 A],** and subsequently in the DA and PCV specifically. In all cases there was no observable evidence that EC number is impacted by *eng* loss of function **[Figure 3.5 B, C, and D].** This is consistent with the data previously reported (Sugden, Meissner et al. 2017).

In addition to looking at the DA and PCV in older embryos, the development of the intersegmental vessels was observed over time **[Figure 3.3E, 3.3F]**. In wild type embryos, arterial intersegmental vessels (aISVs) and venous intersegmental vessels (vISVs) stay approximately the same size from 52 to 100hpf, although aISVs are slightly smaller than vISVs. Furthermore, at 76hpf there was a significant reduction in vessel size in both aISVs and vISVs in *eng*^{mu130} mutants compared with WT siblings. This change in vessel diameter may be a result of improper development in the ISVs. It was previously reported that ISVs collapse to cessation of blood flow through the ISVs, resulting from increased blood flow through a DA/PCV shunt resembling AVM formation (Sugden, Meissner et al. 2017). To quantify this, I used Fiji image analysis software to plot histograms of the fluorescent data in the ISVs **[Figure 3.6]**. Two peaks indicate that the vessel has a lumen and is therefore "open" **[Figure 3.6 A].** One peak indicated ISVs are "closed" resulting in no blood flow through the ISVs **[Figure 3.6 B].** Percentage of open ISVs in WT *eng*^{mu130} mutants were compared in 3dpf zebrafish embryos. As expected, eng mutants showed a significant decrease in open ISVs. Approximately 50% of *eng*^{mu130} mutant ISVs are developed/open compared approximately 97% in WT siblings **[Figure 3.6 C]**.

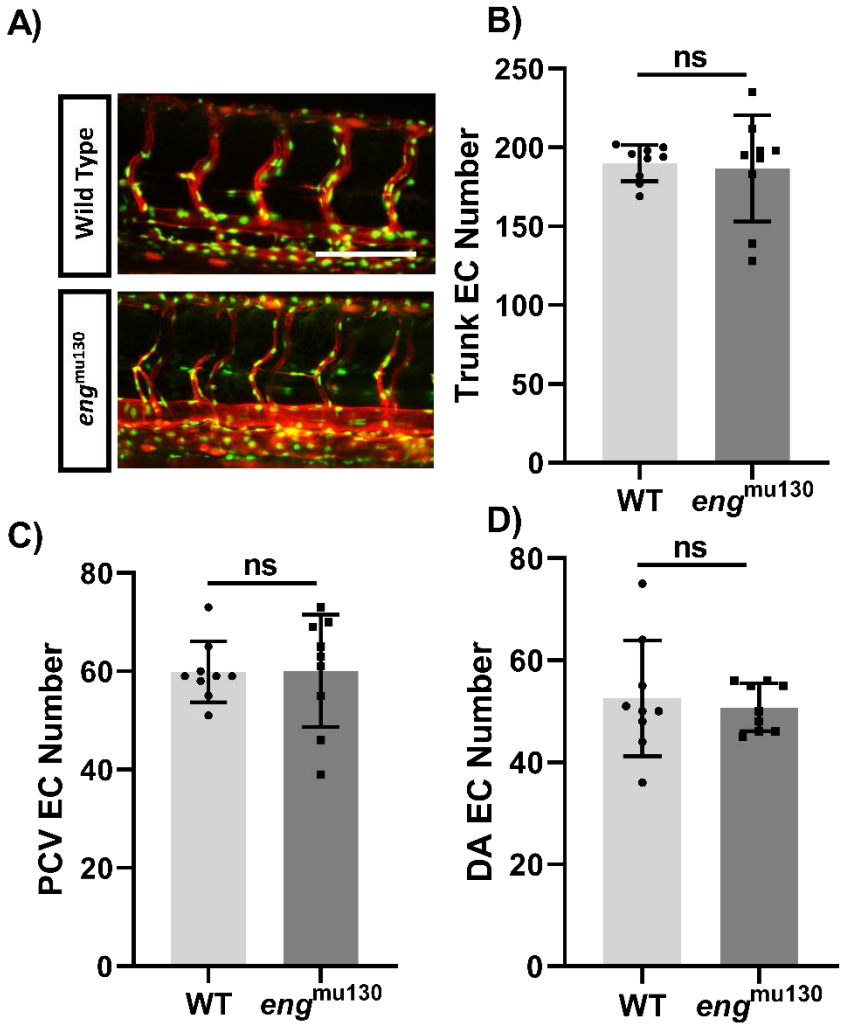

Figure 3.5 *endoglin* loss of function does not affect endothelial cell numbers at 3dpf.

A) Representative maximum intensity projection of the region of interest. *Tg(kdrl:Hsa.HRAS-mCherry)s916* labels endothelial cell membrane and *Tg(fli1a:nEGFP)*^{y7} labels endothelial cell nuclei. B) Quantification of endothelial cell nuclei in all vessels in the region of interest. C) Quantification of endothelial cell nuclei in the dorsal aorta (PCV). D) Quantification of endothelial cell nuclei in the posterior cardinal vein (DA). Data analysed by unpaired student's t-test. n = 8-10/group. Figure taken from Snodgrass *et al*., 2021 (Snodgrass, Arthur and Chico 2021).

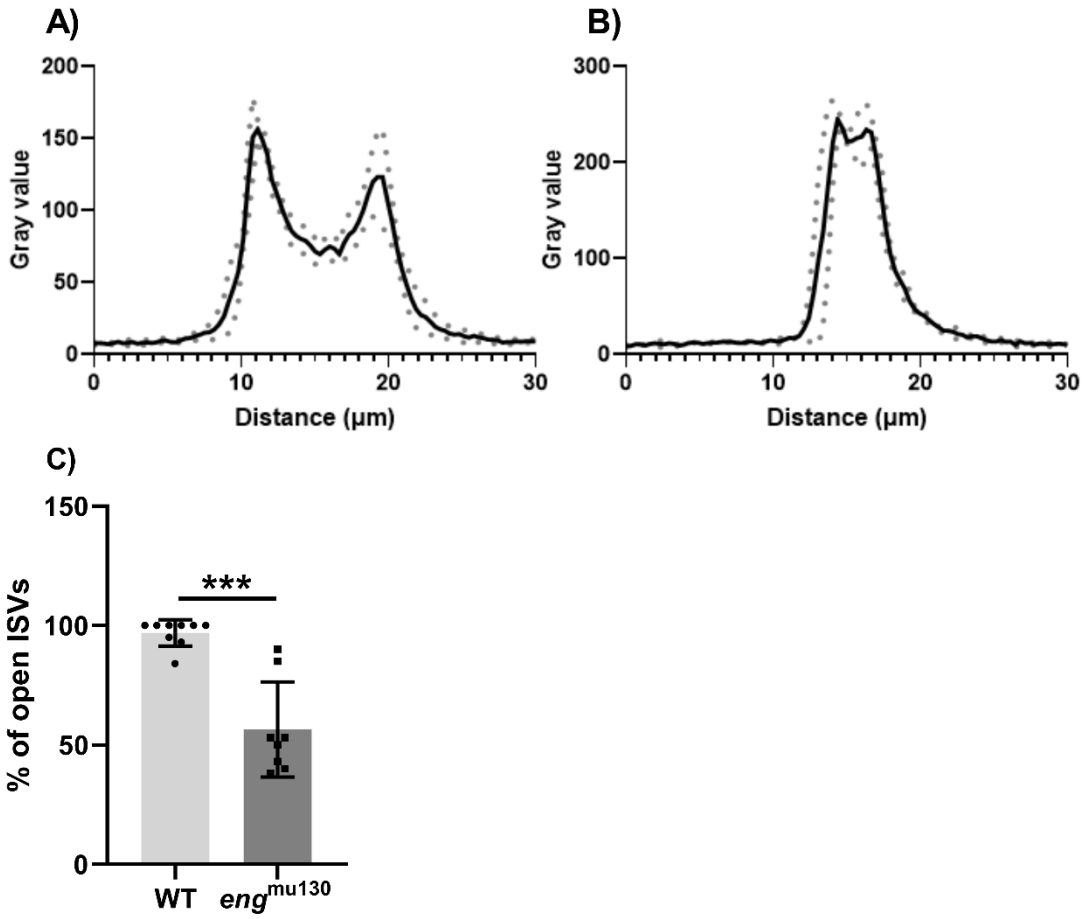

Figure 3.6 *eng*^{mu130} mutant embryos display improper ISV development at 3dpf.

A) An example of a basic intensity profile of an "open" ISV in *Tg(kdrl:Hsa.HRAS-mCherry)s916* zebrafish embryos. Two peaks suggests the existence of a vessel lumen. B) Example of a basic intensity profile of a "closed" ISV in *Tg(kdrl:Hsa.HRAS-mCherry)s916* zebrafish embryos. One peak suggests the absence of a vessel lumen. C) Percentage of open ISVs in WT and *eng*^{mu130} siblings at 72hpf. Data analysed by unpaired student's t-test. n = 10/group.

3.4 Quantification of heart function in *eng*^{mu130} mutant embryos

There are a range of well characterised cell-specific zebrafish transgenic lines available to image the developing heart *in vivo*, for example the *Tg(Kdrl:eGFP)*^{s43} line allows visualisation of the endocardium of the zebrafish. Imaging of fluorescent hearts can be used to assess cardiac functions, such as fractional shortening, chamber size, and heart rate (HR). Therefore, after examining the trunk vasculature of *eng*^{mu130} mutants, short time lapse videos of the hearts were recorded in these same embryos. Fiji image analysis software was subsequently used to quantify chamber size (μm^2) in WT and *eng* mutants. Due to the anatomy of the zebrafish at the time points examined, the heart sits too deeply in the tissue to fully image the ventricle, and therefore only atrial area was measured in this section.

Atrial area was calculated in *eng* mutants and wild type siblings. An example of images used to calculate atrium area in systolic and diastolic phases are shown in **[Figure 3.7 A]**. At 52hpf there was no significant difference in atrium size in the *eng* mutants compared to wild type siblings **[Figure 3.7 B]**. In addition to measuring atrium size, the heart rate of the same embryos was obtained at 52 and 76hpf **[Figure 3.7 C]**. There was no significant difference in heart rate in the *eng* mutants compared to wild type siblings at either time point. This data suggests that embryonic heart rate and atrial chamber size is unaffected by *eng* loss of function at these time points.

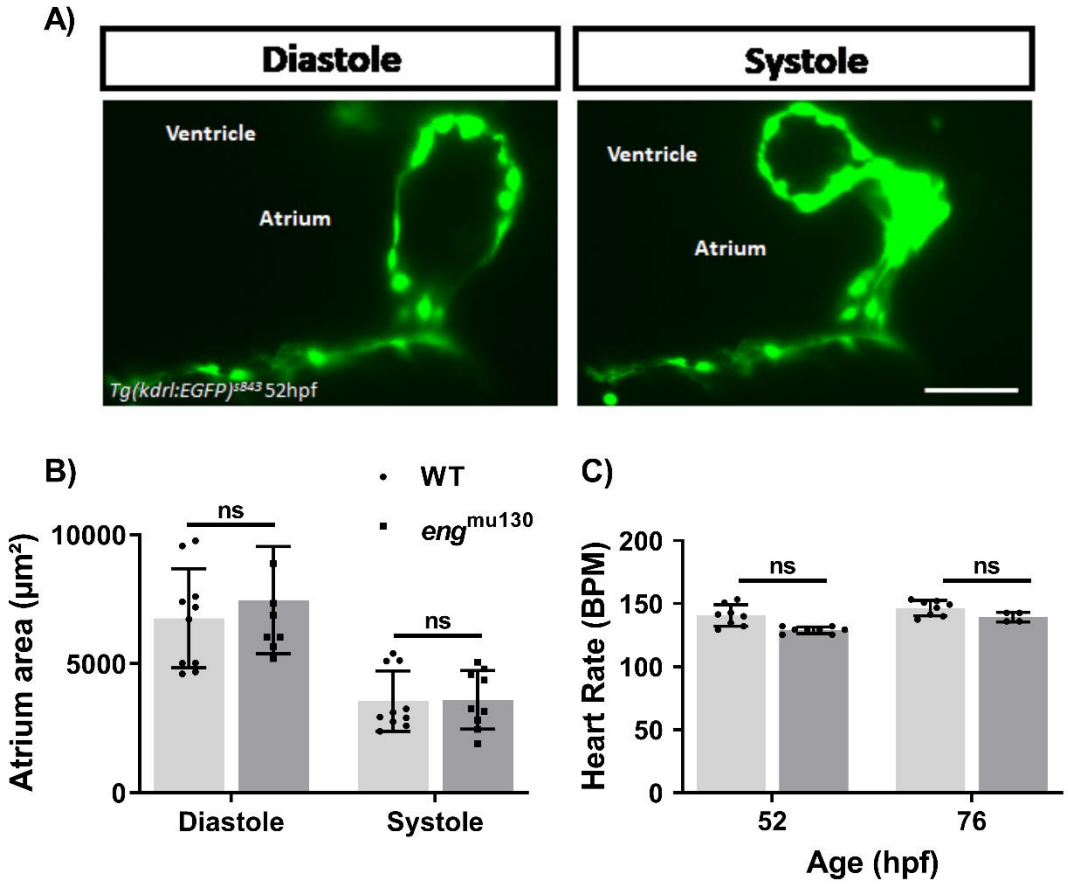

Figure 3.7 Quantification of atrium size and heart rate in WT and e*ng*^{mu130} mutant embryos (52hpf).

Representative images of the zebrafish heart at 52hpf, shown in diastole and systole phases. Scale bar = 100µm B) Quantification of atrium size in *eng*^{mu130} WT and e*ng*^{mu130} mutant siblings at 52hpf. There is no significant difference in atrium size in the compared to WT siblings. C) Quantification of heart rate in WT and e*ng*^{mu130} mutant siblings. There is no significant difference in heart rate in the *eng*^{mu130} compared to WT siblings. Analysed by one-way ANOVA with Tukey post-hoc test. n = 8-10/group.

3.5 Characterisation of embryonic cranial vasculature in *eng*^{mu130} mutants

It was previously reported that *eng* loss of function results in the formation of arteriovenous malformation (AVMs) in the adult brain of zebrafish (Sugden, Meissner et al. 2017). However, the brain vasculature in *eng* mutant embryos has not been characterised. I examined the cranial vasculature of 52, 76, and 100hpf embryos using LSFM. Representative images of the cranial vasculature in wild type, heterozygous and homozygous mutants are shown in **[Figure 3.8]**. Homozygous mutants display no obvious morphological differences during vascular development. However, subtle differences are difficult to identify due to the complicated nature of the cranial vasculature compared to the trunk. Fiji image analysis software was used to quantify the following parameters: basilar artery (BA) diameter, BA cell number, the number of central arteries (CTAs) in the midbrain, and the width of the primordial mid-brain channel (PMBC) **[Figure 3.9]**. An automated image analysis pipeline developed in the group was utilised to asses any gross morphological differences in cerebrovascular development at 3dpf (Kugler, Plant, Chico and Armitage 2019, Kugler, Frost et al. 2020).

PBMC width gives an estimation of the size of the midbrain vasculature. This was measured to investigate if *eng* loss of function results in a change in vascular bed size. The PBMC increases as the embryo develops, however, there was no significant difference in PBMC width between *eng* mutants and WT siblings at any of the time points measured **[Figure 3.9 C].** This data suggests that *eng* loss of function does not affect the overall size of the cranial vasculature.

As *eng* plays a key role in angiogenesis, I therefore observed the number of central arteries in the midbrain over time. This was to investigate if *eng* affects the number of blood vessels rather than just vessel calibre. In wild type embryos, the number of central arteries remains consistent from 52 to 100hpf. Furthermore, there was no significant difference in the number of central arteries between *eng* mutant and WT siblings at any time point measured **[Figure 3.9 B].** This data suggests that *eng* does not affect the number of vessels in the cranial vasculature of zebrafish embryos.

The automated image analysis pipeline was used to quantify total branching points, mean vessel radius (all cranial vessels), and total network length. No statistically significant

difference was observed when comparing *eng*^{mu130} mutant zebrafish cerebral vasculature to WT siblings **[Figure 3.9 D, E, F]**.

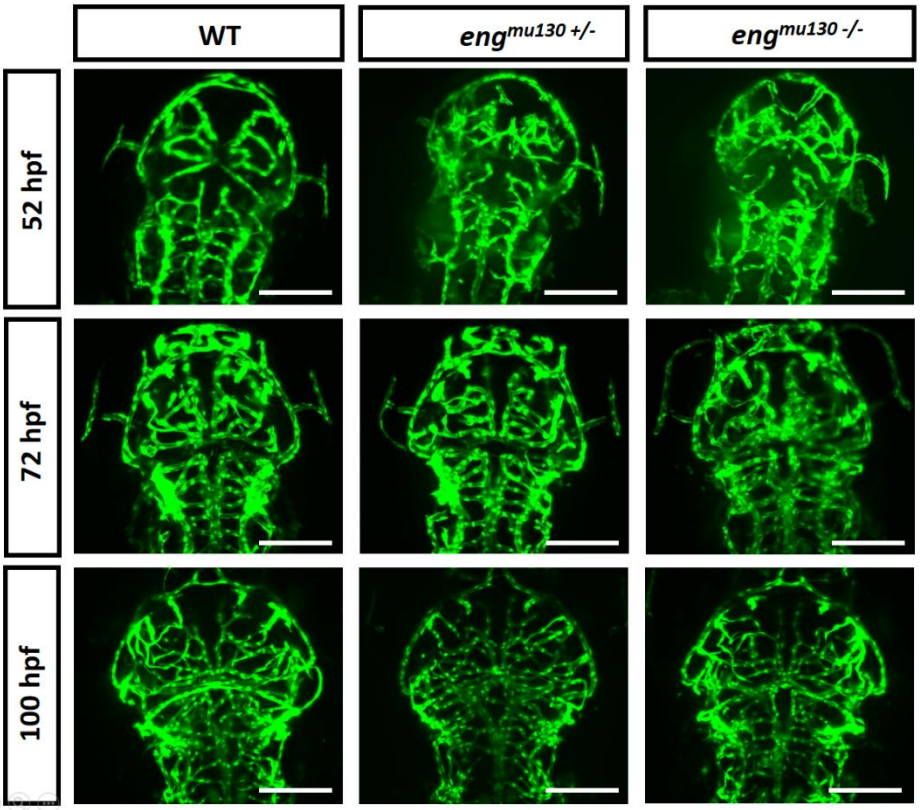

Figure 3.8 *eng*^{mu130} embryonic cranial vasculature compared with heterozygous mutants and wildtypes at 2-4 dpf.

Representative images of the head vasculature of the *eng*^{mu130} wild type (WT), heterozygous (+/-) and homozygous (-/-) mutant siblings from 52-100hpf. Images are maximum intensity projections (MIPs) of z-stacks acquired using LSFM. Scale bars = 100µm.

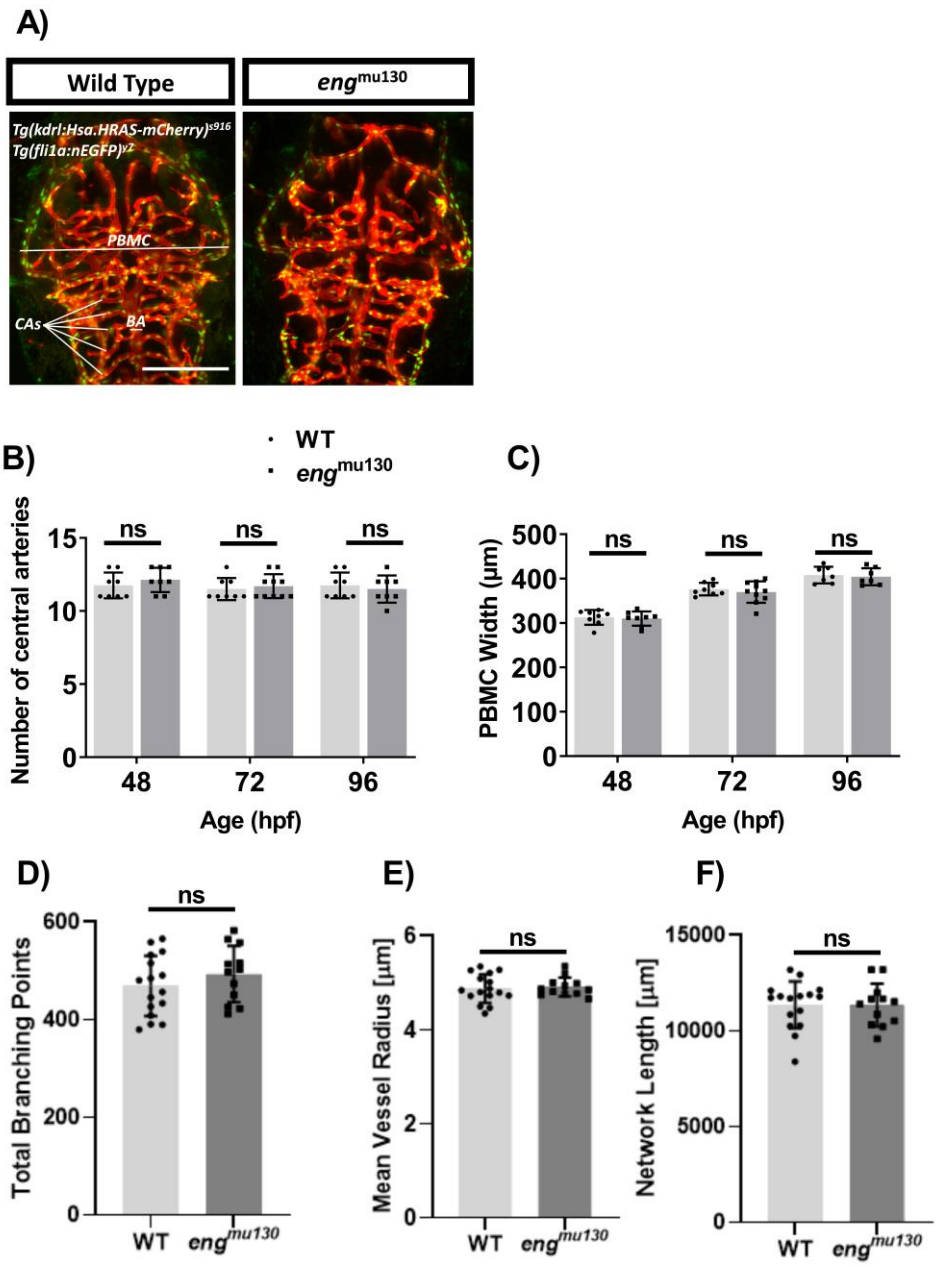

Figure 3.9 *eng*^{mu130} mutant cranial vasculature phenotypic analysis compared with wildtypes at 2-4 dpf.

A) Representative maximum intensity projection of the region of interest in 3dpf embryonic cranial vasculature. *Tg(kdrl:Hsa.HRAS-mCherry)s916* labels endothelial cell membrane and *Tg(fli1a:nEGFP)*^{y7} labels endothelial cell nuclei. Abbreviations: BA, basilar artery; PMBC, primordial midbrain channel; CA, central arteries. Scale bar = 150µm. B) The number of midbrain central arteries is similar in *eng*^{mu130} and wild-type siblings. Data analysed by one-way ANOVA with Tukey post-hoc test. n = 8-10/group. C) PMBC diameter is similar in *eng*^{mu130} and wild type siblings. Data analysed by one-way ANOVA with Tukey post-hoc test. n = 8-10/group. D, E, F) The automated image analysis pipeline was used to quantify total branching points, mean vessel radius, and total network length. Data analysed by unpaired student's t-test. n = 15/group. Figure taken from Snodgrass *et al*., 2021 (Snodgrass, Arthur and Chico 2021).

The zebrafish cranial vasculature is a separate vascular bed to the trunk, and forms independently during development. I therefore measured the vessel diameter of the BA in the brain to investigate if the vessel calibre changes seen in Figures 3.2 and 3.3 are specific to the trunk, or if they develop in other vascular beds. At 3dpf the BA diameter was significantly dilated in the mutant embryos when compared with wild type siblings **[Figure 3.10 B, C]**. Interestingly, at 3dpf the BA was dilated by approximately 10% - a similar increase to the vessel calibre change observed in the DA and PCV at the same age **[Figure 3.10 B, C]**. The basilar artery (BA) had an increased diameter, but no increase in EC number, in *eng*^{mu130} mutants compared with WT siblings **[Figure 3.10 D].** This is similar to the enlarged BA leading to AVM formation in *alk1* and *bmp10* mutant zebrafish (Corti, Young et al. 2011, Capasso, Li et al. 2020).

The *Tg(kdrl:Hsa.HRAS-mCherry)*^{s916} (Chi, Shaw et al. 2008) transgenic reporter line labels the EC membrane, facilitating live imaging of the embryonic trunk and cranial vasculature, and imaging of the adult retinal vasculature in explanted tissue. Recently, this line was used to describe a novel EC behaviour, in which the cerebral vessels form structures termed *kugeln*. *Kugeln* are transient spherical protrusions that extrude abluminally from cerebral blood vessels, and unlike previously described membrane protrusions, *kugeln* are neither driven by blood-flow or cytoplasm (Kugler, van Lessen et al. 2019). *Kugeln* only arise on cerebral vessels, and although their function is currently unclear, they may provide new insights into mechanisms of cerebrovascular development and function. *eng*^{mu130} mutants developed significantly more cerebral vessel *kugeln* compared to WT siblings at 72hpf **[Figure 3.10 E].** Currently, the physiological significance of *kugeln* is not clear, but this is the first work that implicates *kugel* formation in a model of human disease.

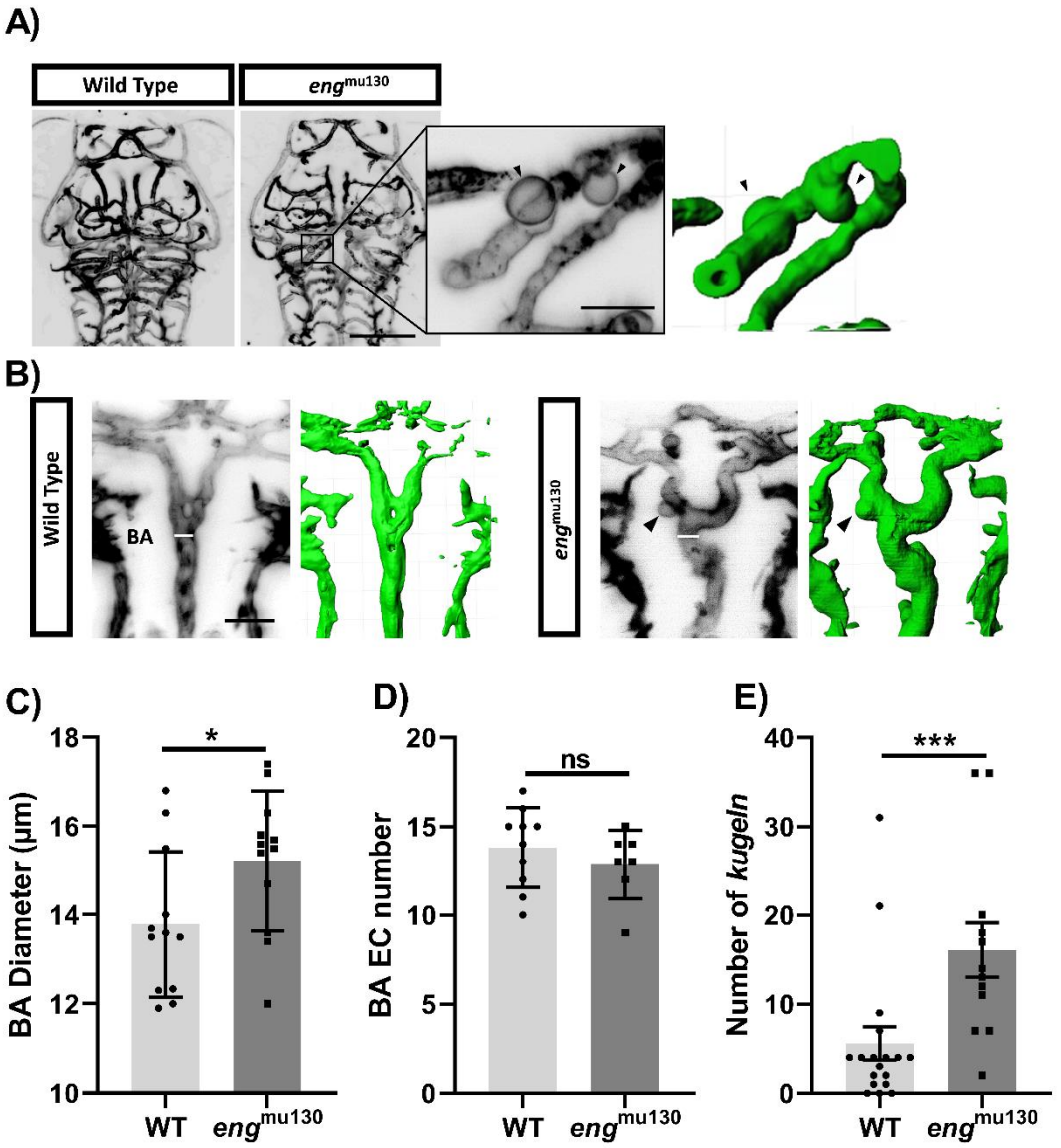

Figure 3.10 *eng*^{mu130} mutant embryos have increased basilar artery diameter and increased number of endothelial *kugeln* at 3dpf.

A) Representative maximum intensity projection of *Tg(kdrl:Hsa.HRAS-mCherry)*^{s916} zebrafish brain vasculature at 72hpf. Black arrowheads indicate individual *kugeln*. Scale bar = 150µm/50µm. Three-dimensional reconstruction of the same image shown in green. B) Representative maximum intensity projection of the basilar artery (BA) at 72hpf. Black arrowheads indicate individual *kugel*. Scale bar = 50µm. Three-dimensional reconstruction of the same images shown in green. C) BA diameter in *eng*^{mu130} mutants and WT siblings (unpaired Student's t-test, 10-12 animals/group). D) *Endoglin* mutation did not alter EC number in the BA (unpaired Student's t-test, 10-12 animals/group). E) *Kugel* number per animal at a single timepoint was increased in *eng*^{mu130} mutants (Mann–Whitney U-test, 12-18/group). Figure taken from Snodgrass *et al.*, 2021 (Snodgrass, Arthur and Chico 2021).

To confirm if this increased *kugel* phenotype is caused by BMP10 dysregulation, I next set out to investigate if this phenotype exists in *acvrl1* (*alk1*) mutants, first described by Capasso and colleagues (Capasso, Li et al. 2020). *acvrl1* mutants in a *Tg(fli1a.ep:mRFP-CAAX)pt50* background were live-imaged using confocal microscopy. All imaging and data processing of *acvrl1* mutants was completed by Erika Dreikorn, University of Pittsburgh, and all data analysis was completed by myself. In this case, *acvrl1* mutants did not display any *kugeln* at 3dpf **[Figure 3.11]**. This is most likely due to the severe presentation of the *acvrl1* mutant. Most kugeln develop in the midbrain on the central arteries (Kugler, van Lessen et al. 2019), which do not develop in the *acvrl1* mutants **[Figure 3.11]**.

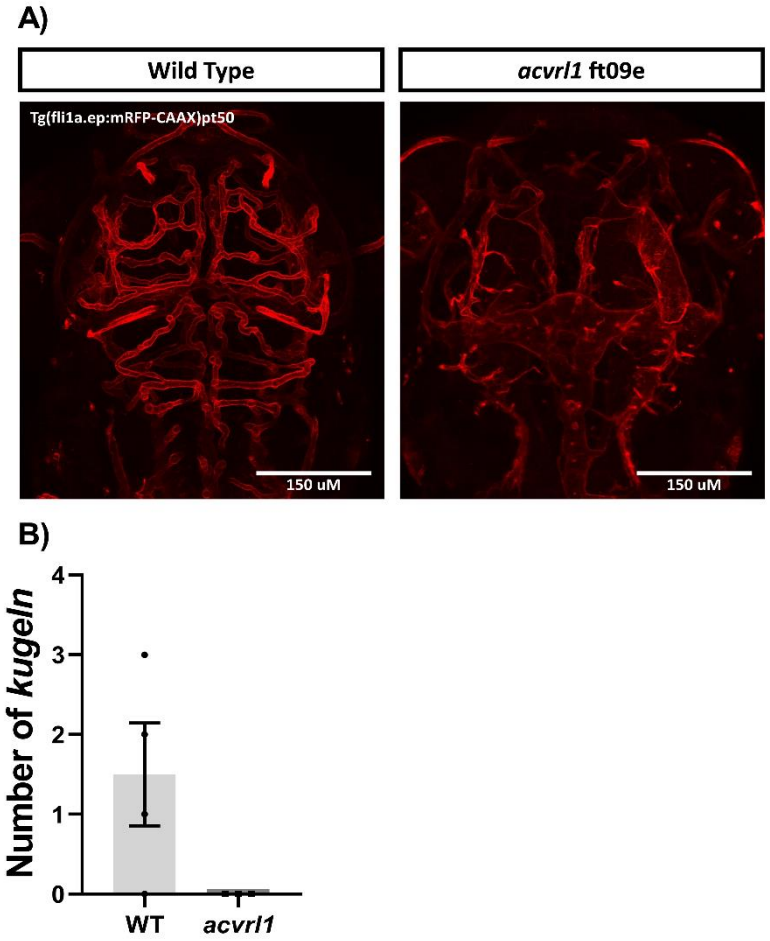

Figure 3.11 *acvrl1* mutant embryos display no endothelial *kugeln* at 3dpf.

A) Representative maximum intensity projection of *Tg(fli1a.ep:mRFP-CAAX)pt50* zebrafish brain vasculature at 72hpf. Scale bar = 150µm. B) E) *Kugel* are not present in *acvrl1* mutants (3/group). 1 experimental repeat.

The function and significance of *kugeln* is currently unclear. However, *eng* mutants have more *kugeln* present in the cerebral vessels, suggesting that *eng* functions to reduce *kugeln* number. I next set out to utilise 3-dimensional scanning electron microscopy to visualise the *kugeln* ultrastructure. For example, the presence of cytoplasm, organelles and cell interactions may give an indication of the role of *kugeln.* 5dpf *eng*^{mu130} or wild type sibling zebrafish embryos were fixed with 2% glutaraldehyde, and subsequently serial sectioned and imaged using electron microscopy. The electron microscopy images were reconstructed using Microscopy Image Browser (MIB) (Belevich, Joensuu et al. 2016). It is not known how fixation of zebrafish tissue affects the presence of *kugeln*, and therefore the harsh fixation and pre-processing techniques required for 3D-SEM may make it impossible visualise *kugeln*. I first set out to investigate this by imaging the same animal pre and post fixation with 4% paraformaldehyde for 2 hours. Although cerebral vessels do collapse during fixation, *kugeln* remain approximately the same size, location, and frequency **[Figure 3.12 A]**. This suggests that the fixation techniques used for SEM do not affect *kugeln* appearance. I next set out to image *kugeln* ultrastructure utilising Serial block face scanning electron microscopy (SBF-SEM). All SBF-SEM imaging and data processing was completed by Tracey Davey, University of Newcastle, and all data analysis was completed by myself. Cranial blood vessels were identified in the 3D-SEM data sets by the presence of red blood cells, which present as small circular dark structures **[Figure 3.12 C]**. Abnormal structures adjacent to cranial blood vessels were identified as possible *kugeln* **[Figure 3.12 D,E].** These structures are spherical protrusions that extrude abluminally from cerebral blood vessels, and do not appear anywhere else in the zebrafish brain. There is therefore evidence that these structures are potential *kugeln*, but further work is needed to validate these structures.

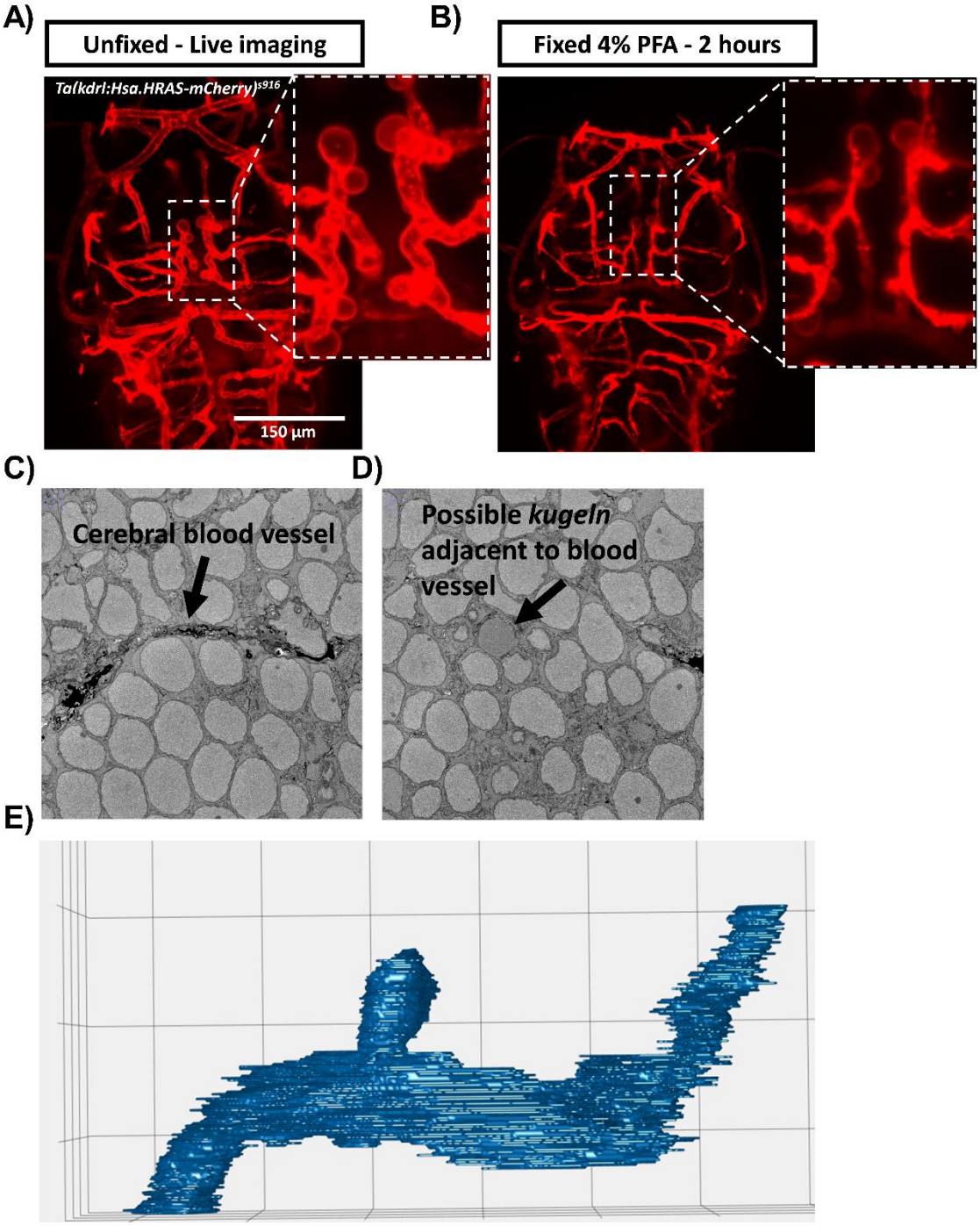

Figure 3.12 Whole-brain 3-dimensional scanning electron microscopy of 5dpf zebrafish embryos at 5dpf.

A) Representative maximum intensity projection of *Tg(kdrl:Hsa.HRAS-mCherry)*^{s916} zebrafish brain vasculature at 5dpf. B) Representative maximum intensity projection of *Tg(kdrl:Hsa.HRAS-mCherry)*^{s916} zebrafish brain vasculature at 3dpf post fixation with 4% paraformaldehyde. C, D) Representative ultrastructure achieved using 3-dimensional scanning electron microscopy**.** E) 3-dimensional reconstruction of cranial blood vessel and possible *kugeln* using Microscopy Image Browser (MIB) (Belevich, Joensuu, Kumar, Vihinen, & Jokitalo, 2016).

3.6 The role of *endoglin* in zebrafish vasculature development with and without cardiac output

It was previously reported that haemodynamic cues drive the development of HHT (Sugden, Meissner et al. 2017). I therefore inferred that preventing the initiation of blood flow would affect the development *of* the *eng* mutant phenotype. To address this, I injected *eng* mutants and WT siblings with *tnnt2a* morpholino to prevent cardiac output (Sehnert, Huq et al. 2002). Firstly, cranial vasculature was observed at 3dpf in *tnnt2a* injected embryos and uninjected controls. The *tnnt2a* morphants were smaller and had an overall reduction of cranial vasculature size **[Figure 3.13 A].** Furthermore, *tnnt2a* morphants showed no evidence of *kugel* formation at 3dpf in WT and eng^{mu130} mutant siblings **[Figure 3.13 E].**

I subsequently set out to investigate how *eng* affects the development of the trunk vasculature in *tnnt2a* morphants. *tnnt2a* knockdown caused a significant decrease in DA and PCV size in both WT and eng^{mu130} mutants, but with a greater effect in eng^{mu130} embryos **[Figure 3.13 B, C].** *tnnt2a* knockdown also reduced the differences ISV behaviour between WT and eng^{mu130} mutants as all aISVs and vISVs presented as collapsed vessels **[Figure 3.13 D]**.

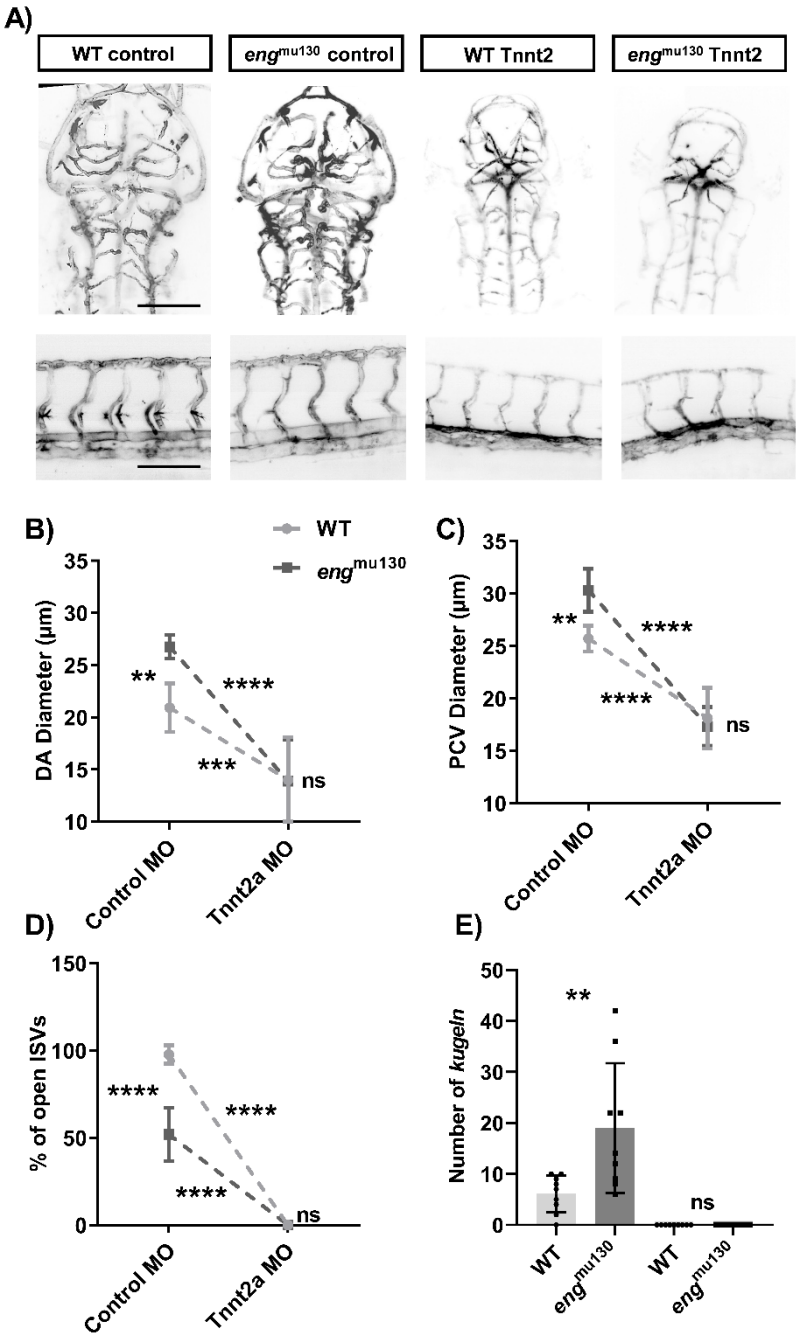

Figure 3.13 The effect of absent blood flow on the *eng*^{mu130} mutant phenotype at 3dpf.

A) Representative maximum intensity projection of *Tg(kdrl:Hsa.HRAS-mCherry)*^{s916} zebrafish trunk and brain vasculature at 72hpf. Scale bar = 150µm/50µm. B) DA diameter in *eng*^{mu130} mutants and WT siblings. C) PCV diameter in *eng*^{mu130} mutants and WT siblings. C) Percentage of open ISVs in *eng*^{mu130} mutants and WT siblings. E) Number of *kugeln* in *eng*^{mu130} mutants and WT siblings. (Two-way ANOVA, 10 animals/group).

3.6 Discussion

In this chapter, I have demonstrated that:

- *eng* loss of function results in a range of adult zebrafish phenotypes not previously described, including skin AVMs, retinal vascular abnormalities, and an enlarged heart.
- *eng* loss of function results in enlarged dorsal aorta and posterior cardinal vein.
- *eng* loss of function results in reduced ISV diameter, resulting from collapse of the vessel lumen.
- *eng* loss of function does not affect atrium size and heart rate during embryo development (2-3dpf).
- Gross morphology of embryonic cranial vasculature was unaffected by *eng* loss of function.
- *eng* loss of function results in an enlarged basilar artery (BA), which is not caused by increased EC number.
- *eng* loss of function results in increased formation of endothelial *kugeln* on cerebral vessels, suggesting *eng* acts to restrict *kugel* formation.
- Preventing cardiac output eliminated differences in DA and PCV diameter between WT and *eng*^{mu130} mutants.

I used light sheet fluorescence microscopy to visualise the vasculature in *eng*^{mu130} mutant zebrafish. In addition to previously described significantly enlarged dorsal aorta and posterior cardinal vein at 3 days post fertilisation, I show for the first time that *eng*^{mu130} embryos had an enlarged basilar artery (BA), and increased formation of endothelial *kugeln* on cerebral vessels. I also show for the first time that adult *eng*^{mu130} fish developed abnormal phenotypes, including skin AVMs, retinal vascular abnormalities, and an enlarged heart.

3.6.1 Adult *eng*^{mu130} fish display cutaneous and retinal vascular malformations similar to HHT and an enlarged heart

My findings substantially expand the previously described vascular phenotype in *eng*^{mu130} mutant zebrafish. For example, adult *eng* mutants display cutaneous vascular lesions on the face, gills and fins. These resemble the telangiectasias that develop on the surface of the skin

HHT patients, particularly on the face, hands and mucosal tissue. Furthermore, these skin lesions resemble the haemorrhagic blood vessels previously described in *bmp10* mutant zebrafish at 20 weeks (Capasso, Li et al. 2020). Similarly, the *bmp10* mutant adults develop these malformations on the face, gills and fins. Together, this is evidence to suggest the *eng* and *bmp10* mutants can be used as models for these features of HHT. Interestingly, there is no evidence that *alk1* mutants display these skin lesions (Roman, Pham et al. 2002, Corti, Young et al. 2011). However, *eng* and *alk1* loss of function in humans results in similar but distinct diseases - HHT1 and HHT2, respectively. It is therefore likely that *eng* and *alk1* loss of function zebrafish would display similar, but distinct phenotypes.

Extensive retinal vessel malformations in adult *eng*^{mu130} mutant zebrafish were observed, including increased capillary interconnections, increased optic artery diameter, and increased vessel branching compared with WT. Currently, the retinal vasculature in *bmp9*, *bmp10* and *alk1* mutants are uncharacterised. Future work would focus on characterising this vasculature bed to fully assess the adult phenotype in these HHT models. I infer that the *bmp10* mutants would recapitulate the *eng* retinal phenotype I have described in this chapter.

Adult *eng*^{mu130} mutant zebrafish heart ventricles were significantly larger than WT siblings. This increase in heart weight was previously noted *bmp10* mutant zebrafish (Capasso, Li et al. 2020). Therefore, *eng*^{mu130} and *bmp10* mutants present with a similar phenotype, including the development of skin lesions and increased heart weight. Furthermore, it was reported that *bmp9* mutant adult zebrafish completely lack a phenotype (Capasso, Li et al. 2020). The striking overlap in vascular phenotypes suggest that *eng* primarily interacts with *bmp10* to form the critical complex for *alk1* signalling in adult zebrafish. This result is somewhat surprising as *eng* primarily interacts with BMP9 in humans to form critical complex that drives ALK1 signalling **[Figure 1.1]** (Saito, Bokhove et al. 2017). For example, BMP9 mutations in humans results in a HHT-like disease, characterised by the development of telangiectasia, and there is no evidence to suggest that BMP10 is linked to any form of HHT **[Figure 1.3]**. This is a potential limitation of this study as it suggests that *eng* regulates angiogenesis via a different mechanism of action in zebrafish, which may affect the validity of using *eng*^{mu130} as a model for screening potential drug therapeutics to treat HHT. Alternatively, this can be explained by the possibility of off target affects in either mutant, resulting in slightly different phenotypes.

It is also known that zebrafish mutants sometimes do not display a phenotype due to genetic compensatory mechanisms (El-Brolosy and Stainier 2017). This is where a an organism with a mutation does not develop the expected phenotype due to compensatory mechanism of another gene.

The increase in cardiac ventricle size I observed in *eng* mutant adult zebrafish is also consistent with the phenotype observed in endothelial-specific *Eng* knockout adult mice, where altered blood flow results in increased venous return and high cardiac output, and consequently and increase in heart size (Tual-Chalot, Garcia-Collado et al. 2020). Future work would focus on further characterising heart size by observing atrium and bulbus arteriosus size/weight. Currently, data is limited to ventricle size due to practical limitation of atrium dissection. This would confirm if the increased size observed in figure 3.1 is specific to the ventricle or the whole heart. I hypothesise that a similar increase in atrium and ventricle size would be present based on the previous murine models of HHT (Tual-Chalot, Garcia-Collado et al. 2020)

Cardiac function was assessed in the *eng*^{mu130} mutant embryos by looking at chamber size and heart rate (HR). Atrium area and heart rate measurements were obtained from 2-3dpf. These heart rate measurements at 2 and 3dpf were similar to those previously described, indicating my results are consistent with published literature and likely to be technically reliable (Liu, Asnani et al. 2014).

There was no significant difference in atrium size and HR in the *eng* mutants compared to wild type siblings at either time point. This data suggests that heart function during development is unaffected by *eng* loss of function. However, this study is limited as it utilised 2D measurements of a 3d organ, which impacts the ability to measure volume. The above data is an imprecise indicator of heart size based on the area of the heart in one frame. In the future, 3D reconstructions using Arivis can be implemented to assess cardiac volume in systole and diastole. Furthermore, due to the anatomy of the zebrafish at the time points measured chamber area measurements were limited to the atrium. An alternative method to quantify ventricle size is to stain the embryonic heart using *in situ* hybridisation. The *myl*7 probe specifically binds to the myocardial cells and can therefore be used to visualise the ventricle using a compound microscope, thus removing this limitation of the light-sheet microscope.

Ex vivo light sheet imaging could be performed to evaluate the effect of *eng* loss on cardiac formation in adult zebrafish. The coronary vasculature develops between 2 and 4 months, and it was previously described that the coronary vessel cell population originates from the endocardium (Harrison, Bussmann et al. 2015). It is therefore possible that coronary vasculature development will be affected in the *eng*^{mu130} mutants. In the future, the *eng*^{mu130} mutant can be crossed with the Tg(fli1:EGFP)^{y1} transgenic to visualise coronary vasculature (Lawson and Weinstein 2002). Adult zebrafish would be raised to various time points and culled. Dissected hearts would be imaged using light-sheet fluorescent microscopy. Coronary vasculature would be assessed at various time points to characterise the development of coronary vasculature in *eng* mutants. Once assessed, angiogenesis in response to cardiac damage can be investigated to characterise the role of *eng* in response to cardiovascular damage.

3.6.2 *endoglin* loss of function affects embryonic blood vessel calibre in the trunk

eng mutants displayed a significant increase in the diameter of the DA. This is due to an increase in EC size and not increased EC number (Sugden, Meissner et al. 2017)**.** Increased flow through the enlarged major vessels in *eng*^{mu130} mutants leads to correspondingly reduced flow in ISVs, which leads to a delayed opening of their lumens (Sugden, Meissner et al. 2017). This blood flow pattern resembles that found in arteriovenous malformations – one of the characteristic symptoms of HHT. I also confirm this finding, suggesting *eng* plays an important role in determining vessel calibre in the zebrafish embryo.

Embryos at 2dpf and 4dpf were observed to investigate when this increase in vessel diameter occurs throughout early zebrafish embryonic development. There was a significant increase in vessel diameter at all the time points measured. Furthermore, the increase in vessel diameter correlates with the age of the embryos i.e older embryos have a greater increase in vessel diameter of the DA and PCV. This data confirms that *eng* plays a role in vascular remodelling during embryo development.

Intersegmental vessels (ISVs) development was observed over time between 2-4dpf. There was a significant reduction in vessel size in both aISVs and vISVs in *eng*^{mu130} mutants compared with WT siblings. This change in vessel diameter may be a result of improper development in the ISVs. As discussed above this is due to the DA/PCV shunt in the *eng*^{mu130} mutants resulting

in increased flow through the major vessels, and thus bypassing the ISVs. The phenotype was confirmed by two methods: firstly, mCherry intensity was used to establish ISV diameter size. Secondly, mCherry intensity was used to establish existence of an open lumen or collapsed vessel. Both of these methods confirmed that *eng*^{mu130} mutants have significantly more collapsed ISVs, resulting in an overall decrease in ISV diameter. Further work is needed to characterise if this ISV behaviour persists in zebrafish after embryonic development. Currently, vessel diameter data is limited to <5dpf due to Home Office licence limitations on adult zebrafish experiments. ISV collapse post 5dpf would most likely severely affect development of adult zebrafish due to lack of oxygenation in the dorsal tissue. However, adult zebrafish appear relatively normal with the exception of skin lesions and smaller size. It is most likely that the ISVs open again at some point during development, and thus restored oxygenation to the dorsal tissue.

3.6.4 *endoglin* loss of function affects embryonic blood vessel calibres in the brain and increases *kugel* formation

In zebrafish embryos, I uncover a cerebrovascular phenotype of enlarged basilar artery (BA) and increased endothelial *kugel* formation in *eng* mutants. It was previously reported that *eng* loss of function results in the formation of arteriovenous malformation (AVMs) in the adult brain of zebrafish (Sugden, Meissner et al. 2017). However, the brain vasculature in *eng* mutant embryos is currently uncharacterised. A key characteristic of brain AVMs is an increased diameter of cranial vessels. I found that at 2–4dpf the BA diameter was significantly dilated in homozygous mutant embryos compared with wild type siblings. Interestingly, at 3dpf the BA was dilated by approximately 30% (wt 19.6μm ± 0.9μm, mut 23.2μm ± 0.9μm, n=8-10/group, $p<0.05$) - a similar increase to the vessel calibre changes observed in the DA and PCV at the same time point.

The increase in BA diameter is similar to the *alk*1 and *bmp*10 mutant phenotype in zebrafish (Corti, Young et al. 2011, Capasso, Li et al. 2020). This is expected as *eng* is the co-receptor for *alk1* in the BMP9/BMP10 signalling pathway **[Figure 1.1]**. Corti and colleagues proposed that the increased BA size in the *alk1* mutants is driven by increased EC number in the BA. Interestingly, Sugden and colleagues suggest that *eng* drives vessel calibre changes due to endothelial cell shape changes, and therefore endothelial cell number is unaffected by *eng*

loss of function. I therefore set out to investigate if BA EC cell number is changed in *eng*^{mu130} mutants. The BA showed no increase in EC number in *eng*^{mu130} mutants compared with WT siblings. It is therefore likely that the increase BA size in *eng*^{mu130} mutants is a result of increased cell size, similar to the DA and PCV phenotype.

Corti and colleagues showed that *alk*1 loss of function results in AVM formation in the cranial vasculature of zebrafish embryos (Corti, Young et al. 2011). They showed that blood flow from the heart passes through the aortic arches towards the BA. Subsequently, blood perfuses into the brain through the capillary like central arteries into the venous primordial midbrain channel (PBMC). Loss of function results in the direct connection between the BA and PBMC, and therefore the development of brain AVMs. Currently, there is no evidence that this phenotype is recapitulated in *eng*^{mu130} mutants. Various manual and automatic quantification methods were utilised to assess vascular phenotype. In this case, *eng*^{mu130} mutant embryos display no obvious morphological differences in embryonic head vasculature, including AVM formation. Furthermore, *violet beauregarde* (*vbg*) mutants – another zebrafish knockout model for HHT2, develop dilated cranial blood vessels, but this phenotype is much more severe, and the embryos die between 7 and 10 dpf (Roman, Pham et al. 2002). Thus, this is further evidence to suggest that *eng* and *alk1* mutants have similar though distinct vascular phenotypes.

Kugeln are large transient spherical structures protruding from cerebral blood vessels that are Notch-dependent, NO-enriched, and VEGF-sensitive (Kugler, van Lessen et al. 2019). Currently, the physiological significance of *kugeln* is not clear, but this is the first work that implicates *kugel* formation in a model of human disease. I found that *eng* mutants have more *kugeln* present in the cerebral vessels, suggesting that *eng* functions to reduce *kugeln* number. I next set out to utilise 3-dimensional scanning electron microscopy to visualise the *kugeln* ultrastructure, which may give some insight into the role of kugeln in zebrafish cranial vasculature development. For example, the presence of cytoplasm, organelles and cell interactions may give an indication of the role of *kugeln*, and it is currently not feasible to observe this precise detail in light-sheet microscopy datasets. Cranial blood vessels were identified in the 3D-SEM data sets by the presence of red blood cells, and potential *kugeln* were identified in this pilot data. These structures appear as spherical protrusions from

cerebral blood vessels. However, this pilot data is currently limited to three datasets due to lengthy process and expense of imaging. Further work is needed to characterise these structures and validate if these structures are kugeln or not. The primary complication of this study is the dearth of literature on *kugeln* and SEM of zebrafish embryos. The next aim of this study is to therefore develop a protocol to reliably identify *kugeln* in SEM datasets. My proposed criteria for identifying *kugeln* is as follows: 1) *kugeln* most likely appear as spherical protrusions 2) These structures should always protrude from blood vessels. 3) Structures should only be found in the cranial vasculature. 4) eng^{mu130} mutants should display more structures than WT siblings. The presence of cytoplasm, organelles and cell interactions can be studied once *kugeln* can be reliably identified in SEM data sets.

3.6.5 Absence of blood flow modifies the *eng*^{mu130} mutant phenotype

tnnt2a knockdown reduced the vessel diameters differences between WT and *eng*^{mu130} mutants **[Figure 3.13]**. Therefore, it can be inferred that blood flow is required to influence the development of the zebrafish HHT phenotype. This is consistent with the previously published literature, which suggests blood flow critically influences EC size. Cessation of blood flow using tricaine treatment prevented the development of abnormal EC cell shape in *eng*^{mu130} mutants (Sugden, Meissner et al. 2017). In the future, tricaine treatment can be used as a secondary method to prevent cardiac output - this would be used to confirm the findings in Figure 3.13. One benefit of using tricaine treatment is that it can be used at any time point during the first 5 days of development to stop blood flow, as opposed to *tnnt2a* knockdown, which is limited to the one-cell stage and prevents initiation of blood flow. This allows precise manipulation of cardiac output and, if implemented can be used to determine the time point in zebrafish development when *eng* expression is critical.

4. The interaction between *endoglin* and VEGFA signalling in zebrafish embryonic vascular development

4.1 Introduction

ENG promotes BMP9/10/ALK1 signalling to couple haemodynamic cues to enable EC migration against blood flow during development and remodelling of the vasculature (Baeyens, Larrivée et al. 2016). Disruption of this pathway leads to AVMs, and depending on their size and location can cause significant complications. However, the underlying molecular mechanisms leading to AVM formation in HHT are still not fully understood, and advances in understanding are required to improve treatment.

Targeting VEGF signalling ameliorates the morbidity of HHT. The anti-VEGF inhibitor bevacizumab reduces epistaxis and high cardiac output in HHT patients with hepatic AVMs (Dupuis-Girod, Ginon et al. 2012). Furthermore, blocking VEGF signalling reduces vascular malformations in mouse models of HHT1 and HHT2 (Han, Choe et al. 2014, Tual-Chalot, Garcia-Collado et al. 2020). However, recent studies have highlighted the increased risk of serious adverse cardiovascular complications when targeting VEGF signalling in cancer patients (Totzeck, Mincu and Rassaf 2017), and unlike cancer treatment which often only lasts months, HHT patients are likely to require life-long therapies, making them particularly susceptible to side effects. VEGFA signalling is complex and drives numerous downstream pathways **[see Figure 1.6 page 42]**, making it possible that targeting specific downstream pathways may provide benefit with reduced risk of side-effects. To address which pathway (or combination of pathways) could efficiently achieve this goal, I took advantage of the zebrafish embryo's suitability for drug-screening assays, including its rapid cardiovascular development, ease of drug administration and transgenic tools for imaging. In this chapter, I pharmacologically inhibit either global VEGF signalling or components of different pathways downstream of VEGFR2 in zebrafish *eng* mutant and control embryo, to identify which signalling pathway/s are most critical to AVM formation.

4.2 Prevention of the *endoglin* mutant phenotype by VEGFR2 inhibition

As loss of *eng* disrupts integration of BMP9/10 and VEGFA signalling pathways, I investigated the VEGFA pathway in *eng*^{mu130} zebrafish in more detail. First, treating *eng*^{mu130} embryos

between 2dpf and 3dpf with the VEGF receptor tyrosine kinase inhibitor AV951 (Tivozanib) prevented progression of the DA and PCV mutant phenotypes, but did not affect the vessel calibre of WT animals **[Figure 4.1 B, C, D].** This indicates the HHT-like phenotype in zebrafish *eng* mutants can be mitigated by inhibiting VEGF signalling. I next asked whether the abnormal cerebral phenotype of *eng* mutants is caused by a similar dysregulation of VEGF signalling. Treating *eng*^{mu130} embryos between 2dpf and 3dpf with AV951 prevented increased *kugel* formation in the mutant embryos, but did not affect *kugel* number in WT siblings compared with DMSO control **[Figure 4.1 G]**. The increased BA diameter in *eng* mutants was also prevented by treatment with AV951 **[Figure 4.1 H].**

AV951 treated embryos were examined for signs of drug toxicity. Bright field microscopy revealed no evidence of pericardial oedema **[Figure 4.3 A]**. Heart rate was unaffected in *eng*^{mu130} and wild types ± AV951 (25nM) treatment for 24h **[Figure 4.3 A]**. Furthermore, 100% (45/45) of *eng*^{mu130} and wild type embryos survived AV951 treatment. Overall, AV951 treated embryos did not show any overt signs of toxicity, suggesting the results in **[Figure 4.1]** are a result of specific modulation of the dysregulated VEGF signalling in *eng*^{mu130} zebrafish embryos rather than off-target effects due to toxicity.

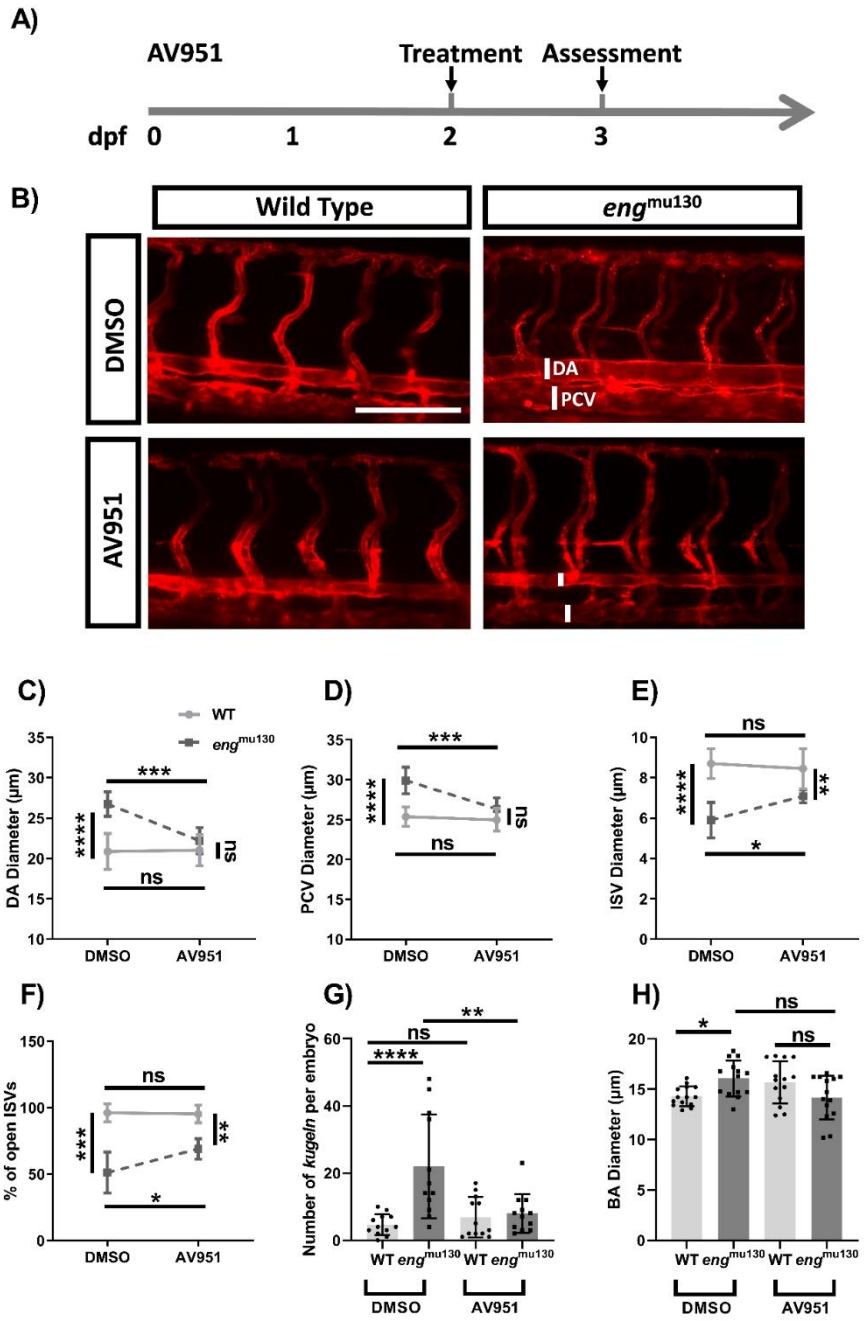

Figure 4.1 VEGFR2 inhibition between 2-3dpf rescues the abnormal trunk and cerebral vessel phenotypes of *eng*^{mu130} mutants.

A) Experimental plan for rescuing *endoglin* mutant phenotype in zebrafish using AV951 (dpf, days post fertilization) B) Representative maximum intensity projection of *eng*^{mu130} and WT embryos ± AV951 (25nM) treatment for 24h. Scale bar = 150µm. C) DA diameter in *eng*^{mu130} and WT embryos ± AV951 treatment. D) PCV diameter in *eng*^{mu130} and WT embryos ± AV951 treatment. E) ISV diameters in *eng*^{mu130} and WT embryos ± AV951 treatment. F) Percentage of open ISVs in *eng*^{mu130} and WT embryos ± AV951 treatment. G) Number of *kugeln* in *eng*^{mu130} and WT embryos ± AV951 treatment. H) BA diameter in *eng*^{mu130} and WT embryos ± 25nM AV951 treatment. (two-way ANOVA with Tukey post-hoc test, n=10/group.) Figure taken from Snodgrass *et al.*, 2021 (Snodgrass, Arthur and Chico 2021).

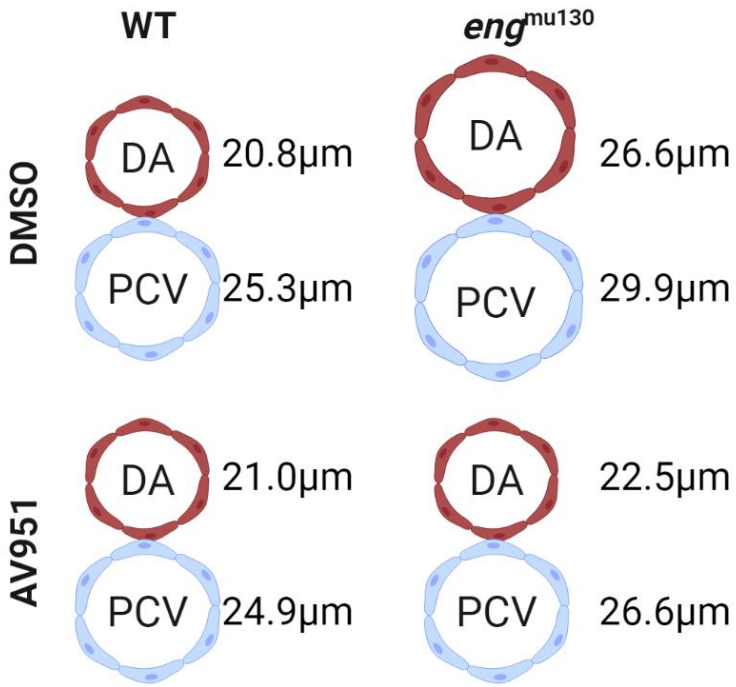

Figure 4.2 Schematic summarising the vessel calibre changes observed in *eng*^{mu130} ± AV951 (25nM) treatment for 24h.

Abbreviations: DA, dorsal aorta; PCV, posterior cardinal vein. Significantly enlarged vessel diameters in *eng*^{mu130} fish are rescued with AV951 treatment. WT vessel diameters are unaffected by AV951 treatment. Mean vessel diameters are shown for each group. Figure created with BioRender (https://biorender.com/).

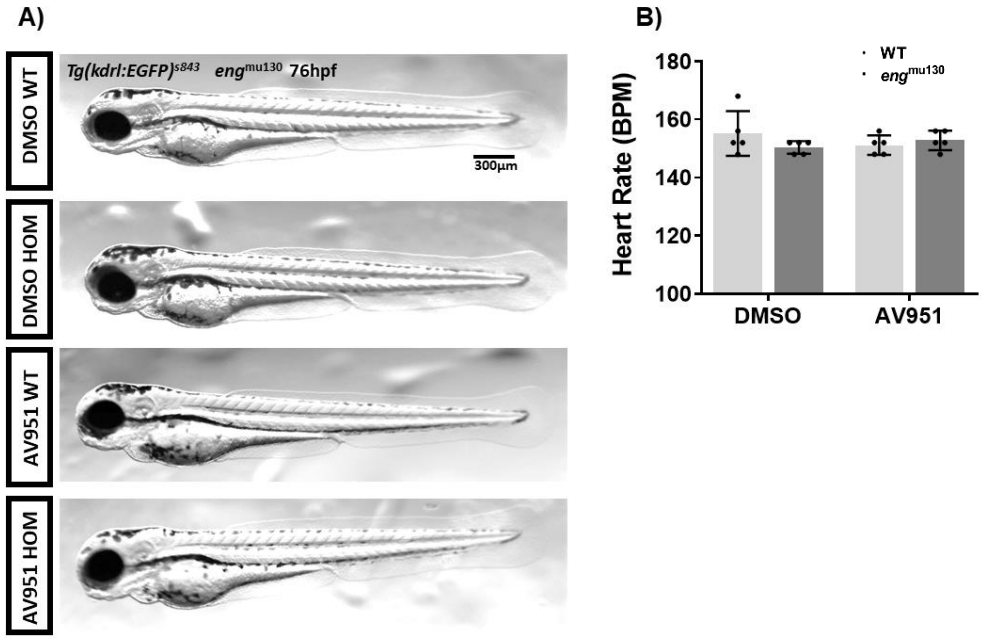

Figure 4.3 WT and *eng*^{mu130} mutant embryos display no obvious morphological differences when treated with VEGF inhibitors.

A) Representative images of 3dpf WT and *eng*^{mu130} mutant embryos with and without AV951 (25nM) treatment for 24h. B) Quantification of heart rate for WT and *eng*^{mu130} mutant embryos with and without AV951 treatment for 24h. 1 experimental repeat, n = 5/group. From Snodgrass *et al*., 2021 (Snodgrass, Arthur and Chico 2021).

4.3 The effect of VEGFR2 downstream inhibitors on the *endoglin* mutant phenotype

VEGFR2 signalling is complex and signals downstream via several pathways. In vitro, BMP9 decreases VEGFA signalling, and loss of BMP9 signalling through ALK1 or ENG depletion leads to increased pERK levels (Alsina-Sanchís, García-Ibáñez et al. 2018, Tual-Chalot, Garcia-Collado et al. 2020). Treatment of embryos at 2dpf for 24h with 10µM PD0325901 to inhibit MEK, upstream of ERK, prevented the enlarged DA and PCV of *eng*^{mu130} embryos without affecting vessel diameter of WT siblings **[Figure 4.4 A,B]**. Furthermore, 10µM PD0325901 prevented the abnormally increased number of *kugeln* in *eng*^{mu130} embryos, but did not affect *kugel* number in WT animals. This suggests that upregulation of MEK/ERK signalling due to *eng* loss of function contributes to the trunk vessel abnormalities and increased *kugel* formation in *eng* mutants **[Figure 4.5 A]**.

A second major pathway downstream of VEGFR2 is the PI3K/AKT pathway, which affects both mTOR and eNOS function to regulate cell survival and vasoregulation, respectively **[Figure 1.4]**. Targeting PI3K can reduce AVMs in murine HHT2 models (Ola, Dubrac et al. 2016). Furthermore, in a model of HHT caused by loss of BMP9 and BMP10 ligands, endothelial mTOR levels are increased and targeting mTOR reduces vascular defects (Ruiz, Zhao et al. 2020). Therefore, I assessed the effect of rapamycin (also known as Sirolimus) to inhibit TOR in *eng*^{mu130} zebrafish embryos and found that both DA and PCV diameters were normalised in *eng*^{mu130} zebrafish whilst WT embryos were unaffected **[Figure 4.4 C,D]**. Rapamycin also prevented the increase in *kugel* number in *eng* mutant embryos **[Figure 4.5 B]**. Interestingly, although rapamycin treatment does not affect *kugel* number, it did affect *kugel* size. The average size of *kugeln* per embryo was significantly increased in *eng*^{mu130} and wild type embryos treated with rapamycin. This experiment also suggests *eng*^{mu130} mutants may have increased *kugel* diameter **[Figure 4.6].**

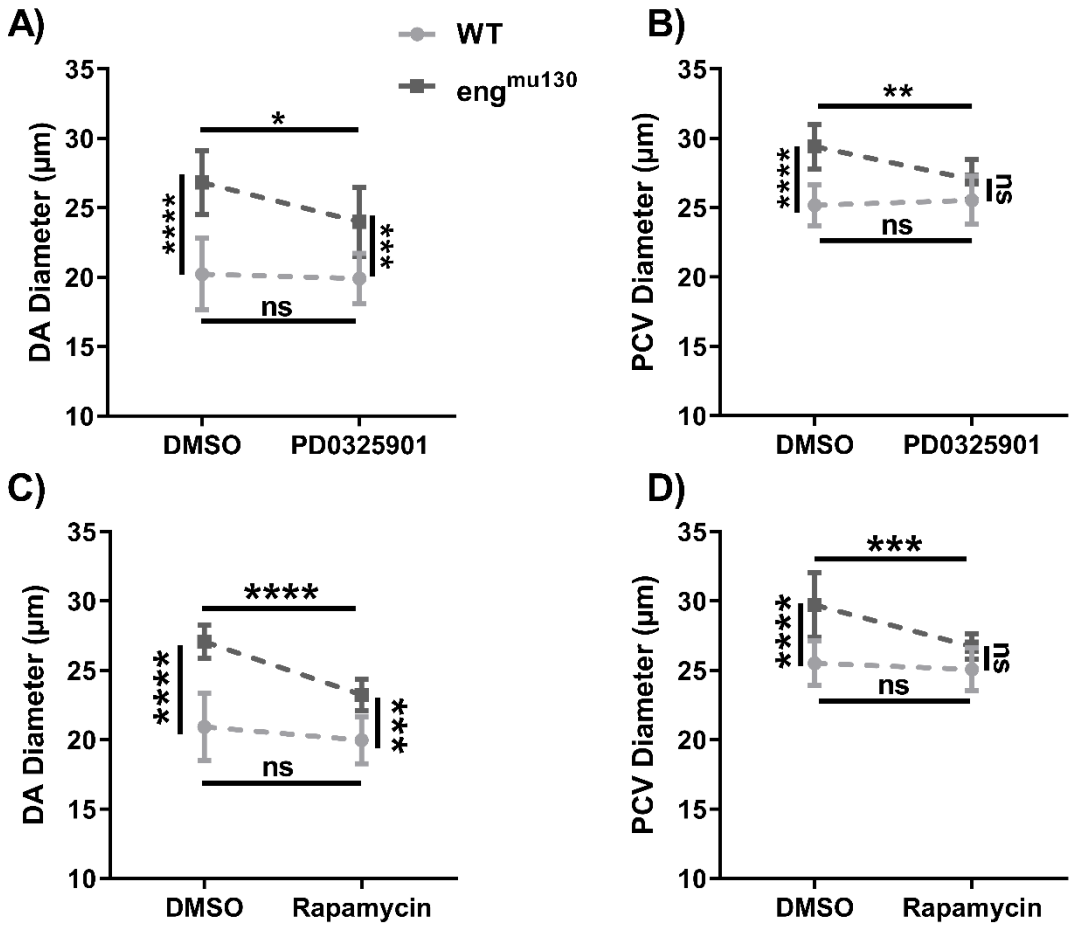

Figure 4.4 Either mTOR or MEK inhibition normalise the trunk vascular phenotype of *eng*^{mu130} zebrafish embryos.

WT and *eng*^{mu130} mutant embryos were treated with the mTor inhibitor Rapamycin (2.5µM) or with the MEK inhibitor PD0325901 (10µM) for 24h between 2-3dpf, or with DMSO vehicle. A, B) *eng*^{mu130} mutant embryos show reduced DA diameter and normal PCV diameter following PD0325901 treatment. C, D) *eng*^{mu130} mutant embryos show reduced DA and normal PVC diameter following rapamycin treatment. Data were analysed by two-way ANOVA with Tukey post-hoc test. 3 experimental repeats, n = 11-14/group. Figure adapted from Snodgrass *et al*., 2021 (Snodgrass, Arthur and Chico 2021).

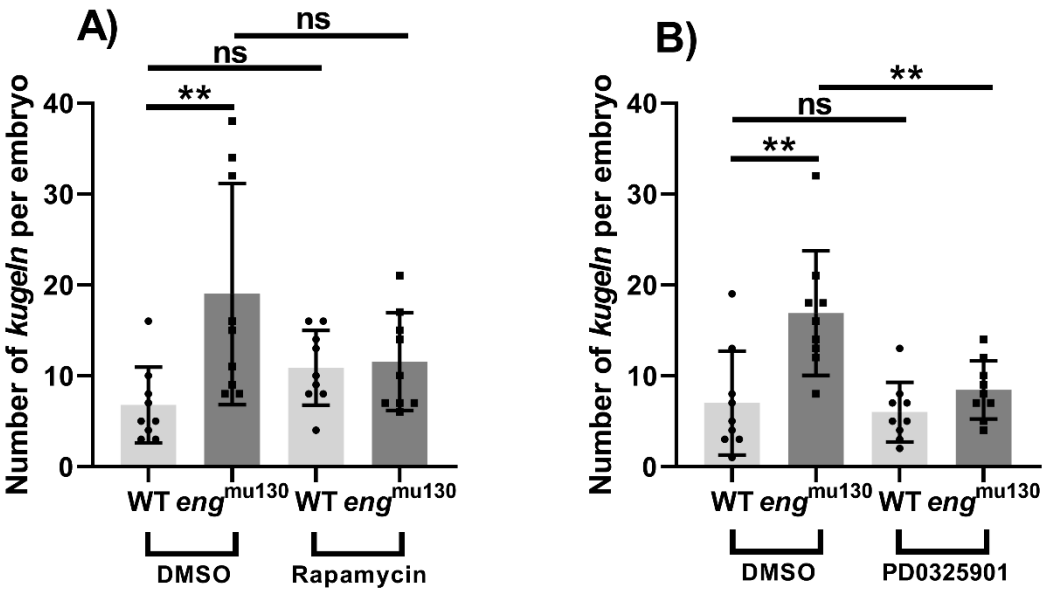

Figure 4.5 Either TOR or MEK inhibition normalises the excess *kugel* phenotype of *eng*^{mu130}.

WT and *eng*^{mu130} mutant embryos were treated with the TOR inhibitor Rapamycin (2.5µM) or the MEK inhibitor PD0325901 (10µM) for 24h between 2-3dpf, or with DMSO vehicle. A) *eng*^{mu130} mutant embryos show reduced *kugel* formation following Rapamycin treatment. B) *eng*^{mu130} mutant embryos show normalised *kugel* formation following PD0325901 treatment. (two-way ANOVA with Tukey post-hoc test. n = 10-14/group. Figure adapted from Snodgrass *et al*., 2021 (Snodgrass, Arthur and Chico 2021).

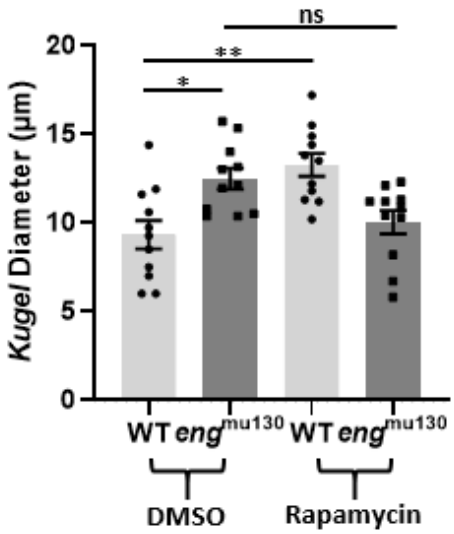

Figure 4.6 TOR inhibition normalises the increased *kugel* diameter phenotype of *eng*^{mu130}.

WT and *eng*^{mu130} mutant embryos were treated with the TOR inhibitor Rapamycin (2.5µM) for 24h between 2-3dpf, or with DMSO vehicle. Data points show average kugel diameter per embryo. *eng*^{mu130} mutant embryos show decreased *kugel* diameter in DMSO control group. *eng*^{mu130} mutant embryos show reduced *kugel* diameter following Rapamycin treatment. Wild type embryos show increased *kugel* diameter following Rapamycin treatment. (two-way ANOVA with Tukey post-hoc test. n = 10-14/group. Figure adapted from Snodgrass *et al*., 2021 (Snodgrass, Arthur and Chico 2021).

Endothelial NOS is a critical enzyme regulating the levels of nitric oxide (NO) available for diffusion to neighbouring smooth muscle cells (SMCs) where it leads to vasodilation. eNOS is upregulated both by flow and by VEGFA signalling, and there is evidence that *eng* regulates coupling of eNOS activity (Toporsian, Gros et al. 2005). However, I found no detectable effect on DA or PCV vessel size in *eng*^{mu130} embryos following L-NAME, consistent with the lack of vascular smooth muscle cells supporting these vessels at this stage of development **[Figure 4.7 A, B].** L-NAME prevented the increase in *kugel* number in *eng* mutant embryos, suggesting that NOS activity is not critical to the formation of the trunk phenotype, but may be important in the development of the excess kugel phenotype in *eng* mutants **[Figure 4.8].**

Treatment with the P38 MAPK inhibitor SB 203580 had no detectable effect on DA or PCV vessel size in *eng*^{mu130} or wild type embryos **[Figure 4.7 C, D]**, suggesting that MAPK activity is not critical to AVM formation.

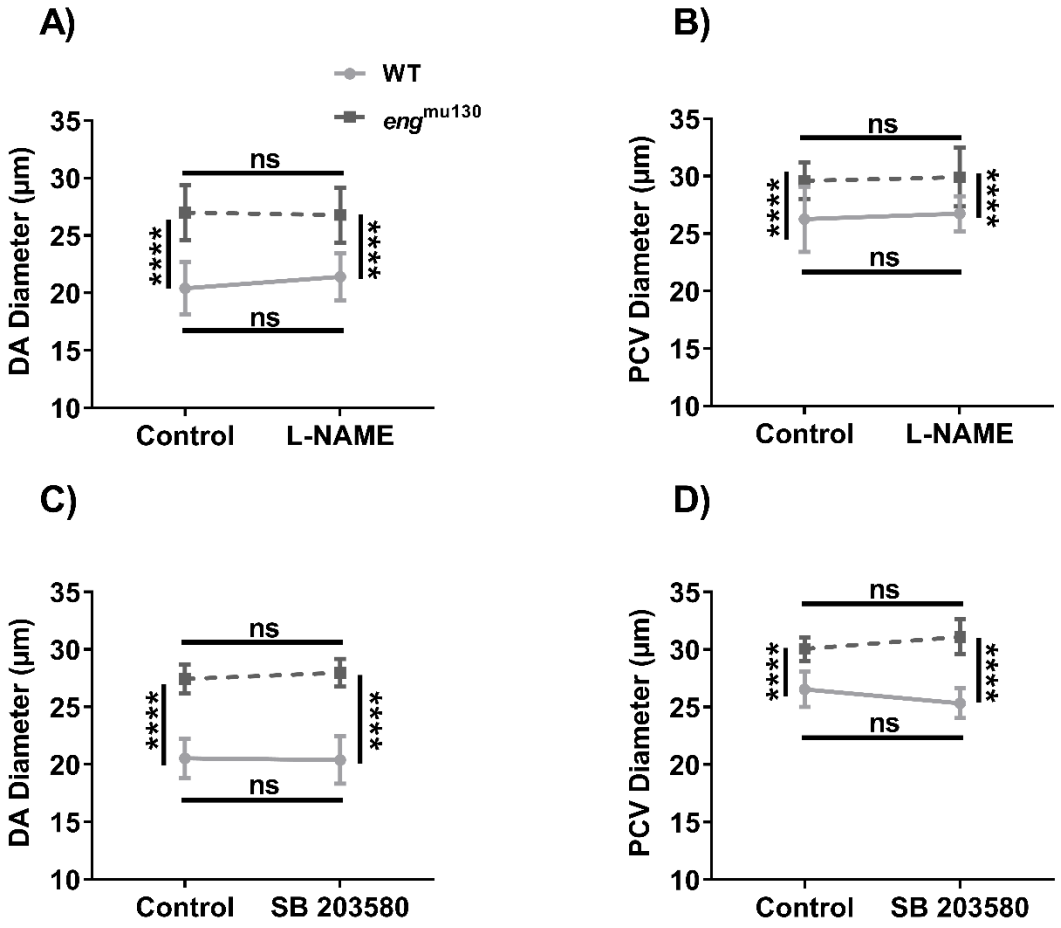

Figure 4.7 NOS or p38 MAPK inhibition between 2-3dpf does not affect the phenotype of *eng*^{mu130} and WT embryos.

WT and *eng*^{mu130} mutant embryos were treated with the NOS inhibitor L-NAME (1µM) or the P38 MAPK (25µM) for 24h between 2-3dpf, or with E3 control vehicle. A, B) Quantification of vessel diameter for the DA and PCV in WT and *eng*^{mu130} mutant embryos with and without L-NAME treatment. C, D) Quantification of vessel diameter for the DA and PCV in WT and *eng*^{mu130} mutant embryos with and without SB 203580 treatment. (two-way ANOVA with Tukey post-hoc test. n = 10-15/group.) Figure adapted from Snodgrass *et al*., 2021 (Snodgrass, Arthur and Chico 2021).

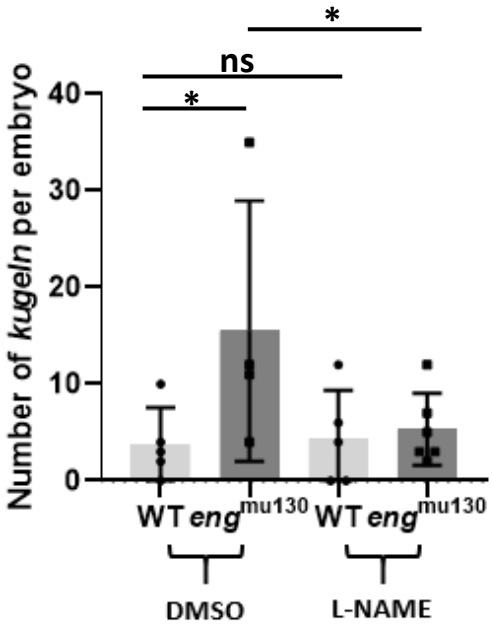

Figure 4.8 NOS inhibition normalises the excess *kugel* phenotype of *eng*^{mu130}.

WT and *eng*^{mu130} mutant embryos were treated with the NOS inhibitor L-NAME (1µM) 2-3dpf, or with E3 vehicle. *eng*^{mu130} mutant embryos show normalised *kugel* formation following L-NAME treatment. (two-way ANOVA with Tukey post-hoc test. n = 5-8/group.

4.4 The effect of combined VEGFR2 downstream inhibitors on the *endoglin* mutant phenotype

I next set out to investigate if combined low dose mTOR and MEK inhibition prevents abnormal trunk vasculature in *eng*^{mu130} embryos. Neither 2µM Rapamycin nor 7.5µM PD0325901 alone altered the vascular phenotype of *eng*^{mu130} mutants, but co-treatment normalised both DA and PCV diameters and reduced the excess *kugel* formation phenotype **[Figure 4.9 A, B, C],** suggesting that upregulation of both MEK/ERK and AKT/mTOR pathways contribute to the abnormal vessel phenotype in *eng* mutants.

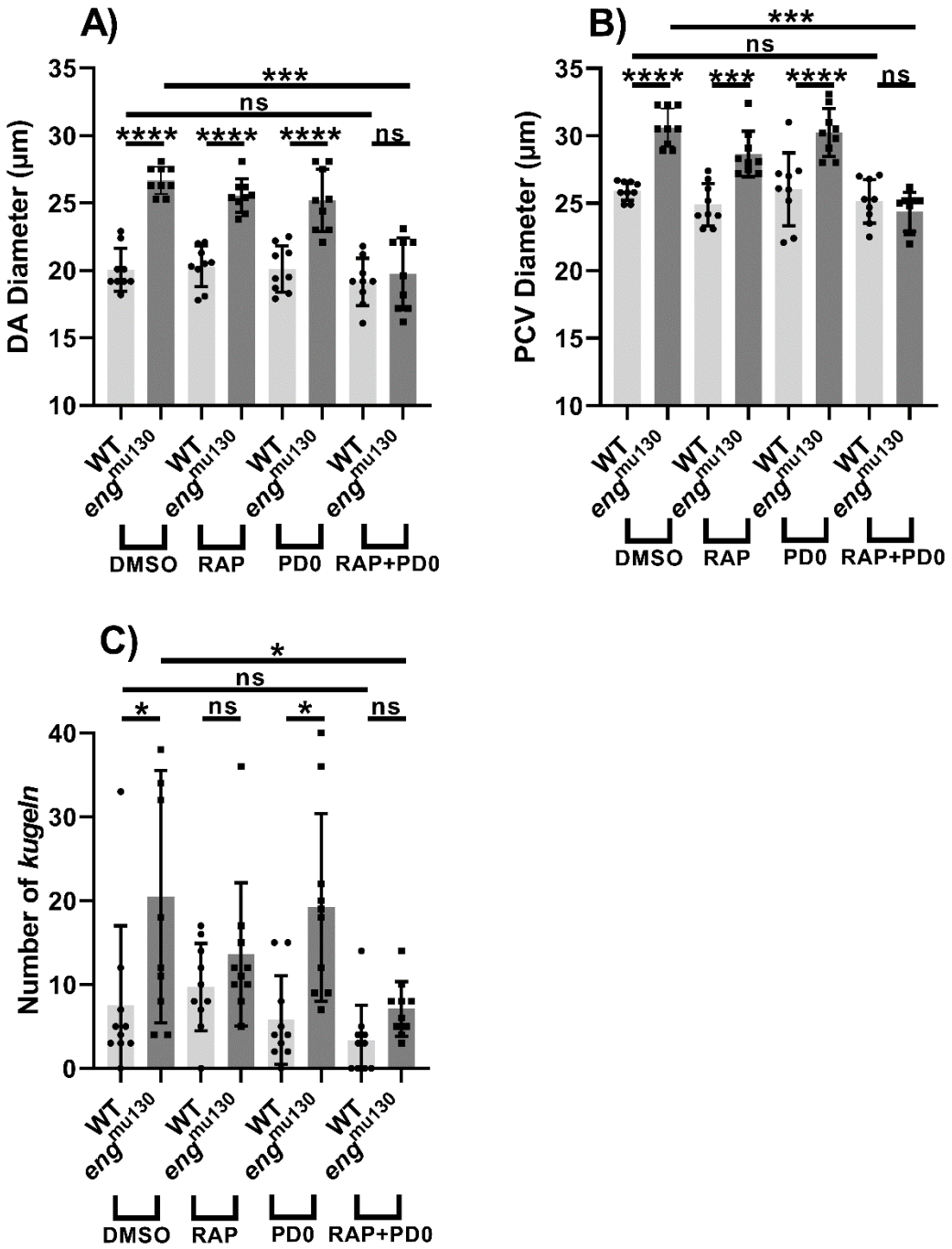

Figure 4.9 Combined low dose TOR and MEK inhibition prevents abnormal trunk vasculature and excess *kugel* formation in *eng*^{mu130} zebrafish embryos.

A,B,C) Neither 2µM Rapamycin (RAP) nor 7.5µM PD0325901 (PD0) alter the vascular phenotype of *eng*^{mu130} mutants, but combined treatment resulted in normalised DA and PCV diameters, as well as reduced *kugel* formation in *eng*^{mu130} zebrafish embryos. (two-way ANOVA with Tukey post-hoc test (10-14/group.) Figure adapted from Snodgrass *et al.*, 2021 (Snodgrass, Arthur and Chico 2021).

4.5 Recapitulation of the *endoglin* mutant phenotype using VEGFA Inducers

Having found that modulating various aspects of the VEGFA signalling pathway prevents the *eng*^{mu130} zebrafish pathway, I subsequently set out to investigate if the *eng* mutant phenotype can be recapitulated by overstimulation of VEGF signalling in WT embryos. VEGF signalling was therefore overstimulated by the addition of GS4012 into the E3 media.

Firstly, the trunk vasculature was observed at 3dpf. GS4012 treated WT embryos developed an enlarged PCV, similar to *eng*^{mu130} mutants **[Figure 4.10 A, C].** Furthermore, there was non-significant increase in DA diameter **[Figure 4.10 A, B].** The *eng*^{mu130} mutant ISV phenotype was recapitulated in GS4012 treated embryos. aISV and vISV dimeter was significantly decreased due to collapsing of vessels during development **[Figure 4.10 A, D, E].** This data provides further evidence that the *eng*^{mu130} mutant phenotype, and therefore the HHT-like phenotype is a result of dysregulated/excess VEGF signalling.

I subsequently set out to investigate if the *eng*^{mu130} mutant cranial phenotype is recapitulated by GS4012 treatment. *Kugeln* number was unaffected by GS4012 treatment **[Figure 4.10 A, G]**, suggesting the cranial vasculature phenotype is less likely to be related to an excess VEGF signalling, However further work is needed to characterise the effect of GS4012 treatment on zebrafish cranial vasculature development. A technical explanation could be the lack of penetration of the drug into the deeper tissues of the head compared with the trunk.

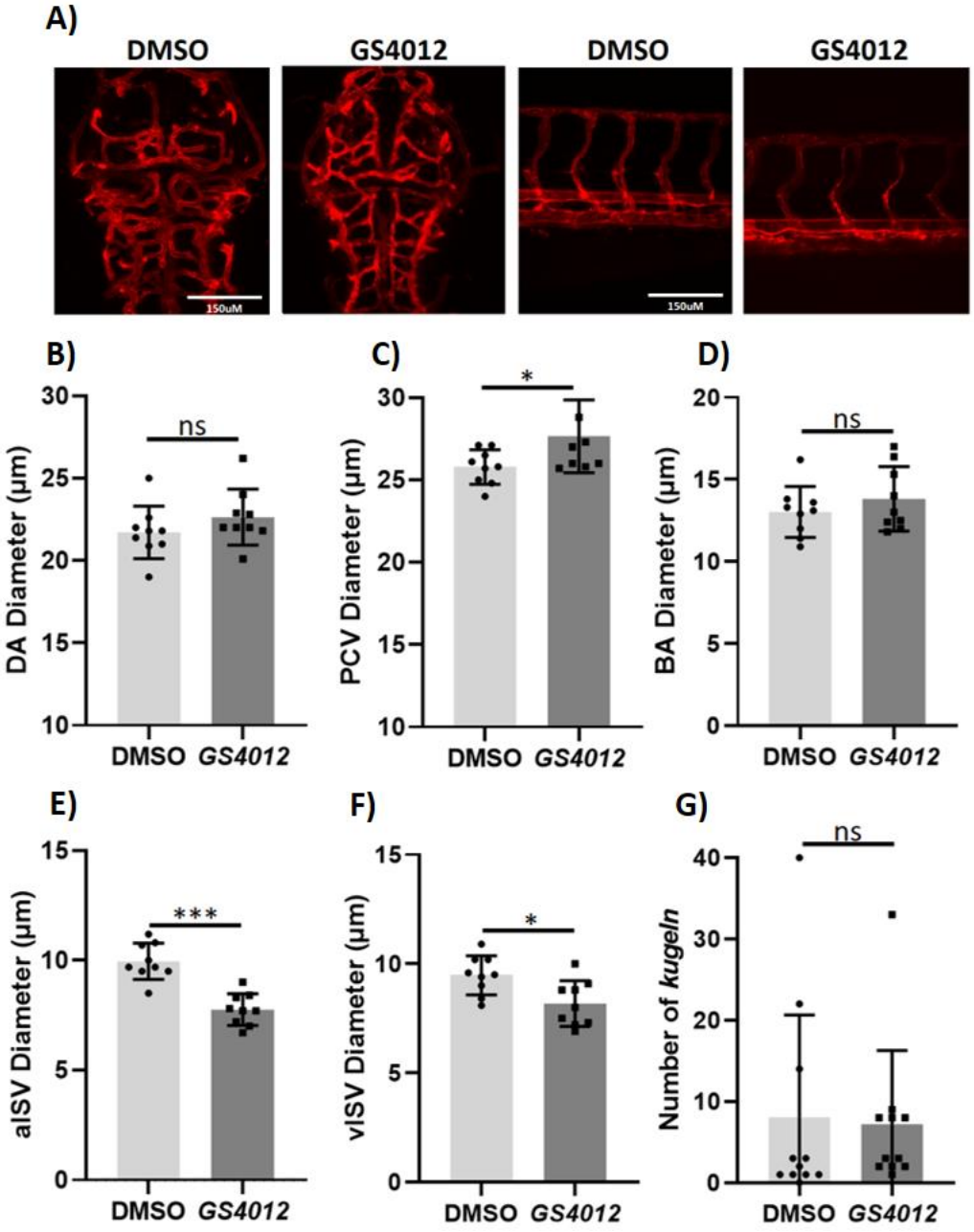

Figure 4.10 VEGF induction by GS4012 between 1-3dpf partially recapitulates the abnormal trunk phenotypes of *eng*^{mu130} mutants.

A) Representative maximum intensity projection of WT embryos ± GS4012 (50µM) treatment for 48h. B) DA diameter in *eng*^{mu130} and WT embryos ± GS4012 treatment. C) PCV diameter in *eng*^{mu130} and WT embryos ± GS4012 treatment. D) BA diameter in *eng*^{mu130} and WT embryos ± GS4012 treatment. E) aISV diameter in *eng*^{mu130} and WT embryos ± GS4012 treatment. F) vISV diameter in *eng*^{mu130} and WT embryos ± GS4012 treatment. G) Number of *kugeln* in *eng*^{mu130} and WT embryos ± GS4012 treatment. (Unpaired Student's t-test, 11 animals/group.).

4.6 Prevention of the *endoglin* mutant phenotype by Notch inhibition

Having found that modulating various aspects of the VEGFA signalling pathway prevents the *eng*^{mu130} zebrafish phenotype, I subsequently set out to investigate if a secondary vascular signalling pathway, Notch is critical to AVM formation (Siekmann and Lawson 2007). Previously, it was reported that Notch signalling reduces *kugel* formation (Kugler, van Lessen et al. 2019), making it an ideal candidate to rescue the *eng* phenotype. In agreement with previously reported data inhibition of Notch signalling by DAPT significantly reduced *kugel* number in wild types (Kugler, van Lessen et al. 2019), but did not significantly affect the kugel number in *eng*^{mu130} embryos **[Figure 4.11 C].** Furthermore, there was no detectable effect on DA or PCV vessel size in *eng*^{mu130} embryos following DAPT treatment **[Figure 4.11 A, B]**.

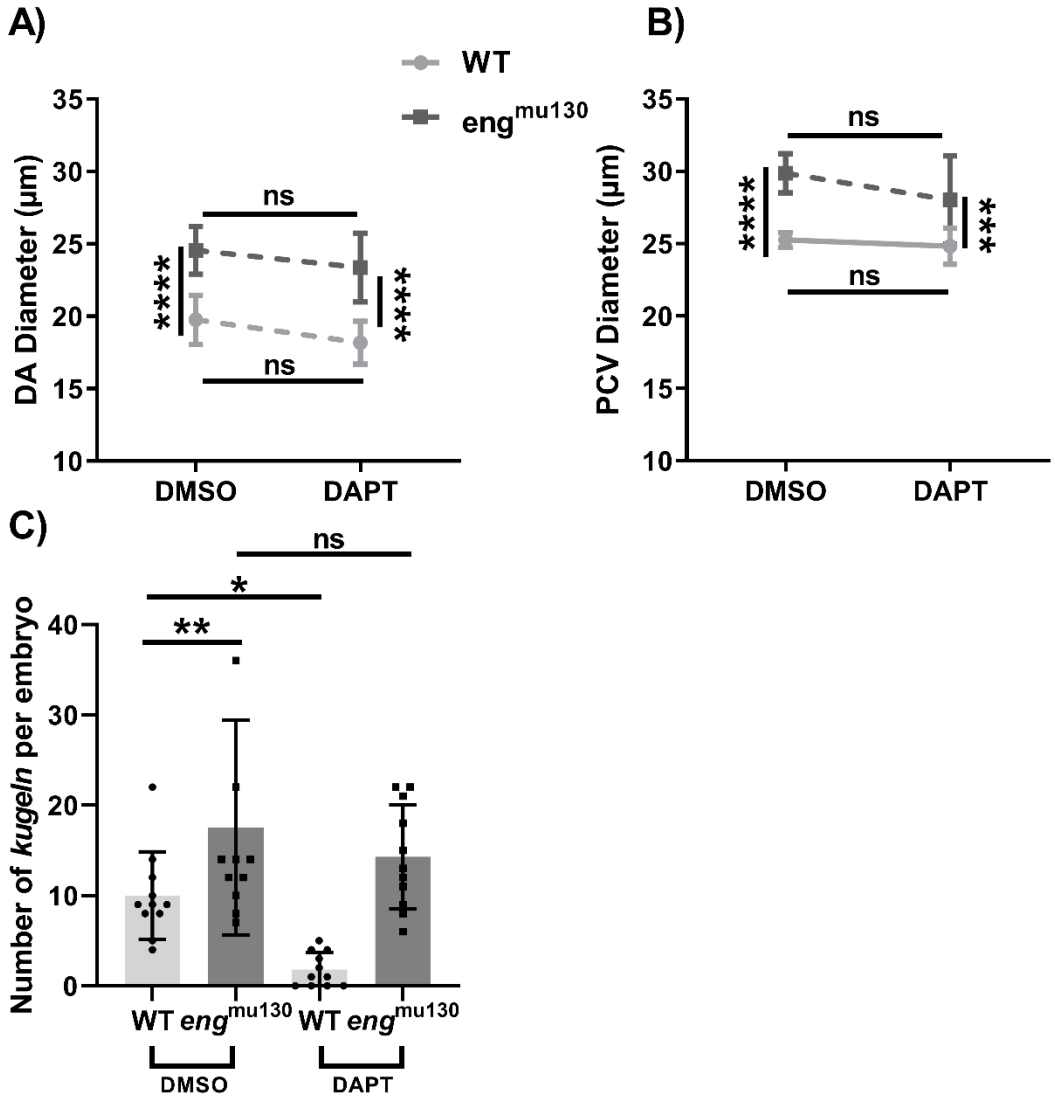

Figure 4.11 Notch inhibition between 2-3dpf does not affect the phenotype of *eng*^{mu130} and WT embryos.

WT and *eng*^{mu130} mutant embryos were treated with the Notch signalling inhibitor DAPT (50µM) 2-3dpf, or with DMSO vehicle. A, B) Quantification of vessel diameter for the DA and PCV in WT and *eng*^{mu130} mutant embryos ± DAPT (50µM) treatment. C) Number of *kugeln* in *eng*^{mu130} and WT embryos ± DAPT treatment. (two-way ANOVA with Tukey post-hoc test. n =11/group.)

4.7 Discussion

In this chapter, I have demonstrated that:

- Inhibiting global VEGFR prevents the development of abnormally enlarged major vessels and normalised the number of *kugeln* in *eng*^{mu130} embryos.
- Inhibiting TOR or MEK prevented the abnormal trunk and cerebral vasculature embryonic phenotype.
- Targeting NOS, P38 MAPK, or Notch had no observable effect on the *eng* loss of function phenotype.
- Combining subtherapeutic TOR and MEK inhibition prevented the vascular phenotype, suggesting synergy between TOR and MEK/ERK signalling pathways.
- Induction of VEGF signalling using GS4012 partially recapitulated the *eng* loss of function phenotype.

I used various VEGF drug treatments to prevent the development of abnormally enlarged major vessels and normalised the number of *kugeln* in *eng*^{mu130} embryos. Inhibiting signalling pathways downstream of VEGFR2 in *eng*^{mu130} embryos gave further insights. Inhibiting TOR or MEK prevented the abnormal trunk and cerebral vasculature embryonic phenotype, whilst targeting NOS and MAPK had no effect. Combining subtherapeutic TOR and MEK inhibition prevented the vascular phenotype, suggesting synergy between TOR and MEK/ERK signalling pathways. These results indicate the HHT-like phenotype in zebrafish *eng* mutants can be mitigated through modulation of VEGFA signalling, and implicate combination low dose MEK and TOR pathway inhibitors as a therapeutic strategy in HHT. A summary of all the drug regimens used rescue or recapitulate the *eng*^{mu130} mutant phenotype is shown in Figure 4.12.

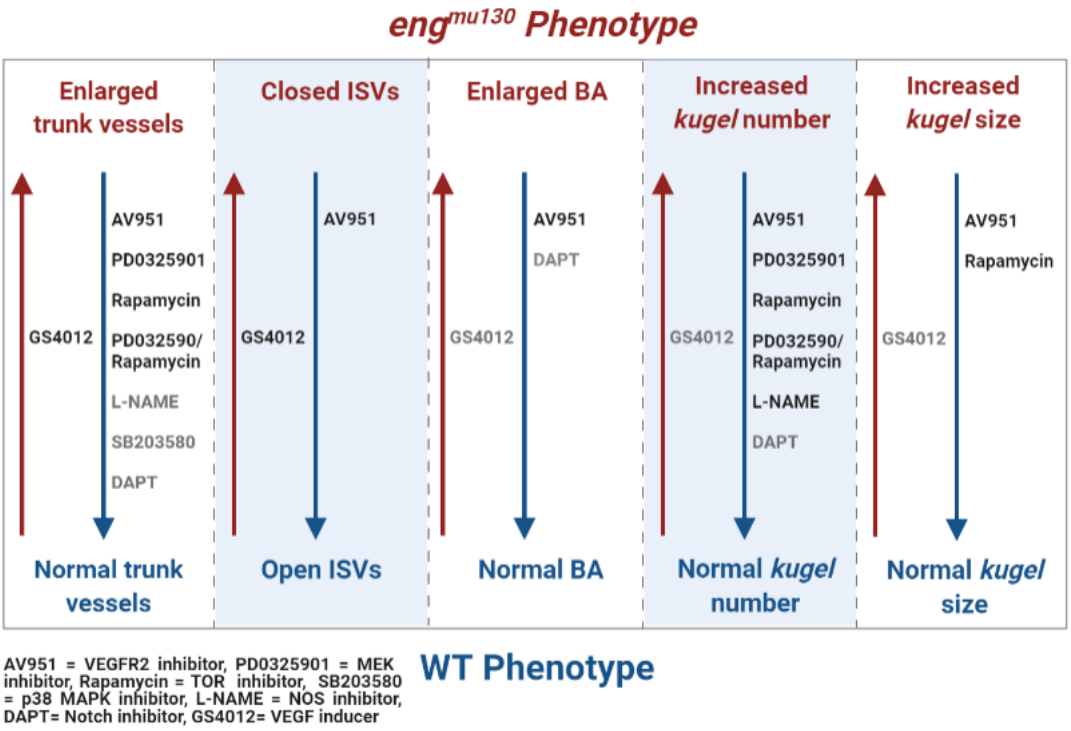

Figure 4.12 Schematic diagram summarising the various drug regimens used to rescue or recapitulate the *eng*^{mu130} mutant phenotype.

Abbreviations: ISV; intersegmental vessels, BA; Basilar artery. Figure created with BioRender (**https://biorender.com/**). Red arrows show drugs that were used treat WT embryos to recapitulate the *endoglin* mutant phenotype. Blue arrows show drugs that were used treat *eng*^{mu130} embryos to rescue the mutant phenotype. Drugs in black = statistically significant effect, drugs in grey = statistically non-significant effect.

4.7.1 Abnormal brain and trunk vasculature of *eng*^{mu130} zebrafish embryos is prevented by VEGFR2 inhibition

Treatment of *eng*^{mu130} embryos with Tivozanib to target VEGFR signalling prevented development of the abnormally enlarged major vessels and normalised cerebrovascular *kugel* number. This indicates that the HHT-like phenotype in zebrafish *eng* mutants can be mitigated by inhibiting VEGF signalling, in agreement with other studies in mouse models of HHT (Han, Choe et al. 2014, Jin, Muhl et al. 2017, Tual-Chalot, Garcia-Collado et al. 2020) and current clinical therapies targeting VEGF in HHT patients (Dupuis-Girod, Ginon et al. 2012). However, anti-VEGF treatment must be continuous or semi-continuous to maintain suppression of abnormal angiogenic responses, and anti-VEGF therapies such as Bevacizumab have severe side effects and require repeated intravenous delivery (Totzeck, Mincu and Rassaf 2017). Furthermore, VEGFA signalling activates numerous downstream pathways **[see Figure 1.6 page 38]**,and knowing which of these is dysregulated in HHT will help to guide more focused therapeutic interventions.

4.7.2 TOR and MEK inhibition prevents abnormal brain and trunk vasculature of *eng*^{mu130} zebrafish embryos

I took advantage of the zebrafish embryo's suitability for drug-screening assays to target separate signalling pathways downstream of VEGFR2 in *eng*^{mu130} embryos. As *Eng* mutants show increased phosphorylated ERK (pERK) activity in endothelial cells downstream of VEGFA signalling, and increased pERK was observed in ECs associated with AVMs (Tual-Chalot, Garcia-Collado et al. 2020) this may represent a key pathway to target downstream of VEGFA. Indeed, sporadic human cerebral AVMs also have an exaggerated pERK response suggesting aberrant pERK activation is a common feature of AVMs (Nikolaev, Vetiska et al. 2018, Jakobsson and Arthur 2020). Treatment of embryos for 24h between 2 and 3dpf with PD0325901 to inhibit MEK, upstream of ERK, normalised the enlarged vessels and reduced the excess *kugel* formation in *eng*^{mu130} zebrafish embryos. These timings were chosen as pERK is present at an early stage (from 18hpf) in the developing DA, and predefines ECs that are going to contribute to ISV formation (Nagasawa-Masuda and Terai 2016). However, this initial process is completed by 2dpf when MEK inhibition was initiated. Importantly, development and vessel size (including ISV) of wild type embryos was unaffected by exposure to

PD0325901. Thus, targeting MEK effectively prevented occurrence of the *eng* mutant vascular phenotype.

In contrast, targeting p38 MAPK, a second pathway downstream of VEGFA signalling, had no detectable effect on the enlarged trunk vessels in *eng*^{mu130} mutants, suggesting that altered p38 regulated cell migration was not involved in the HHT phenotype.

I next set out to look at the PI3K/AKT pathway downstream of VEGFA. Inhibition of PI3K in *Alk1* mouse neonates has previously been shown to protect against development of vascular abnormalities (Ola, Dubrac et al. 2016, Alsina-Sanchís, García-Ibáñez et al. 2018). *Alk1*-deficient endothelial cells show enhanced activation of the PI3K/AKT pathway (Ola, Dubrac et al. 2016, Alsina-Sanchís, García-Ibáñez et al. 2018, Hwan Kim, Vu et al. 2020), which would be expected to increase both eNOS and mTOR activity downstream. I therefore next targeted NOS using L-NAME, but found no detectable effect on DA or PCV vessel size in *eng*^{mu130} embryos. Although previous evidence has suggested eNOS may be involved in HHT due to eNOS uncoupling in Eng mutant endothelial cells (Toporsian, Gros et al. 2005), our data would suggest that increased NOS activity in the developing zebrafish vasculature does not drive vascular malformations, at least not prior to the recruitment of vascular smooth muscle. Finally, I targeted TOR downstream of pI3K/AKT and found that rapamycin treatment normalised the enlarged vessels and reduced the excess *kugel* formation in *eng*^{mu130} embryos. This is consistent with previous findings in a mouse neonatal retinal model caused by loss of BMP9/10 ligands where targeting mTOR had beneficial effects (Ruiz, Zhao et al. 2020).

4.7.3 Combined TOR and MEK inhibition prevents abnormal brain and trunk vasculature of *eng*^{mu130} zebrafish embryos

In this chapter, I demonstrate that independently targeting two separate pathways, MEK/ERK and mTOR, downstream of VEGFA could prevent the mutant vascular phenotype in eng^{mu130} embryos. I then asked whether there was synergy between these two pathways by combining low dose TOR and MEK inhibitors. At low dose neither TOR nor MEK inhibitor had any detectable effect on the developing vasculature of *eng*^{mu130} mutant embryos. However, when used together in combination they efficiently reduced the vascular phenotype. These results indicate that the HHT- like phenotype in zebrafish *eng*^{mu130} mutants can be mitigated through modulation of VEGFA signalling and implicate synergistic targeting of ERK and mTOR

pathways as therapeutic strategy in HHT. The ability to combine subtherapeutic doses of these inhibitors might reduce the risks of toxicity while providing amelioration of the consequences of HHT.

I did not look more in depth at VEGFA expression levels before and after drug treatment. Thus, I have not demonstrated that signalling through these various pathways is increased *eng*^{mu130} embryos, nor have the drugs effectively inhibited the pathways of interest in this model. However, the dosing regimens were determined from the Ki values and the published literature. All the drugs used in this chapter were previously used to inhibit the respective signalling pathway in zebrafish embryos, strengthening the validity of why I chose these doses **[Table 2.5]**. Future work would focus on providing molecular evidence that these doses inhibit the targeted pathways. pERK immunostaining has been established in zebrafish (Shin, Beane et al. 2016). I hypothesise that pERK is upregulated in mutants, and therefore rescued with MAPK inhibition. I provided preliminary data to show that ERK is phosphorylated in the developing ISVs at 3dpf **[Figure 7.1].** This work is ongoing, and the immediate aim is further optimise this pERK experiment and to subsequently investigate pERK expression in *eng*^{mu130} embryos. Additionally, mTOR levels can be measured in zebrafish by monitoring pS6 expression (Diekmann, Kalbhen and Fischer 2015). Alternatively, qPCR for VEGFA and downstream signalling components would have been a more quantifiable way of testing VEGFA induction by these various drug treatments. This type of corroborating evidence would greatly strengthen conclusions in this chapter.

Furthermore, there is limited investigation into the overall effects on angiogenesis in response to these agents. It would strengthen this chapter to further prove that eng loss directly results in dysregulation of these pathways in vivo, and that drug treatment rescues defects without otherwise affecting embryonic/larval blood vessel development. I would approach this using an EC membrane stain such as CD31 to mark membranes and quantify cell size post phenotype rescue. Sugden and colleagues showed that DA and PCV dimeter increase is a result of EC cell changes (Sugden, Meissner et al. 2017). Therefore, rescuing EC cell shape changes would further ensure the mechanism of disease is rescued as well as the overall phenotype.

Finally, it is possible that some drug treatments halted or dramatically slowed angiogenesis. To investigate this, I measured drug toxicity looking at, presence of pericardial oedema, and overall embryo body size and trunk vasculature in response to all drug regimes. Any drug treatments that affected these parameters were omitted from these experiments. To further validate these finding other vascular beds should be monitored, for example, the head vasculature and the sub-intestinal vessels should be imaged to ensure they develop normally through development.

4.7.4 GS4012 treatment between 2-3dpf partially recapitulates the abnormal trunk phenotypes of *eng*^{mu130} mutants

GS4012 is a potent inducer of VEGF-mediated vessel formation in zebrafish (Peterson, Shaw et al. 2004). GS4012 treated embryos developed enlarged PCV and collapsed ISVs - recapitulating the abnormal trunk phenotypes of *eng*^{mu130} mutants. This data provides further evidence that the HHT-like phenotype is a result of deregulated/excess VEGF signalling. I infer from this data that the increased PCV diameter is a result of increased cellular footprint leading to vessel enlargement. To test this, an EC membrane stain such as CD31 could be used to mark membranes and quantify cell size. Furthermore, the *Tg(kdrl:EGFP;fli1:nGFP)*^{y7} line can be used to quantify EC number in the PCV. I hypothesise that, GS4012 treated embryos will show increased EC footprint in the PCV and EC cell number will be unaffected. This would confirm whether GS4012 treatment recapitulates the cellular mechanism as well as the vessel size phenotype.

Future GS4012 studies should be undertaken to dissect the role of VEGF in *eng* mutants. Currently this data is limited to recapitulating the *eng*^{mu130} mutant phenotype. In the future, *eng*^{mu130} mutant should be treated with GS4012 and the phenotype should be assessed. I hypothesise that this would exacerbate the HHT-like phenotype in *eng* mutants, potentially resulting in increased kugeln numbers, vessel calibre, and premature death.

4.7.5 Abnormal brain and trunk vasculature of *eng*^{mu130} zebrafish embryos is not prevented by Notch inhibition

Whilst there are other experiments with regards to the VEGF signalling pathway I would have liked to complete, I also moved my attention to the Notch signalling pathway. Previously, it was demonstrated that Notch inhibition results in excessive sprouting of ISVs leading to

malformations that resemble to those observed with ALK1 and *eng* mutants (Siekmann and Lawson 2007). It is therefore possible that notch influences the clinical outcome of HHT in patients although this has not been studied. The aim of this study was to use our zebrafish screening techniques to investigate if there is any evidence of crosstalk between eng/bmp10 and Notch signalling.

In agreement with previously reported data inhibition of Notch signalling by DAPT significantly reduced *kugel* number in wild types (Kugler, van Lessen et al. 2019), but did not significantly affect the kugel number in *eng*^{mu130} embryos**.** Likewise, DA or PCV vessel size in *eng*^{mu130} embryos following DAPT was unaffected. This data suggests that altered notch signalling is not involved in the HHT phenotype.

4.7.6 Future directions

Automated high throughput screening assays are now possible due to the development of liquid handling robotics and automated imaging systems. Burns and colleagues developed an automated microscopy assay for measuring the heart rate of embryos expressing GFP in the myocardium (Burns, Milan et al. 2005). This assay allows heart rate analysis of multiple embryos per well enabling a throughput of approximately 500 embryos per 96-well plate. Furthermore, they tested determined concentration-dependent effects of two proof of concept drugs over time, nifedipine and terfenadine. A wide range of conditions analysed in this thesis chapter can be quickly tested using systems like this, including heart rate and vessel diameter. Continued technological advances in imaging techniques and automated zebrafish screening platforms will increase functionality and effectiveness of the zebrafish model.

In this chapter, I studied the effects of PD0325901 and rapamycin on vascular abnormalities and kugel formation, but as yet there is no evidence to suggest that these inhibitors have any effects on heart size and retinal vessel malformations. Future work may focus on performing these experiments in adult homozygous *eng* mutants to assess the adult phenotype. However, currently the literature is limited to testing these to water-soluble compounds by adding them to the E3 growth media during development. Further work is therefore needed to develop a reliable protocol to expose adult zebrafish to these compounds.

5. The role of *endoglin* in other models of cardiovascular disease

5.1 Introduction

Endoglin regulates processes known to be protective after heart injury. The aim of this chapter is therefore to investigate the role of *eng* in response to a range of models of cardiovascular disease, including cardiac damage and diabetes. Firstly, I expose *eng*^{mu130} mutants to doxorubicin as a model of chemotherapy induced heart failure. I subsequently examine how doxorubicin treatment affects cardiac function and structure of *eng*^{mu130} mutants compared to wild types. Furthermore, I utilise a glucose-exposure model of diabetes mellitus to induce hyperglycaemia in *eng*^{mu130} mutants and examine the effects on the developing vasculature.

To investigate the role of *eng* in the heart regeneration response, I intended to use a cryoinjury model to induce cardiac damage. I planned to use this technique to induce cardiac cryoinjury in adult wild type and *eng*^{mu130} mutants and apply the established transgenic lines to examine the effect of the *eng* mutation on angiogenesis at the site of cardiac injury, and regeneration of the heart tissue. Preliminary work started on these experiments, but these studies were significantly curtailed by the effects of the pandemic (see COVID-19 mitigation statement).

5.2 *In vivo* cardiotoxicity induced by doxorubicin

Doxorubicin (DOX) is an anthracycline used to treat a range of cancers including breast cancer and leukaemia. The use of anthracyclines are limited by the risk of inducing cardiotoxicity, and patients treated with anthracyclines have a significantly increased risk of developing heart failure (Suter and Ewer 2013). Therefore, developing novel therapies to protect the heart during doxorubicin treatment is of great importance. This could benefit cancer patients by reducing the risk of cardiotoxicity and allowing the use of increased doxorubicin doses.

eng is expressed in endothelial cells, mesenchymal cells and myofibroblasts of the heart and regulates a range of processes known to be protective after heart injury (Jonker and Arthur 2002). The role of *eng* after cardiac injury is therefore of great relevance to developing therapies to treat cardiovascular disease. Previously, it was shown that administration of

chemotherapeutic drugs used in humans induces heart failure in embryonic zebrafish (Liu, Asnani et al. 2014). In this chapter, I utilise this model to investigate if *eng* mutants are sensitised to chemotherapy-induced heart failure.

Wild type zebrafish embryos were treated at 1dpf with 50, 100, and 150μM of doxorubicin (DOX). This timing was to ensure that the heart had initiated normal development, and blood circulation had started prior to DOX treatment. Embryos were treated for 48 hours from 1 to 3dpf and then assessed for signs of cardiotoxicity. The proportion of embryonic lethality was determined in DOX treated embryos **[Figure 5.1 B].** No lethal effect was observed in embryos treated with 50μM of DOX, while only 20% of embryos survived the full 48 hours of 150μM DOX exposure **[Figure 5.1 B]**. Examination under a bright field microscope revealed no evidence of pericardial oedema. To further assess heart function, heart rates were recorded. Changes in heart rate were found to occur in a dose-dependent manner, and a significant decrease in heart rate was observed in embryos treated with 100 and 150μM DOX compared to the DMSO control and thus blood cell circulation in the trunk, was significantly reduced in DOX treated embryos. 150μM of DOX induced approximately a 30% decrease in heart rate, suggesting cardiotoxicity **[Figure 5.1 C].** This data suggests that doxorubicin is toxic at high concentration (150μM).

Light sheet microscopy was used to visualise the trunk vasculature after 48 hours of DOX exposure. Representative images of the trunk vasculature in DOX and DMSO treated embryos are shown in **[Figure 5.1 A].** DOX treated embryos display no gross morphological differences during vascular development. However, more detailed visual assessment using Fiji image analysis software revealed altered DA and PCV sizes in the embryos treated with 100 and 150μM DOX in a dose-dependent manner. At 3dpf DA diameter was significantly reduced in embryos treated with 100μM and 150μM DOX, compared to DMSO control. Treatment with 100μM or 150μM of DOX induced a 15% or 30% decrease in DA diameter, respectively **[Figure 5.1 D]**. Furthermore, the PCV diameter was significantly increased in embryos treated with 100 and 150μM DOX, compared to DMSO control. 100μM or 150μM of DOX induced a 15% or 25% increase in PCV diameter, respectively **[Figure 5.1 E].**

Next, atrial area was calculated in wild type embryos ± 100μM DOX to assess heart function. Short time lapse videos of the hearts were recorded in vivo at 3dpf. Atrial area in systolic and

diastolic phases are shown **[Figure 5.2]**. At 3dpf, there was a significant decrease in diastolic atrial size in the DOX treated embryos compared with controls, suggesting heart function is impaired by DOX treatment. There was no significant difference in systolic atrial size in the DOX treated embryos **[Figure 5.2]**.

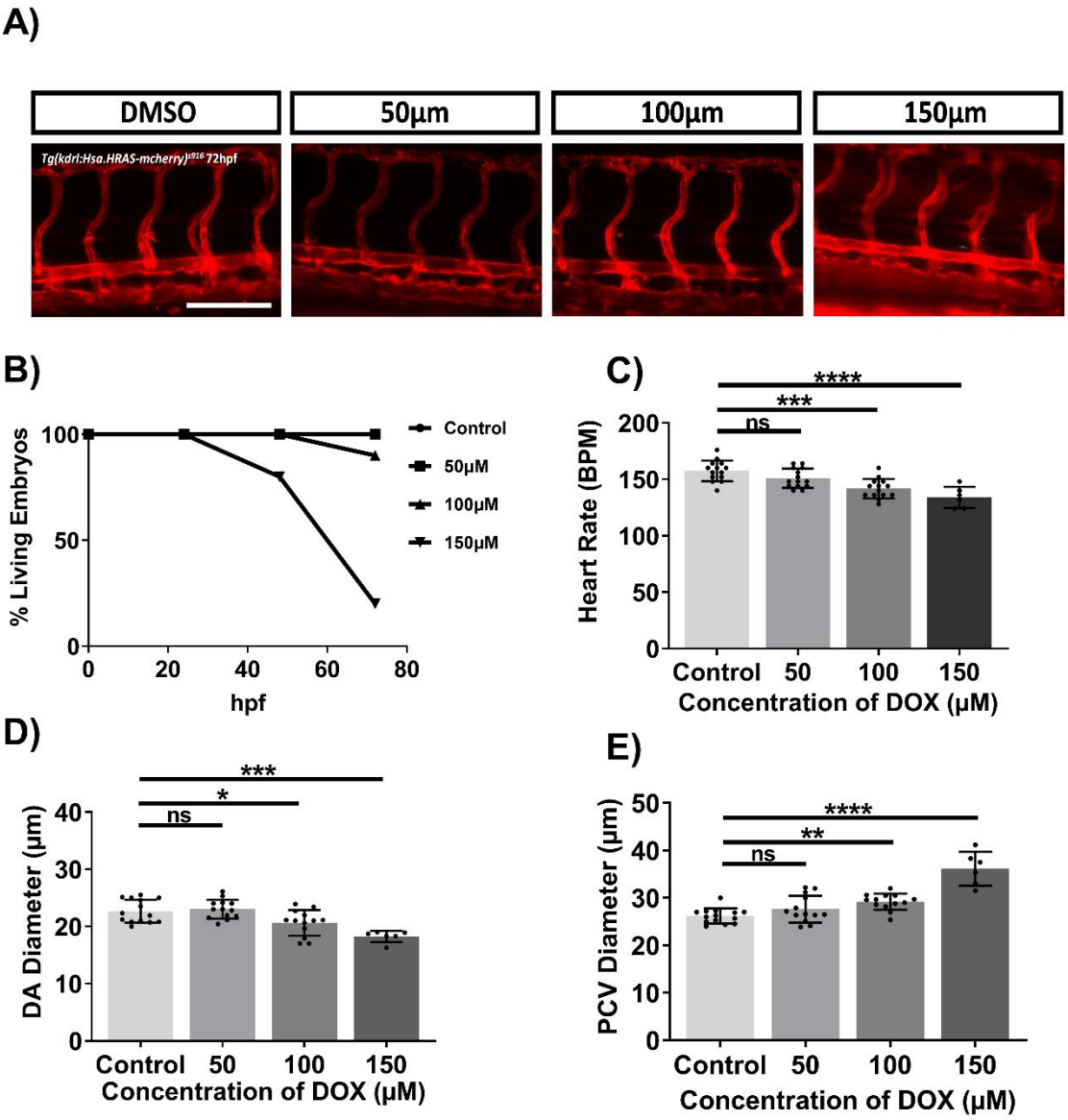

Figure 5.1 Optimisation of a doxorubicin-induced cardiomyopathy model in wild type zebrafish.

A) Representative maximum intensity projection of WT embryos ± DOX (50-150µM) treatment for 48h. Scale bar = 100µm. B) Survival rate of zebrafish treated with doxorubicin. Each point represents the mean average from 3 experimental repeats. C) Heart rate in WT embryos ± DOX treatment. D) DA diameter in WT embryos ± DOX treatment. E) PCV diameter in WT embryos ± DOX treatment. (One-way ANOVA with Tukey post-hoc test, 8-15/group.).

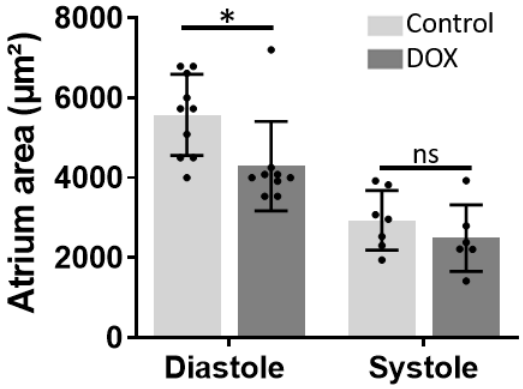

Figure 5.2 doxorubicin treatment reduces diastolic atrial area in embryonic zebrafish.

WT Atrium area of WT embryos ± 100µM treatment for 48h. (One-way ANOVA with Tukey post-hoc test, n=6-10/group.).

5.3 Investigating the role of *endoglin* in response to doxorubicin-induced cardiomyopathy

The changes in cardiac function, blood circulation and vasculature described above were used to assess if *eng* loss of function results in increased sensitivity to doxorubicin-induced cardiomyopathy compared with WT. At 100µM, doxorubicin caused small, but significant changes in survival rate, heart rate, DA diameter and PCV diameter in WT embryos. Indicating this dosage has the lowest observed adverse effect level (LOAEL) (Panzica-Kelly, Zhang and Augustine-Rauch 2015), 100µM of DOX was therefore chosen for the following experiments due to its mild, but significant, effect on cardiac function. Heterozygous adult *eng*^{mu130} mutants in a *Tg(Kdrl:eGFP)*^{s438} background were in-crossed to generated clutches of embryos that were predicted to have 25% homozygous mutations.

Embryos were treated for 48 hours with 100µM DOX and then assessed for signs of cardiotoxicity. Embryos were genotyped at the end of the experiment to ensure image acquisition and analysis was blinded. Heart rates of DOX treated embryos were reduced compared to their untreated siblings, which confirms the results from section 3.2.1. However, there was no difference in heart rate between *eng* mutant and wild type siblings after DOX treatment **[Figure 5.3 A]**. Furthermore, atrium area at 3dpf was unaffected by *eng* loss of function with and without 48h DOX treatment **[Figure 5.3 B].** Finally, there was no difference in DA and PCV diameter between *eng*^{mu130} mutant embryos treated with DOX compared to their untreated siblings **[Figure 5.3 C, D].** This data suggests that *eng* loss of function does not result in an increased sensitivity to chemotherapy-induced heart failure.

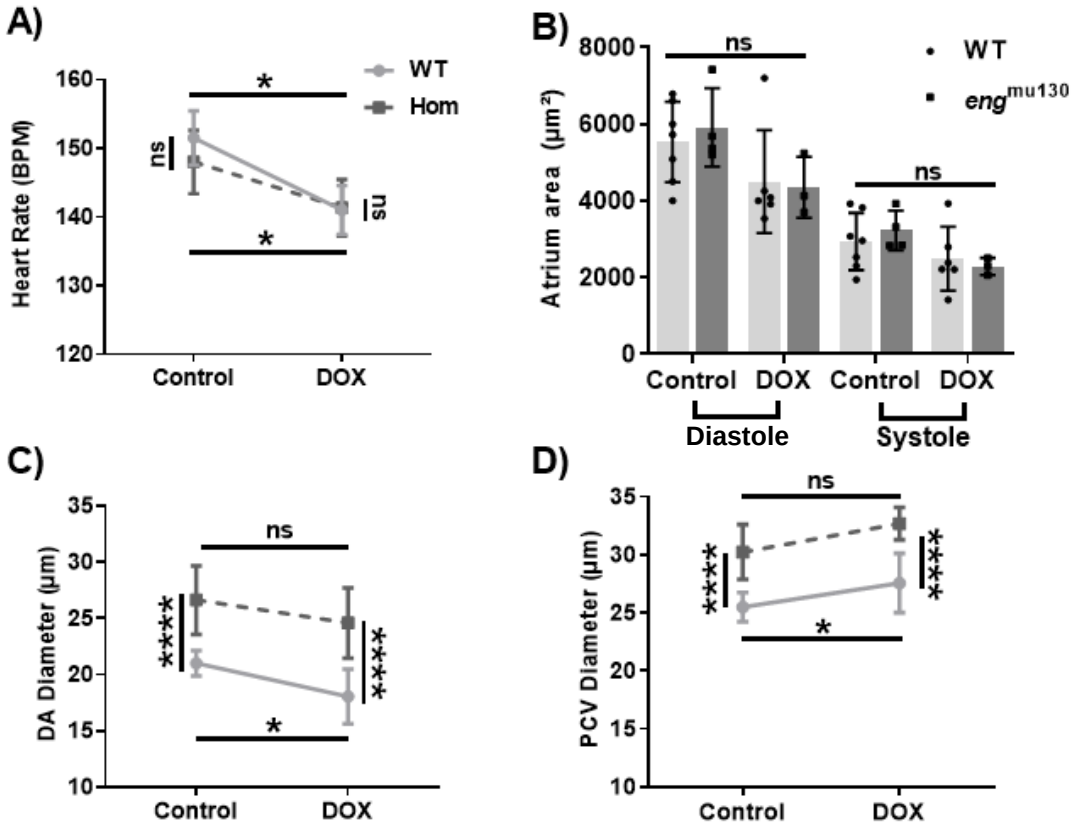

Figure 5.3 *eng*^{mu130} mutant embryos are not sensitised to doxorubicin-induced cardiomyopathy.

A) Quantification of heart rate in *eng*^{mu130} and WT embryos ± Doxorubicin (100µM) treatment for 48h. Data indicate there is no difference in heart rate in the *eng*^{mu130} compared to WT siblings. In both cases heart rate is significantly reduced following 48h treatment with 100µM doxorubicin. B) Quantification of atrium area in *eng*^{mu130} and WT embryos ± Doxorubicin (100µM) treatment for 48h. C) Quantification of DA diameter in *eng*^{mu130} and WT embryos ± Doxorubicin (100µM) treatment for 48h. D) Quantification of PCV diameter in *eng*^{mu130} and WT embryos ± Doxorubicin (100µM) treatment for 48h. (two-way ANOVA with Tukey post-hoc test, 8-10/group.).

I next set out to investigate if *eng*^{mu130} mutant embryos show impaired response/recovery to doxorubicin-induced cardiovascular damage. Firstly, to assess damage in response to DOX at 4dpf, embryos at 1dpf were treated for 72 hours with 100µM DOX and then assessed for signs of vessel damage. DA and PCV diameter was subsequently quantified at 4dpf. At 4dpf DA diameter decreased in *eng* mutants treated with DOX compared with their genotype matched untreated controls **[Figure 5.4 A].** Similarly, at 4dpf PCV diameter increased in both WT and *eng*^{mu130} treated with DOX compared with their genotype matched untreated controls, but this was only significantly different ($p<0.05$) in *WT* embryos **[Figure 5.4 B]**. *eng*^{mu130}mutants retained their characteristically increased DA and PCV diameters whether DOX treated or control treated.

To assess rescue of cardiac damage, WT and *eng*^{mu130} mutant embryos were exposed to DOX for 48h to induce cardiac damage, and embryos were transferred to E3 media for 24 hours. At 4dpf, embryos were assessed for rescue of vessel diameters. WT and *eng*^{mu130} mutant embryos showed complete rescue of vessel diameters **[Figure 5.4 C, D],** suggesting *eng*^{mu130} mutant embryos are able to recover from doxorubicin induced defects in a similar way to WT embryos.

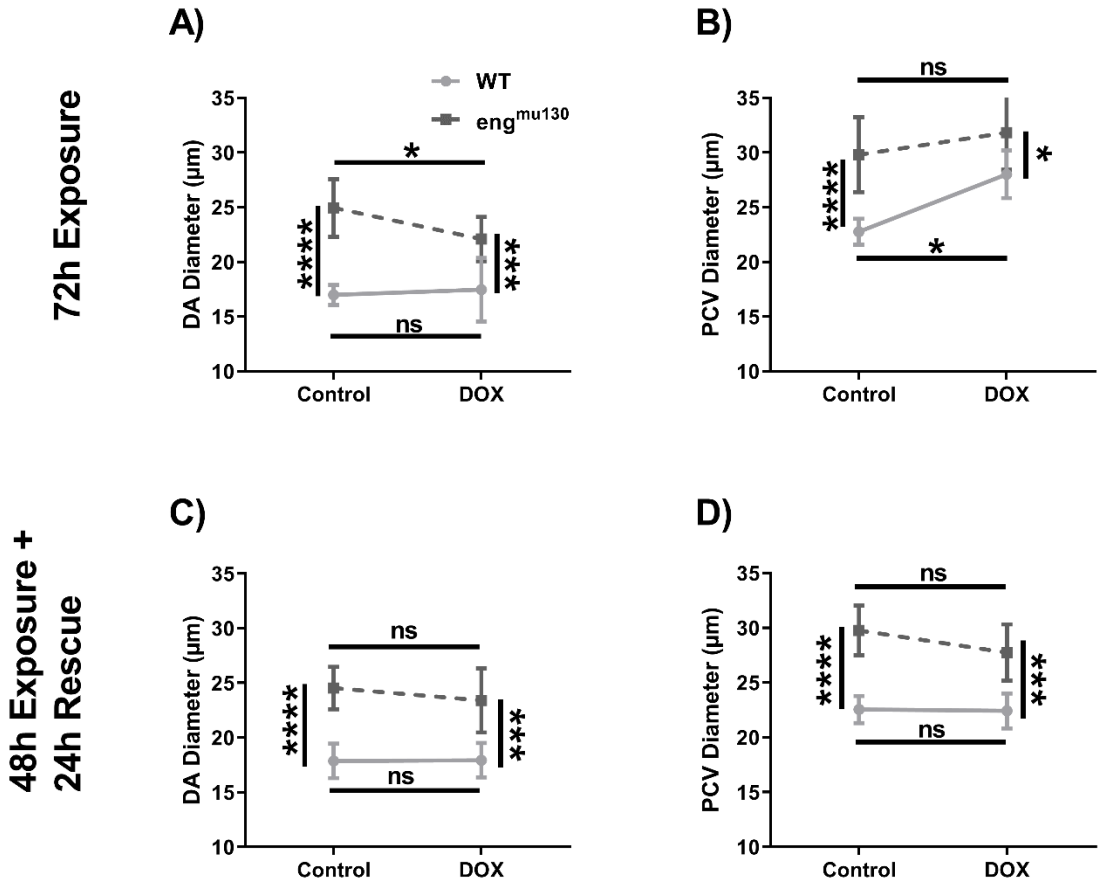

Figure 5.4 *eng*^{mu130} mutant embryos do not show impaired recovery of doxorubicin-induced effects

A) Quantification of DA diameter (4dpf) in *eng*^{mu130} and WT embryos ± Doxorubicin (100µM) treatment for 72h. B) Quantification of PCV diameter (4dpf) in *eng*^{mu130} and WT embryos ± Doxorubicin (100µM) treatment for 72h. C) Quantification of DA diameter (4dpf) in *eng*^{mu130} and WT embryos ± Doxorubicin (100µM) treatment for 48h, and 24h in E3 growth medium. D) Quantification of PCV diameter (4dpf) in *eng*^{mu130} and WT embryos ± Doxorubicin (100µM) treatment for 48h, and 24h in E3 growth medium. (two-way ANOVA with Tukey post-hoc test, n=12/group.)

5.4 Investigating the role of *endoglin* in response to glucose induced hyper proliferation

Diabetes is a metabolic condition characterised by chronic hyperglycaemia. Hyperglycaemia causes various vascular complications in diabetic patients such as atherosclerotic disease, retinopathy and nephropathy (Paneni, Beckman, Creager and Cosentino 2013). Hyperglycaemia leads to increased dicarbonyl methylglyoxal (MG), but it is currently unclear how MG affects the development of vascular complications *in vivo* (Bierhaus, Fleming et al. 2012). Previously, a zebrafish model for hyperglycaemia was described (Jörgens, Stoll et al. 2015). Hyperglycaemia induced by the addition of D-(+)-glucose in the E3 growth media increased MG concentrations in zebrafish embryos. This resulted in the development of vessel malformation sprouting from the ISVs, which resemble AVMs. Furthermore, it was reported that DA and PCV development was unaffected in this hyperglycaemia model.

I utilised this model to assess if *eng* loss of function results in sensitivity to hyperglycaemia induced vessel malformations. Zebrafish embryos were incubated in 55mM D-(+)-glucose starting at 1 hpf, and imaged using light sheet microscopy at 4dpf. Consistent with previously reported data (Jörgens, Stoll et al. 2015), glucose did not affect the development of major blood vessels. **[Figure 5.5 A]**. ISVs also developed normally with the exception of additional vessel branches developing out of ISVs **[Figure 5.5 A]**. These hyperbranches are small vascular structures that grow horizontally toward adjacent ISVs, and in some cases connecting to neighbouring hyperbranches. The response to D-(+)-glucose treatment was quantified by observing the percentage of ISVs in the region of interest that develop hyperbranches. Approximately 10% of untreated WT ISVs develop hyperbranches **[Figure 5.5 B]**, as consistent with previously reported data (Jörgens, Stoll et al. 2015). Furthermore, there was no significant difference in hyperbranches in *eng*^{mu130} siblings **[Figure 5.5 B]**. WT and *eng*^{mu130} mutant embryos developed a significant increase in ISV hyperbranches. However, there was no evidence that *eng*^{mu130} embryos developed a different number of hyperbranches than WT siblings branches **[Figure 5.5 B]**, suggesting *eng*^{mu130} mutant embryos do not show altered response to hyperglycaemic-induced vessel malformations.

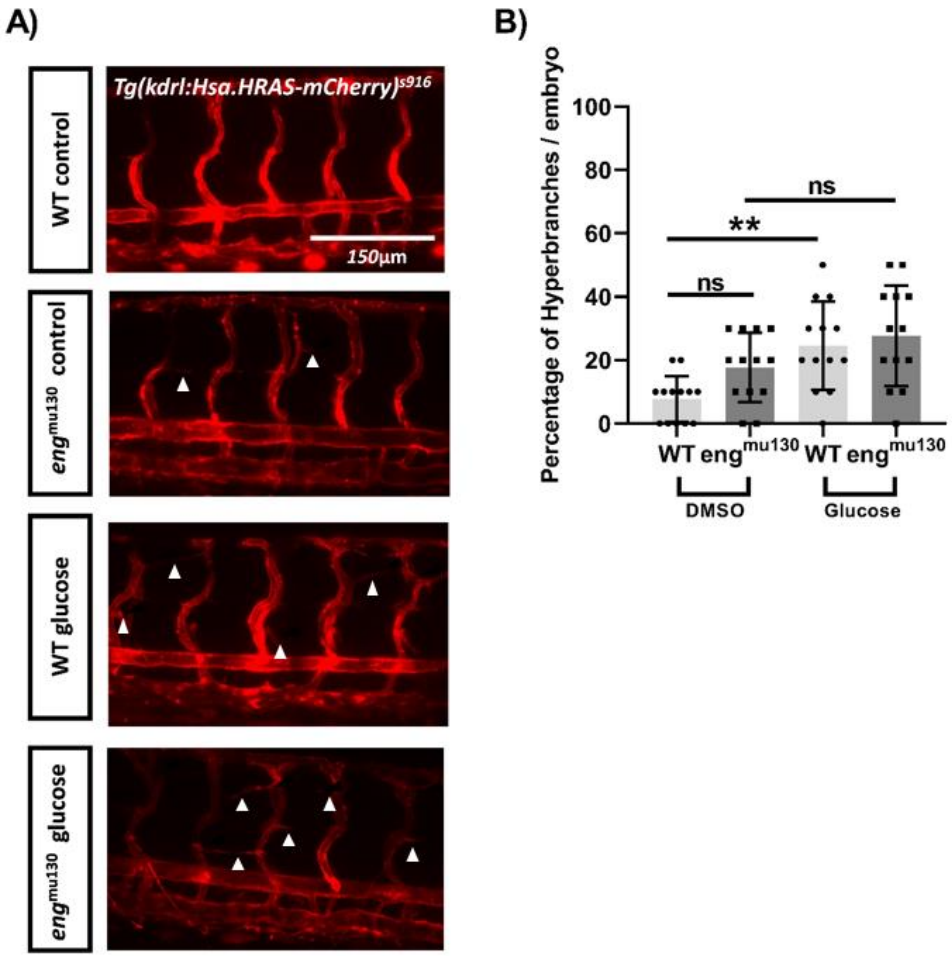

Figure 5.5 *eng*^{mu130} mutant embryos are not sensitised to the development of glucose-induced ISV hyperbranches.

A) Representative maximum intensity projection of *eng*^{mu130} and WT embryos ± D-(+)-glucose (55mM) at 1hpf until 4dpf. White arrows show the development of ISV hyper branches. B) Quantification of ISV vessel malformations at 96hpf. (Two-way ANOVA with Tukey post-hoc test, n=13/group.

5.5 Investigating the role of *endoglin* in adult cardiovascular development

I next set out to investigate the role of *eng* in the heart regeneration response. The aim was to use the cryoinjury model to induce cardiac damage in adult wild type and *eng*^{mu130} mutants. Preliminary work started on these experiments. I was trained in the technique in the lab of Dr Caroline Pellet-Many at the Royal Veterinary College London. Adult fish were raised to the appropriate age, culled, and uninjured hearts were dissected, sectioned and stained with AFOG as a control to investigate cardiomyocyte damage **[Figure 5.6**]. I utilised histological AFOG-staining of all cross-sections of the heart **[Figure 5.6]**. AFOG staining labels healthy muscle cells (orange), damaged cells with plasma (dark red), and collagen (blue). *eng*^{mu130} mutants showed no evidence of cardiomyocyte damage, but further data is needed to characterise cardiac development. I also completed preliminary work utilising the cryoinjury technique **[Figure 5.7]**. This shows example of an adult zebrafish heart with cardiac damage induced by cryoinjury utilising the *Tg(cmlc2:EGFP)* line (Huang, Tu et al. 2003) (line by Dr Caroline pellet-Many). Unfortunately, these experiments were not performed due to the closure of the aquarium and lab facilities for several months followed by reduced capacity meaning I could only access these facilities alternate weeks and so had to prioritise completion of studies in previous chapters.

The proposed plan for these experiments was to assess cardiac repair in WT and *eng*^{mu130} in response to cryoinjury. The cryoinjury procedure would be completed on 30 WT and 30 *eng*^{mu130} siblings at 6 months old. 5 Fish in each group would be culled at 1 day post injury (dpi), 7 dpi, 14 dpi, 30dpi, and 60 dpi. Furthermore, 5 fish in each group would be culled at 1dpi that were not exposed to the copper probe, this is known as a sham surgery and would be used as a negative control. Zebrafish would be sorted based on their phenotype at 3dpf and then raised in equal numbers. Genotyping would be performed at the end of experiment. All fish would be culled, and hearts dissected. Dissected hearts would be fixed and AFOG stained. Cardiomyocyte damage would be quantified at all time points to measure repair over the 60-day period. By 60 days, WT hearts should show complete regression of cardiomyocyte damage (González-Rosa and Mercader 2012). The hypothesis for these experiments is that eng^{mu130} would show impaired response to cardiac damage repair. Hypothetically, if these experiments confirm that *eng* mutants show impaired heart regeneration, this will raise the

question if this result is due to the mutation directly or secondary to other phenotypes such as AVM formation, small size etc. Further work could be done to investigate this, such as repeating this experiment at an earlier age before the adult phenotype develops e.g. at 3 months post fertilisation.

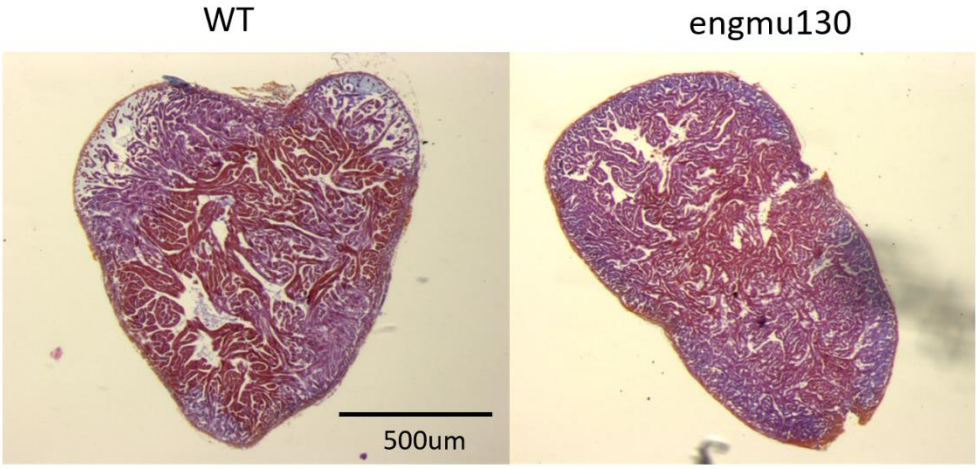

Figure 5.6 WT and *eng*^{mu130} mutant adult heart (150 days) sections.

Example sections of WT and *eng*^{mu130} mutant adult heart (150 days) stained with Acid Fuchsin Orange G, which labels cardiomyocytes in orange, fibrin in red and collagen in blue. n=3/group.

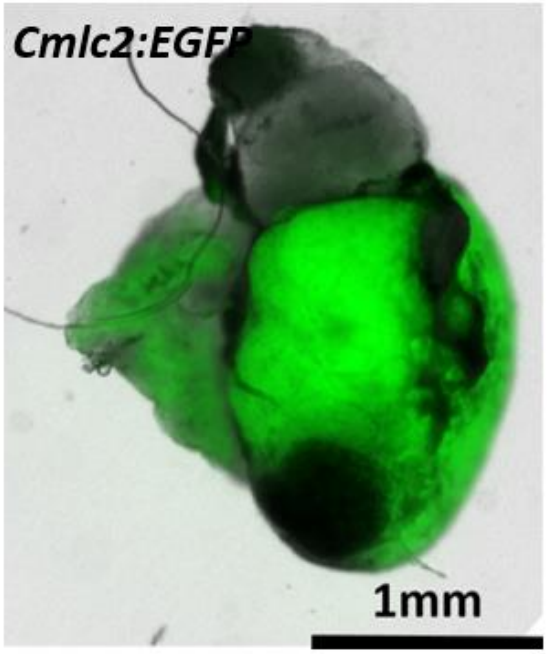

Figure 5.7 example of cryoinjury damage in *Tg(cmlc2:EGFP)* adult (6 Months) zebrafish. *Tg(cmlc2:EGFP)* adult zebrafish heart imaged approximately 1 hour post cryoinjury procedure.

5.6 Discussion

I have demonstrated that:

- *eng*^{mu130} embryos are not sensitised to doxorubicin induced cardiomyopathy.
- *eng*^{mu130} embryos display signs of ISV vessel malformations, which resemble AVMs.
- *eng*^{mu130} embryos are not sensitised to glucose-induced ISV hyperbranches.

One of the key aims of my PhD project was to ascertain the role of *eng* during the cardiovascular response to models of disease including cardiac injury and diabetes. To answer this, I needed a model to observe blood vessels and cardiovascular development response to damage *in vivo*. In this chapter, I utilised two possible models for inducing cardiovascular disease in zebrafish embryos, and presented preliminary data to assess response to cardiovascular damage in zebrafish adults but was unable to perform the cryoinjury studies planned.

I demonstrated reproducibly induction of chemotherapy-induced heart toxicity in zebrafish embryos. Changes in survivability, cardiac function, blood circulation and vascular calibre were detected in doxorubicin-treated embryos. These findings confirm that doxorubicin inhibits development of normal cardiac functions. The doxorubicin-induced cardiomyopathy model was therefore used to investigate if *eng*^{mu130} mutants are sensitised to chemotherapy-induced heart failure. Heterozygous adults with a *Tg(kdrl:Hsa.HRAS-mCherry)*^{s916} background were in-crossed by pair-mating to generate clutches of embryos of mixed wild type, heterozygous and homozygous mutants. Light sheet fluorescence microscopy was used to evaluate the role of *eng* in response to chemotherapy-induced heart failure. This data suggests that *eng* loss of function does not result in a sensitivity to chemotherapy- induced heart failure. Furthermore, I characterised the role of *eng* in response to glucose induced hyper proliferation. WT embryos developed a significant increase in ISV hyperbranches, but *eng* loss of function did not affect the development of hyperbranches.

5.6.1 Optimisation of a doxorubicin-induced cardiomyopathy model in zebrafish

in vitro human cell culture systems or *in vivo* mammalian models such as rodents are most often used to determine drug toxicity. However, research is limited due to the disadvantages of these model systems. For example, *in vitro* cell culture does not recapitulate the complexity

of whole organs in human patients, and *in vivo* methods are limited as they are expensive, low through-put, and ethically questionable. Zebrafish embryos therefore are a useful model organism as they overcome many of these limitations. Firstly, they can be used for high-throughput screening due to the large number of embryos that are produced during breeding techniques. Furthermore, their rapid development of complex organ systems reduces the experimental period, thus reducing cost and time constraints. In addition, zebrafish embryos are mostly transparent which allows real time imaging of the cardiovascular system. All the above arguments therefore support the use of zebrafish as an animal model for rapid screening of *in vivo* cardiotoxicity.

Embryos were treated for 48 hours and then assessed for signs of cardiotoxicity. The proportion of embryonic lethality was determined in DOX treated embryos, and the data suggested that doxorubicin is toxic at high concentration (150µM). Changes in survivability, cardiac function, blood circulation, and trunk vessel calibre were also detected in doxorubicin treated embryos. These findings confirm that doxorubicin strongly inhibits development of normal cardiac functions, which is consistent with previous reports (Liu, Asnani et al. 2014). However, examination under bright field microscope revealed no evidence of pericardial oedema. This is in contrast to what was reported by Liu and colleagues. It was reported that at two days after doxorubicin exposure embryos displayed “extensive pericardial oedema”. However, this was not quantified in the report, and therefore cannot be compared with data from section 5.2.

Further work is needed to further characterise cardiotoxicity in doxorubicin treated fish. This can be done by examining cardiac function directly. Imaging of fluorescent hearts *in vivo* can be used to assess cardiac functions such as fractional shortening, chamber size, and heart rate (HR). However, as discussed in chapter 3, this study is limited as it utilised 2D measurements of a 3d organ, and therefore the primary aim moving forward is to develop a robust method of quantifying cardiac volume in systole and diastole. Future work would also include whole-mount active caspase 3 antibody staining to quantify the level of apoptosis in the heart. I hypothesise that this will confirm that zebrafish recapitulate the cardiomyocyte apoptosis observed in patients treated with doxorubicin, and thus ensuring reliability of the doxorubicin-induced heart failure model.

At 3dpf, I found a significant decrease in diastolic atrial size in the DOX treated embryos compared with controls, suggesting heart function is impaired by DOX treatment. There was no significant difference in systolic atrial size in the DOX treated embryos **[Figure 5.2]**. Interestingly, reduction of diastolic volume but not systolic suggests impairment of relaxation not contraction. This is analogous to heart failure with preserved ejection fraction (Murphy, Ibrahim and Januzzi 2020). This therefore supports doxorubicin treatments as a model for chemotherapy induced heart failure. Future work would focus on characterising ejection fraction in our models to confirm this data. Ejection fraction of *eng*^{mu130} mutants and wild types can be measured by echocardiography at 3dpf (Gao, Ren et al.2016).

5.6.2 endoglin mutant embryos are not sensitised to doxorubicin-induced cardiomyopathy

eng is required to maintain normal development of embryonic vasculature. Loss of function results in vasculature malformations in trunk and cranial vascular beds, as well increased *kugel* formation. I therefore hypothesised that *eng*^{mu130} mutants will be sensitized to chemotherapy-induced heart failure. The changes in cardiac function, blood circulation and vasculature described in section 4.2 were easily detected and reliable. Doxorubicin was therefore used to assess if *eng* loss of function results in sensitivity to chemotherapy-induced cardiomyopathy.

Embryos were treated for 48 hours and then assessed for signs of cardiotoxicity. The proportion of embryonic lethality was determined in DOX treated embryos, and data suggested the *eng*^{mu130} mutants were not sensitised to the toxic effects of doxorubicin. Likewise, heart rate and vessel diameter were unchanged in *eng*^{mu130} mutants. This data suggests that *eng* loss of function does not result in a sensitivity to chemotherapy- induced heart failure.

5.6.3 endoglin mutant embryos are not sensitised to the development of glucose-induced ISV hyperbranches

A hyperglycaemia model induced by the addition of D-(+)-glucose in the E3 growth media was previously described (Jörgens, Stoll et al. 2015). This resulted in the development of vessel malformation sprouting from the ISVs, which resemble AVMs.

Firstly, the number of hyperbranches in the embryonic trunk vasculature was quantified in untreated embryos. *eng*^{mu130} mutants showed increased hyperbranching in trunk vessels compared to WT siblings. It could therefore be argued that this is a result of increased glucose sensitivity in *eng*^{mu130} mutants. Embryos were subsequently treated for 72 hours with D-(+)-glucose and then assessed for signs of hyperbranching. Glucose treatment increased the amount of ISV branches in WT embryos, however, the data suggested the *eng*^{mu130} mutants were not sensitised to D-(+)-glucose treatment.

Glucose increases osmotic pressure in aqueous solutions. Therefore, additional experiments in the presence of mannitol should be performed as an osmotic control. However, previous reports suggest that mannitol does not affect the zebrafish embryonic vasculature (Jörgens, Stoll et al. 2015), suggesting the results observed in section 5.4 are not due to an increased osmotic pressure.

This data is limited to chemical models of diabetes mellitus (T2DM) in zebrafish embryos. The *glyoxalase1* (*glo*$^{1-/-}$) knockout model is a robust genetic model of T2DM (Wiggenhauser, Kohl et al. 2017). In this study they used CRISPR-Cas9 to knockout *glyoxalase1,* while simultaneously inducing hyperglycaemic conditions. Mutants were raised to adulthood and assessed for T2DM. Mutants showed increased MG levels and reduced tolerance to glucose. In the future, a double mutant of glyoxalase1 and *eng* would be interesting to assess the role of *eng* in response to diabetes in adult zebrafish.

5.6.4 Future work

Adult zebrafish are capable of heart regeneration after cardiac injury. Several mechanisms are essential to drive this regeneration process, including angiogenesis to provide adequate blood flow to the affected area (Kim, Wu et al. 2010). However, the role of *eng* in zebrafish heart regeneration remain uncharacterised. I therefore hypothesised that cardiac repair will be impaired in *eng* mutants. In order to investigate the role of *eng* in the heart regeneration response, I planned to use a cryoinjury model to induce cardiac damage.

Preliminary work did start on these experiments. I was trained in the technique in the lab of Dre Caroline Pellet-Many at the Royal Veterinary College London. Adult fish were raised to the appropriate age, culled, and uninjured hearts were dissected, sectioned, and stained with

AFOG as a control to investigate cardiomyocyte damage **[Figure 5.6**]. I also completed preliminary work utilising the cryoinjury technique, Figure 5.4 shows an example of an adult zebrafish heart with cardiac damage induced by cryoinjury.

Future directions should focus on assessing the role of *eng* in response to cryoinjury. Infarct size can be measured at different time points after cryoinjury. Damaged cardiomyocytes can be distinguished as they appear as deep red in AFOG stained sections. Cardiac damage can be monitored over a 30-60 day period to assess recovery in WT and *eng*^{mu130} mutants. I hypothesise that *eng* loss of function will affect the recovery of cardiac tissue, and coronary vasculature will present with malformations, which resemble AVMs.

Furthermore, apoptosis in heart sections should be quantified as an additional assessment of cardiomyocyte damage and repair. For example, a TUNEL assay at different time points after injury could be performed to quantify apoptotic cells. I hypothesise that there will be a significant increase in apoptotic cells following cryoinjury, which will recover by approximately 30 days post injury in WT animals.

The zebrafish is powerful model to study heart regeneration, but its limitations must be appreciated. Currently, assessment of cardiac damage is limited to imaging fixed tissue analyses of explanted tissue, and thus it is impossible to image the same animal over time. In the future it may be possible to implement new imaging techniques to assess heart regeneration *in vivo* in the same sample. For example Koth and colleagues, developed a non-invasive magnetic resonance imaging (MRI) method, which included a respiratory and anaesthetic set-up for live adult zebrafish (Koth, Maguire et al. 2017). They also demonstrated that this method can be used to image scar formation in the same animal over time.

6. Conclusions and future work

6.1 Summary

The first aim of this project was to characterise the function of *eng* in zebrafish cardiovascular development. As hypothesised, the *eng*^{mu130} mutant zebrafish display abnormal cardiovascular development. Adult *eng*^{mu130} fish developed abnormal phenotypes, including skin AVMs, retinal vascular abnormalities, and an enlarged heart – recapitulating the human HHT disease. Here it was also confirmed that mutations in *eng* affect embryonic trunk vasculature throughout development. No change in heart function was detected in the *eng*^{mu130} mutant line, but vessel calibre changes in the basilar artery were noted throughout development. Furthermore, increased endothelial *kugel* formation was observed in *eng* mutants. This is the first evidence that *eng* KO leads to vessel deformities in the embryonic cranial vasculature, and is the first work first work that implicates *kugel* formation in a model of human disease.

My second aim was to investigate the interaction between BMP9/BMP10 and VEGFA signalling in zebrafish embryonic development. I demonstrated that AV951, a VEGF receptor tyrosine kinase inhibitor, prevented development of the abnormally enlarged major vessels and normalised the number of *kugeln* in *eng*^{mu130} embryos. Furthermore, Inhibiting also TOR or MEK prevented the abnormal trunk and cerebral vasculature embryonic phenotype. Finally, combining subtherapeutic doses of TOR and MEK inhibitors prevented the vascular phenotype, suggesting a combination of low dose MEK and TOR pathway inhibitors as a therapeutic strategy in HHT. A graphical summary of these results are shown in **[Figure 6.1].**

Finally, the third aim of this project was to characterise the function of *eng* in response to models of cardiovascular disease. I utilised two models of cardiovascular disease – a chemotherapy induced heart failure model and diabetes mellitus model. These results suggest that *eng*^{mu130} mutants are not sensitised to cardiac damage. Preliminary work started on a third model of cardiac damage, but these studies require further experimentation.

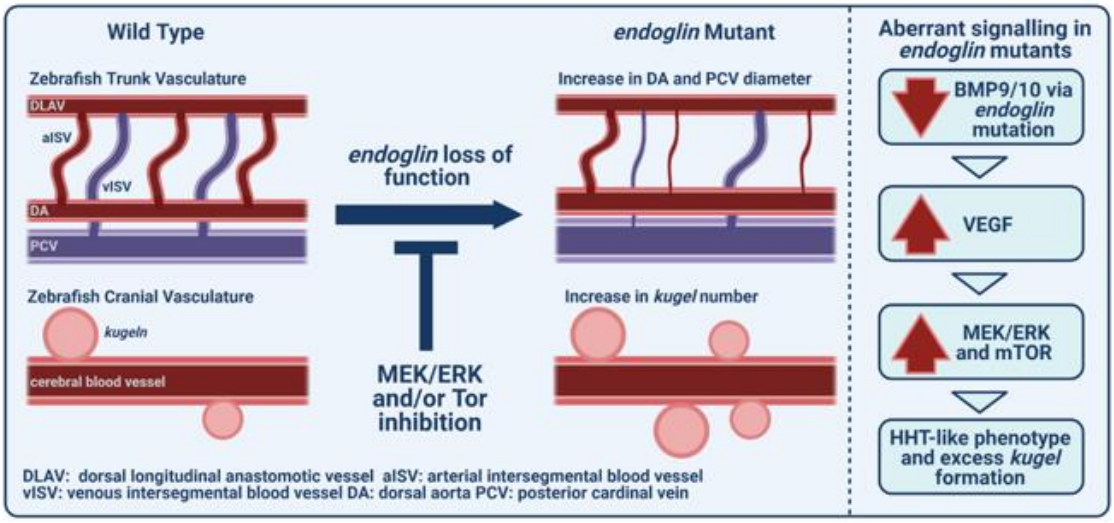

Figure 6.1 Graphical summary of the main findings of chapter 3 and 4.

eng^{mu130} embryos had an enlarged basilar artery (BA), and increased formation of endothelial *kugeln* on cerebral vessels. TOR and/or MEK inhibition prevented development of the abnormally enlarged major vessels and normalised the number of *kugeln* in *eng*^{mu130} embryos, suggesting synergy between TOR and MEK/ERK signalling pathways.

The results of each experiment and suggested future work is discussed in the relevant chapters above. In this chapter the overall findings, overall limitations, and additional further work will be discussed.

6.2 Overall limitations

The zebrafish allows real time imaging of the vasculature following *eng* loss of function. It therefore offers great promise to investigate the cellular and molecular events that lead to AVM formation. Furthermore, it is a useful model for drug screening to develop therapeutics that may help treat cardiovascular diseases such as HHT. Zebrafish also offer further advantages such as low cost and practical simplicity. There are therefore many compelling arguments for using the zebrafish model to study cardiovascular disease and development, but the limitations of the zebrafish model must be discussed. For example, zebrafish are not as closely related to humans as traditional mammalian model organisms such as rodents. This is important because in order to draw conclusions from animal models of genetic disease there must be a high degree of evolutionary conservation. For example, approximately 90% of human genes have orthologues in rodents, whereas this number is approximately 70% in zebrafish (Howe, Clark et al. 2013). Furthermore, zebrafish, like many teleost fish, are believed to have experienced a partial genome duplication event, which makes studying certain genes more complicated due to the presence of paralogous genes. Zebrafish have two paralogous loci chromosome 5 containing the *eng* gene. However, following the duplication event, there was most likely a gene loss event on the paralogous chromosomes resulting in one functional *eng* orthologue in zebrafish (Sugden, Meissner et al. 2017). Sugden and colleagues, confirmed that the eng^{mu130} mutant line used in this project has complete *eng* loss of function.

A further limitation is that adult zebrafish are capable of heart regeneration after cardiac injury and humans are not. This limits the application of the results that are discovered in this study, but it does allow a deeper understanding of the mechanisms behind heart regeneration, with the aim of one day stimulating similar regeneration in human patients. For these reasons, any findings in zebrafish would benefit from further validation using mammalian models such as rodents or human cell culture where possible. However, BMP9/10 signalling is highly conserved in zebrafish, and there have been multiple studies that show that the zebrafish is an appropriate model organism to study HHT (Roman, Pham et al. 2002,

Corti, Young et al. 2011, Sugden, Meissner et al. 2017, Capasso, Li et al. 2020). Furthermore, the zebrafish, as an *in vivo* model, allows visualisation and therefore simple analysis of angiogenesis. This allows observation of blood vessel formation and development in response to each experimental assay. I believe that the zebrafish is therefore a powerful in *vivo* model for studying vascular development, which is fundamental reason why I have utilised the zebrafish model throughout this work.

There are further limitations of utilising zebrafish as a drug screening model. Firstly, the most popular method of drug delivery is through dissolving the chemical in E3 growth media. This means that chemicals with poor solubility cannot be used in these studies. It is possible to inject zebrafish embryos, but this limits the range of drugs that can be tested at high-throughput. Another variable that should be considered is drug penetrance. The zebrafish embryos absorb the chemicals from the E3 growth media, but there may be some variability in penetrance between chemicals. It is therefore difficult to establish an appropriate concentration to use in these experiments. To address this, there were multiple rounds of preliminary experiments to establish a range of doses that can potentially rescue the *eng* mutant phenotype for all drugs used in this project. It is also important to establish if the drug is causing any off-target toxic effects. For example, in the case of AV951 death rate, heart rate and general morphology was assessed to ensure the concentration of AV951 in this study did not induce toxic effects. Future work should ensure all drugs used in this project comply with this toxicity assessment.

The work in this thesis utilises one knockout model of the *eng*. A secondary model of *eng* loss of function can be used to assess the role of *eng* function in zebrafish cardiovascular development. For example, morpholino oligonucleotides (MOs) have been used in zebrafish as a stable but transient form of gene knockdown for many years (Nasevicius and Ekker 2000). The use of morpholino oligonucleotides in zebrafish research have led to many great insights into gene function. However, there are several limitations of MOs, including that they may have off target effects and may activate p53 leading apoptosis knockdown (Nasevicius and Ekker 2000). The TALEN-induced mutant used in my work is a published model of HHT, ensuring the validity of using this model in this project.

6.3 Future work

HHT is characterised by vascular deformities, such as telangiectasias and arteriovenous malformations (AVMs). These malformations can form in lung, liver or brain, leading to severe symptoms and increased morbidity. Endoglin is expressed on endothelial cells, and studies using mice and zebrafish have confirmed that endoglin function protects against AVM formation. Furthermore, it is predicted that AVMs have an arterial origin, but this has not yet been formally tested and it is not known whether the protective role of endoglin is arterial or venous-specific. To test the venous specific role of endoglin, the Apj-Cre-ERT2 mouse line, which is expressed in venous and capillary endothelial cells can be utilised. This will allow the depletion of endoglin specifically in these cells. The incidence of AVMs in the neonatal retina will then be compared with wild type siblings. Previously reported data shows that retinal AVMs is unaffected by venous specific endoglin depletion, and the incidence is similar to that occurring in neonates where endoglin is depleted in all endothelial cells (Singh, Redgrave, Phillips and Arthur 2020). I hypothesise that endoglin is required in venous endothelial cells, but not in arteries, to protect against AVM formation and maintain vessel calibre.

One of the key findings in this project is that combining subtherapeutic doses of TOR and MEK inhibitors prevented the vascular phenotype. The ability to combine sub-therapeutic doses of these inhibitors might reduce the risks of toxicity, while providing amelioration of HHT symptoms. A limitation of this work is that all of this data was found using the relatively high-throughput drug screening zebrafish model. Previously, a comparative analysis of the *in vivo* responses of zebrafish, rat, dog and human to three cardiovascular drugs, propranolol, losartan, and captopril was published (Margiotta-Casaluci, Owen, Rand-Weaver and Winter 2019). They showed that zebrafish and human responses were comparable in approximately 80% of drug combinations. This study clearly demonstrates the zebrafish can be used as an appropriate and robust model for screening cardiovascular drugs (Margiotta-Casaluci, Owen, Rand-Weaver and Winter 2019) However, confirming the data in this project in a mammalian model would strengthen these findings, and therefore, future work should focus on recapitulating these results in a traditional murine model.

The zebrafish is a proven model to study vascular disease mechanisms, including drug screenings and toxicology studies, particularly when complementing mammalian *in vivo* and

in vitro models. I believe the findings of this project are of value to the field of angiogenesis, HHT, and zebrafish vascular development. I believe that the discussed future experiments will be essential further elucidate the roles of endoglin in cardiovascular development, disease and repair.

7. Appendices

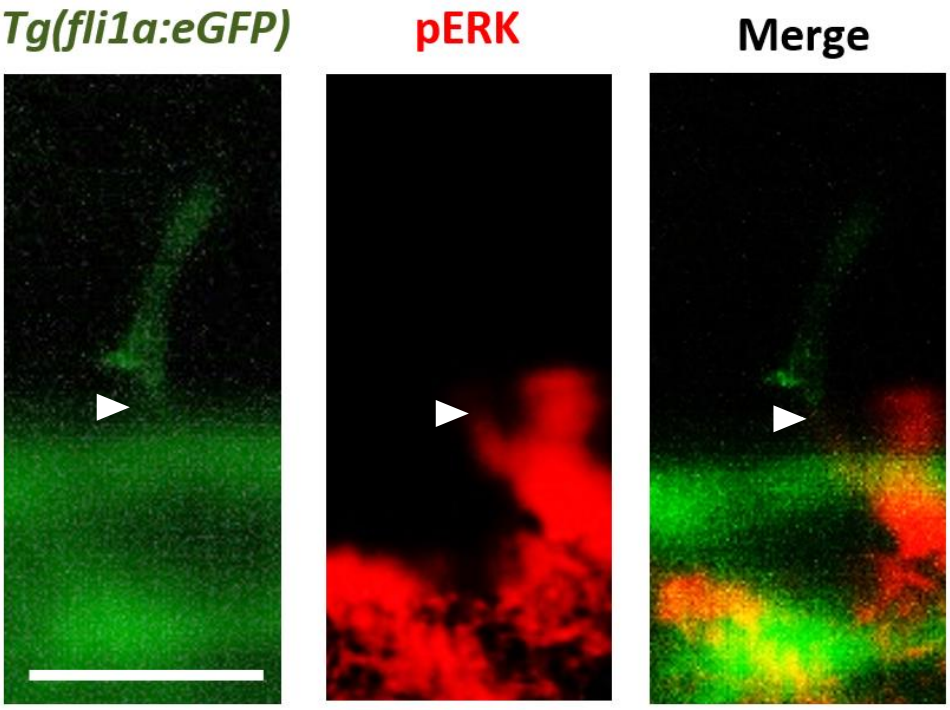

Figure 7.1 ERK is phosphorylated in developing ISV endothelial cells.

Representative maximum intensity projection of the region of interest. *Tg(fli1a:egfp)*^{y1} (green) labels EC cytoplasm, embryos were immunostained to detect pERK (red). Scale bar = 100µm. White arrows indicate overlap between ISV (GFP) and pERK.

genes

Review

Hereditary Haemorrhagic Telangiectasia, an Inherited Vascular Disorder in Need of Improved Evidence-Based Pharmaceutical Interventions

Ryan O. Snodgrass [1], Timothy J. A. Chico [1] and Helen M. Arthur [2,*]

[1] Department of Infection, Immunity & Cardiovascular Disease, Medical School, University of Sheffield, Sheffield S10 2RX, UK; rosnodgrass1@sheffield.ac.uk (R.O.S.); t.j.chico@sheffield.ac.uk (T.J.A.C.)
[2] Biosciences Institute, Centre for Life, Newcastle University, Newcastle NE1 3BZ, UK
* Correspondence: helen.arthur@ncl.ac.uk

Abstract: Hereditary haemorrhagic telangiectasia (HHT) is characterised by arteriovenous malformations (AVMs). These vascular abnormalities form when arteries and veins directly connect, bypassing the local capillary system. Large AVMs may occur in the lungs, liver and brain, increasing the risk of morbidity and mortality. Smaller AVMs, known as telangiectases, are prevalent on the skin and mucosal lining of the nose, mouth and gastrointestinal tract and are prone to haemorrhage. HHT is primarily associated with a reduction in endoglin (ENG) or ACVRL1 activity due to loss-of-function mutations. ENG and ACVRL1 transmembrane receptors are expressed on endothelial cells (ECs) and bind to circulating ligands BMP9 and BMP10 with high affinity. Ligand binding to the receptor complex leads to activation of the SMAD1/5/8 signalling pathway to regulate downstream gene expression. Various genetic animal models demonstrate that disruption of this pathway in ECs results in AVMs. The vascular abnormalities underlying AVM formation result from abnormal EC responses to angiogenic and haemodynamic cues, and include increased proliferation, reduced migration against the direction of blood flow and an increased EC footprint. There is growing evidence that targeting VEGF signalling has beneficial outcomes in HHT patients and in animal models of this disease. The anti-VEGF inhibitor bevacizumab reduces epistaxis and has a normalising effect on high cardiac output in HHT patients with hepatic AVMs. Blocking VEGF signalling also reduces vascular malformations in mouse models of HHT1 and HHT2. However, VEGF signalling is complex and drives numerous downstream pathways, and it is not yet clear which pathway (or combination of pathways) is critical to target. This review will consider the recent evidence gained from HHT clinical and preclinical studies that are increasing our understanding of HHT pathobiology and informing therapeutic strategies.

Keywords: BMP9/10; ENG; ACVRL1; VEGF; angiogenesis; arteriovenous malformation

Citation: Snodgrass, R.O.; Chico, T.J.A.; Arthur, H.M. Hereditary Haemorrhagic Telangiectasia, an Inherited Vascular Disorder in Need of Improved Evidence-Based Pharmaceutical Interventions. *Genes* **2021**, *12*, 174. https://doi.org/10.3390/genes12020174

Academic Editor: Rosemary J. Akhurst
Received: 4 December 2020
Accepted: 20 January 2021
Published: 27 January 2021

1. Introduction

Hereditary Haemorrhagic Telangiectasia (HHT) is an inherited vascular disorder affecting up to 1 in 5000 people. It is an autosomal dominant disorder and the vast majority of patients (>85%) have inherited one allele encoding nonfunctional endoglin (*ENG*) or activin receptor-like kinase 1 (*ACVRL1*, also known as *ALK1*) allele [1]. A minority of HHT cases are due to mutations in *SMAD4* or *BMP9* (*GDF2*), but these have somewhat different clinical presentations. SMAD4 patients have a combined Juvenile Polyposis–HHT syndrome, whilst BMP9 patients display a mild HHT-like phenotype [2,3]. This review will focus on the two major patient groups, HHT1 and HHT2 that are caused by loss-of-function (LOF) mutations in *ENG* and *ACVRL1*, respectively.

HHT1 and HHT2 patients develop very similar clinical symptoms that result from sporadic vascular malformations, with clinical diagnosis based on the "Curacao criteria". Patients with at least three of the following features are considered to have a definitive

diagnosis of HHT: (1) multiple mucocutaneous telangiectases, (2) recurrent nosebleeds, (3) visceral organ arteriovenous malformations (AVMs) and (4) a first degree relative with HHT. Where possible, this diagnosis is confirmed by genetic testing. Telangiectases are small arteriovenous connections found on the skin and mucosal surfaces and are prone to bleeding in the nose and gastrointestinal (GI) tract. In fact, epistaxis from nasal telangiectases is the most highly penetrant phenotype, present in almost all young adults with HHT, and anaemia may be sufficiently severe to necessitate regular iron or blood transfusions. Larger AVMs may be present in the lung, liver and neural tissues. HHT1 and HHT2 patients differ in the incidence of affected tissues, with AVMs in the lung and brain more common in HHT1, whilst a spectrum of hepatic vascular malformations including AVMs are more common in HHT2 [4,5]. The reasons for these differences are not yet known.

2. BMP9/10 Signalling

ENG and ACVRL1 proteins are expressed on the endothelial cell (EC) surface. They are also found in other cell types, for example, in fibroblasts, but overwhelming evidence from preclinical studies points to the critical nature of their *endothelial* role in protecting against vascular malformations in HHT [6]. LOF mutations in *ENG* and *ACVRL1* lead to disruption of bone morphogenetic protein 9/10 (BMP9/10) signalling. BMP9 (encoded by *GDF2*) and BMP10 are ligands of the TGFβ superfamily produced by the liver and right cardiac atrium, respectively, and released into the circulation in active forms [7–10]. ENG and ACVRL1 proteins have a high binding affinity for both BMP9 and BMP10 [11,12] that initiates signalling [13]. ENG has a large glycosylated extracellular domain that can form an ENG–BMP9/10 complex [14] and provides an EC surface reservoir of bound ligand [15]. To promote signalling, ENG forms a BMP9/ENG/ACVRL1 protein complex (or equivalent complex with BMP10 or potentially even a BMP9/10 dimer [16]). In this way, ENG acts as a coreceptor to promote BMP9/10 signalling through the signalling receptor kinase ACVRL1. ENG protein is released from the complex following recruitment of the type II receptor (either BMPR2 or ACTRIIB or ACTRIIA) which phosphorylates ACVRL1 kinase to activate and propagate the signalling cascade via activation of transcription factors SMAD1/5/8 (Figure 1). SMAD4 then associates with phospho-SMAD1/5/8 to form a SMAD transcription factor complex which shuttles to the nucleus to regulate genes that promote quiescence and migration. In parallel, TGFBR2/ALK5 stimulation following binding of TGFβ ligand results in phosphorylation of SMAD2/3. Phospho-SMAD2/3 then interacts with SMAD4 in order to move to the nucleus to regulate multiple genes including those that promote extracellular matrix secretion. Disruption of the BMP9/10 pathway leads to the endothelial cell defects seen in HHT and may be partly explained by a disrupted balance of BMP9/10 and TGF-β1 signalling pathways.

The critical importance of this pathway in HHT is confirmed by evidence from combined loss of BMP9 and BMP10 activities in mouse models that recapitulate the vascular malformations typical of HHT [17,18]. The requirement for loss of both ligands to generate AVMs pointed to functional redundancy. However, BMP10, but not BMP9, plays the critical role in maintaining normal vascular architecture in zebrafish [19,20]. Work in mice suggests some differences between BMP9 and BMP10 functions, where loss of BMP9 affects the lymphatic but not blood vasculature [21], and loss of BMP10 is embryonic lethal at E10.5 due to failure of heart development [8]. Replacing the murine BMP10 coding sequence with that of BMP9 partially rescues defects in heart development, but not sufficiently to survive to birth, pointing to an essential role for BMP10 in cardiogenesis [22]. Further investigations are required to interrogate the overlapping and different functions of BMP9 and BMP10 signalling in ECs in vivo, as they appear to be very similar in vitro [10]. Indeed, signalling outcomes may depend on type II receptor availability as BMP9 shows a preference for ACTRIIB over BMPR2, and low affinity for ACTRIIA, whilst BMP10 has similar binding affinity for all three type II receptors [23]. A better understanding of the roles of BMP9 and BMP10 in the vasculature would inform potential ligand treatment strategies to rescue

clinical features of HHT1 (see below). Moving downstream of the signalling pathway, the critical importance of the canonical SMAD1/5/8 pathway in protecting ECs against vascular malformations is shown by the HHT-like phenotype in SMAD4 LOF mutation patients [2], and by the retinal AVMs that develop in neonatal mice with endothelial loss of either SMAD4 or SMAD1/5 [24,25].

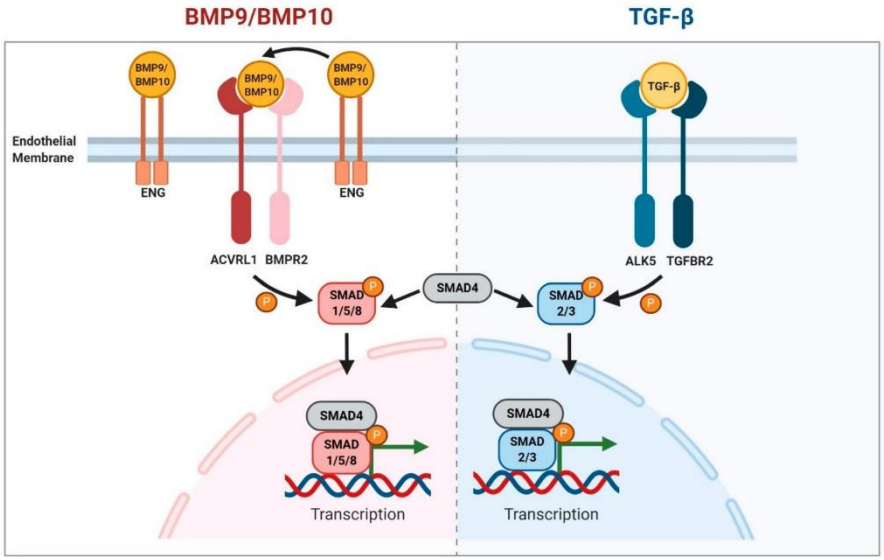

Figure 1. Schematic summary of BMP9/10 and TGFβ1 signalling pathways in endothelial cells. Figure created with BioRender (https://biorender.com/).

Whilst considering the role of this pathway in HHT, it is important to note that there is some confusion in the literature regarding the critical ligands that protect against HHT, because TGFβ1 and 3 were originally thought to be the primary ligands for the ENG/ACVRL1 pathway. As discussed above, it is now clear that BMP9 and BMP10 have much higher affinities for ENG and ACVRL1 proteins than TGFβ1. It is even possible that rather than TGFβ1 signalling being reduced following depletion of ENG or ACVRL1 protein activity, TGFβ1 signalling may actually be increased due to an imbalance between BMP9/10 and TGFβ1 signalling in ECs (Figure 1).

3. Aetiology of HHT Disease

Although there is a growing consensus that HHT is caused by reduced BMP9/10 signalling in ECs, it is not yet clear why the vascular lesions are localised to specific organs and tissues. Nasal telangiectases and nosebleeds seem to be the most highly penetrant feature affecting over 90% of young HHT adults. Dermal and GI telangiectases accrue later in adult life, whilst pulmonary and cerebral AVMs may be present from birth, usually reaching their final size by adult life [26,27]. The first point to emphasise here is that the majority of the vascular architecture in HHT1/2 patients appears to be normal, supporting the conclusion that one wild type allele (for *ENG* or *ACVRL1*) is sufficient for development, maintenance and function of the vast majority of the vasculature. Therefore, to explain the focal nature of vascular lesions, a local second genetic hit has been postulated, and recent evidence has indeed confirmed biallelic loss of *ENG* or *ACVRL1* gene function in dermal telangiectases from HHT1 and HHT2 patients [28]. This mechanism is yet to be confirmed in larger AVMs from HHT patients when such tissue becomes available. However, this

finding is entirely consistent with evidence from preclinical models that reproducibly develop AVMs when functional *Eng* or *Acvrl1* genes are deleted from ECs, but rarely when mice are heterozygous carriers of *Eng* or *Acvrl1* LOF mutations [6]. This second genetic hit event to generate *ENG* or *ACVRL1* null ECs will likely be a stochastic event that is entirely consistent with HHT vascular lesions that accrue with age such as dermal telangiectases.

If biallelic loss of *ENG* or *ACVRL1* drives the formation of sporadic vascular lesions in HHT, this only partly explains the phenotypic complexity of this disease. An explanation is also required as to the tissue location preference for AVMs and telangiectases. Considering the nasal telangiectases first, these lesions are the most highly penetrant defect in HHT1 and HHT2, and the nasal mucosal tissue is also an area of acute inflammation during frequent respiratory infections such as the common cold. Local inflammation would provide two additional stimuli that may be relevant to initiate telangiectasis formation. Firstly, inflammation triggers removal of the endothelial glycocalyx, and is associated with local release of inflammatory cytokines such as tumour necrosis factor-α (TNFα). This cytokine triggers events leading to cleavage of the extracellular domain of ENG protein, which is released as a soluble form into the circulation [29]. As HHT1 patients have baseline levels of 50% of the normal levels of ENG protein [30], then protein cleavage during inflammation may cause this to drop below the levels required to maintain the normal vascular architecture. It is interesting to note in this context that genetic variants of *ADAM17*, which encodes a major regulator of TNFα activity, are associated with pulmonary disease severity in HHT1 [31]. Secondly, inflammation resulting from infection or tissue injury generates a proangiogenic stimulus that has been shown in preclinical models to be required for AVM formation [6,32]. Organs that are frequently affected in HHT are all exposed to environmental and/or inflammatory insults. This is most obvious for the lung, skin, oronasal and GI tract. However, the liver is also exposed to blood draining from the gut which is rich in antigenic material including microbial debris. As a result, local inflammation is a normal part of liver homeostasis [33]. In addition, although cerebral tissue would normally be protected from environmental insults, there is an increased risk of embolic stroke and cerebral abscess caused by microthrombi passing through lung AVMs, even when these are small and clinically silent [26,27]. It therefore logically follows that there is an increased risk of proinflammatory microthrombi reaching the brain that may be insufficient to cause clinical stroke or abscess, but still provide sufficient pathophysiological proinflammatory trigger for vessel remodelling to form brain AVMs (BAVMs). Therefore, it may be no coincidence that lung and brain AVMs are both present in HHT1 patients more frequently than HHT2 patients. Furthermore, the variability of clinical symptoms even within the same HHT family carrying the same mutation (in *ENG* or *ACVRL1*) can be explained by this complex pathogenesis that depends on the timing of the second hit—a stochastic mutation event and/or exposure to an inflammatory or other environmental stimulus that promotes angiogenesis. Indeed, developmental angiogenesis may help drive the formation of congenital AVMs in the presence of biallelic *ENG* or *ACVRL1* LOF mutations. Ultimately, however, the precise reasons for the specific tissue distribution of vascular lesions in HHT remain to be uncovered in detail in future work.

Once an abnormal arteriovenous shunt is formed it becomes extremely challenging to reverse due to the increased blood flow. Added to this is evidence that loss of ACVRL1 signalling alters the endothelial response to shear stress [34,35]. Analysis of zebrafish embryos harbouring a LOF mutation in *acvrl1* showed increased EC numbers in cerebral arteries that further increased in response to blood flow to generate stabilised AVMs [35]. This increase in EC number to generate an AVM is not due to increased proliferation, but rather to reduced migration of ECs against blood flow leading to an accumulation of ECs that would normally have migrated towards the heart [36]. This reduced migration defect has also been confirmed in a mouse model of HHT1 [37]. In this way, due to a failure of normal EC migration against blood flow, congenital AVMs may further enlarge during developmental angiogenesis. Furthermore, additional local secondary events likely come into play as blood shunting via an AVM and bypassing a local capillary bed cannot

efficiently exchange oxygen leading to local tissue hypoxia. Low oxygen leads to a local increased expression of many genes, including VEGF, which potentially drives a positive feedback scenario in HHT causing further angiogenic stimulation and AVM expansion.

Another important contributory element to AVM formation is the disruption of crosstalk between ECs and pericytes. Following loss of ENG, there is reduced pericyte–EC contact that may affect vasoregulation and vessel stability in HHT. Evidence from mouse models of HHT shows reduced vascular smooth muscle coverage and reduced pericyte–endothelial integration leading to vessel instability [38,39]. Reduced pericyte number and coverage have also been reported in sporadic brain AVMs (BAVMs) [40], and may also be the case in BAVMs in HHT patients.

To summarise, in addition to genetic loss of *ENG* or *ACVRL1*, developmental angiogenesis, blood flow and local environmental triggers driving neovessel formation, such as hypoxia and inflammation, are critical players driving the formation of AVMs in HHT.

4. Overlapping Endothelial Cell Abnormalities in HHT and Spontaneous BAVMs

Although up to 5% HHT patients develop BAVMs, the majority of BAVMs in patients presenting at neurology clinics are spontaneous. There is an inherent high risk of haemorrhage from a BAVM which accounts for the majority of haemorrhagic strokes in young adults. This risk has driven major efforts to better understand BAVM pathobiology, and in light of recent progress in this area it is important to consider whether there are overlaps between the downstream molecular changes that give rise to spontaneous and HHT BAVMs. Recent seminal work has revealed that somatic activating mutations in *KRAS* are associated with the majority of spontaneous BAVMs [41]. These constitutively active (CA) *KRAS* mutations are present in ECs of spontaneous BAVMs in a mosaic fashion. This parallels evidence from a mouse model of HHT1, where mosaicism for *Eng* mutations in ECs is sufficient to generate AVMs [37]. Thus, only a proportion of ECs need to harbour a new mutant allele to develop AVMs in both HHT and in spontaneous BAVMs. In HHT, the new mutation is a loss of the second functional *ENG* or *ACVRL1* allele, whereas in spontaneous brain AVMs it is gain of a CA-*KRAS* mutation. It is striking that ECs with gain of KRAS activity or LOF *ENG* mutations both show elevated phospho-ERK activity, suggesting that this may be a common pathway associated with AVM formation [42,43]. Furthermore, as inhibiting MEK signalling can reverse established AVMs due to activated KRAS in the zebrafish model [42], this finding may be relevant to HHT (as discussed below). However, it is not yet clear whether the proproliferative role of the activated RAS/RAF/MEK/ERK pathway makes a direct contribution to AVMs [42]. Similarly, it is not known to what extent loss of the antiproliferative role of BMP9 signalling in the absence of ENG or ACVRL1 proteins drives the increased EC proliferation seen in telangiectases from HHT2 patients and in AVMs in preclinical models of HHT [17,44–47]. Nevertheless, the similarities in cellular responses in AVMs in HHT and spontaneous BAVMs suggest that scientific progress in these two fields may be mutually informative [48].

5. Treatment Options for HHT

There are currently limited options for treating HHT. To date, the majority of therapeutic approaches in severe disease have focussed on invasive procedures to cauterise bleeding telangiectases or occlude phenotypic AVMs (where accessible) to reduce disease symptoms or risk of complications such as stroke. Depending on the location of symptomatic vascular lesions and severity of symptoms, the feeding artery of an AVM can be physically occluded to prevent arteriovenous shunting of blood. This is frequently achieved by implantation of intravascular metal coils to occlude pulmonary AVMs to successfully restore blood oxygenation levels. However, access to symptomatic AVMs in the brain and liver is more challenging and presents a higher risk. Importantly, embolization of asymptomatic AVMs is not recommended in HHT. Liver transplant is recommended where hepatic VMs are sufficiently severe to cause high output heart failure. The advances in understanding the molecular and cellular defects that drive HHT and the availability of reproducible preclini-

cal models have driven further investigations to identify optimal pharmaceutical strategies to prevent or reverse established AVMs. Translation of these fundamental findings to the clinic ultimately depends on the availability of suitable safe drugs. These research efforts are summarised below and in Table 1.

Table 1. Pharmaceutical rescue of Hereditary haemorrhagic telangiectasia (HHT)-related phenotypes in patients and preclinical models.

Drug	Target	Number of HHT Patients	Outcomes	Reference
Bevacizumab (Avastin)	Anti-VEGFA antibody	24	Reduced epistaxis and improved cardiac function in liver VM patients with HOHF	[49]
Bevacizumab (Avastin)	Anti-VEGFA antibody	238	Reduced epistaxis	[50]
Tacrolimus (FK506)	Increased activation ACVRL1	24 (+24 placebo)	Reduced epistaxis	[51]
Pazopanib	TKI	7	Some improvement in Hb and epistaxis	[52]
Timolol	β-adrenergic blocking agent	28 (+28 placebo)	No change in epistaxis	[53]
Thalidomide	Increased PDGFB expression	7	Reduced epistaxis	[38]
Drug	**Target**	**Mouse Model**	**Outcomes**	**Reference**
Wortmannin, Pictilisib	PI3K inhibitor	*Acvrl1-iKOe* and *Eng-iKOe* neonates	Reduced retinal AVMs	[17,37]
Nintedanib and Sirolimus	TKI and mTOR inhibitor	Neonatal antibody blockade of BMP9/10	Combination therapy reduced and reversed retinal AVMs	[54]
DC101	Anti-VEGFR2 antibody	*Eng-iKOe* adult	Prevents AVMs and HOHF	[43]
G6.31	Anti-VEGFA antibody	*Acvrl1-iKOe* adult	Prevention of wound induced dermal AVMs; possible reversal of established wound AVMs	[55]
Sorafenib and Pazopanib analogue (GW771806)	TKI	*Acvrl1-iKOe* adult	Each drug alone significantly improved Hb and GI bleeding but did not prevent wound-induced skin AVMs.	[56]
SU5416	VEGFR2 inhibitor	*Eng-iKOe* neonate	Significant reduction in retinal AVM size	[37]
Thalidomide	Increased PDGFB expression	*Eng*+/− and *Acvrl1-iKO* adult	Increased SM coverage of dermal and cerebral vessels, reduced cerebral haemorrhage	[38,57]
LC10	ANGPT2 inhibitor	*Smad4-iKOe* neonate	Prevents retinal AVMs	[58]

Abbreviations: GI, gastrointestinal; Hb, haemoglobin; HOHF, high output heart failure; -iKO(e), inducible gene knockout (Endothelial Cell (EC)-specific); TKI, tyrosine kinase inhibitor. VM: vascular malformation; AVM: arteriovenus malformation.

5.1. Increasing Expression of ENG or ACVRL1 Genes

Using a myoblast cell line stably expressing an *Id1* reporter (C2C12BRA) to screen 700 FDA-approved drugs, Tacrolimus (also known as FK506 or Fujimycin) was identified as a potent activator of the BMP9-ACVRL1-BMPR2-SMAD1/5/8 signalling cascade [59]. This drug is widely used clinically as an immunosuppressant, for example, in organ transplantion, but has also been shown to increase *ENG* and *ACVRL1* expression [60]. Tacrolimus is also suggested to be useful in the treatment of pulmonary arterial hypertension (PAH), a disease associated with genetic defects in BMP signalling. Three end stage PAH patients all showed stabilized cardiac function and an increase in BMPR2 expression following Tacrolimus treatment [61]. A case report shows clinical improvements following Tacrolimus

therapy in an *ACVRL1* patient with a combined HHT PAH syndrome [62]. However, a recent randomised trial showed only minor effects of topical Tacrolimus nasal treatment on epistaxis [51] and further work is needed to evaluate this therapy in HHT.

Recent work has shown that ectopic expression of human/mouse ACVRL1 in mouse models of HHT1 and HHT2 can prevent AVMs [63]. Although this finding is in line with the recessive nature of LOF *ENG* and *ACVRL1* mutations in the presence of exogenous ACVRL1 expression, this type of approach is difficult to apply clinically. If Tacrolimus increases expression of the unaffected allele in HHT patients, this has the potential to be beneficial, but only if the vascular lesions in HHT are caused by haploinsufficiency. This may be true if a localised bout of inflammation led to a temporary loss of ENG or ACVRL1 protein, but if the majority of lesions arise from biallelic LOF mutations (due to the genetic two hit mechanism), this strategy would not be useful. Increased understanding of disease mechanisms in HHT patients is clearly essential and awaits genetic analysis of larger AVMs, as discussed above.

Patient-specific mutant allele correction using a CRISPR/Cas9 approach is possible in principle but is currently too high risk due to risk of uncontrolled off-target effects. In terms of a personalised gene therapy approach, patient-specific exon skipping has moved to clinical trials in genetic diseases such as Duchenne muscular dystrophy (DMD). This uses a therapeutic antisense oligonucleotide that allows the transcriptional machinery to bypass pathogenic DMD mutations in specific exons (amenable to exon skipping) to produce a slightly shorter but still partially functional dystrophin protein [64]. This approach is less likely to be useful for *ACVRL1* and *ENG*, where there are no known redundant protein regions. However, treatments enabling stop codon read-through [65] may be applicable to specific HHT1 and HHT2 patients where the disease-causing mutation is a premature stop codon in the *ENG* or *ACVRL1* coding region. This type of mutation leads to premature termination of translation and a truncated nonfunctional ENG or ACVRL1 protein. Although its efficacy is highly variable, stop codon readthrough is now under evaluation in clinical trials for some cystic fibrosis patients and may offer hope to those HHT patients with disease-causing nonsense mutations.

5.2. Increasing BMP9/10 Ligand Availability

As discussed above, HHT1 is likely due to a reduced level of BMP9/10 signalling through depleted ENG protein levels. Therefore, it may be possible to bypass the requirement for ENG and increase BMP9/10 signalling through ACVRL1 kinase by increasing the amount of circulating BMP9/10 ligand. Clearly, this approach would be ineffective to bypass local loss of ACVRL1 signalling kinase activity in HHT2. However, a major potential problem using exogenous BMP9/10 is the propensity of both these ligands to drive heterotrophic bone formation [10]. Some exciting progress has been made in reducing the osteogenic properties of BMP9 whilst maintaining its EC signalling properties [10] and potentially similar changes could be applied to BMP10, which may have a higher protective effect in HHT [20].

5.3. Targeting Proangiogenic Growth Factor Signalling

VEGF(A) signals through VEGFR2 receptor to activate a range of downstream pathways regulating cell metabolism, proliferation, survival and permeability (Figure 2). BMP9/10 signalling affects the endothelial cell's response to VEGF stimulation in at least two ways. First, BMP9/10 signalling prevents inactivation of PTEN, consequently inhibiting PI3K activity and reducing AKT activation responses. Second, downstream BMP9/10 signalling inhibits VEGF signalling outcomes in ways that remain to be defined but require a minimum of two hours, implying requirement for downstream gene expression [44]. In consequence, loss of BMP9/10 signalling leads to an untempered response of VEGF such as increased endothelial cell proliferation, which contributes to AVM formation. Drugs targeting VEGFA/VEGFR2 signalling and downstream mediators that have shown benefit

in HHT (patients and/or preclinical models) are indicated in Figure 2 and summarised in the table.

A marked improvement of HHT disease symptoms was noted when the anti-VEGF antibody Bevacizumab was used to treat cancer in an HHT patient [66]. This initial serendipitous finding led to the realisation that reducing VEGF activity was beneficial in HHT and was followed up by successful (nonrandomised) clinical trials showing improved cardiac function in HHT patients with hepatic VMs and reduced epistaxis [49,50]. A major caveat is that to be effective intravenous Bevacizumab is repeated over a substantial period and can incur significant side effects including hypertension, thrombosis and impaired healing. Targeting VEGF signalling has also been shown to be effective in protecting against AVM formation in many animal models of HHT [37,43,55]. However, VEGF signalling is complex and drives numerous downstream pathways, and it is not yet clear which pathway (or combination of pathways) is critical to target. Furthermore, there is limited understanding to date of the molecular interaction between VEGF signalling and BMP9/10 signalling, or how this is disrupted in HHT. Advances in this area are essential to optimise and improve therapies targeting VEGF signalling.

Multisite phosphorylation of the VEGFR2 receptor following VEGF ligand binding leads to activation of various signalling pathways that regulate EC proliferation, migration and adhesion, all of which are required to regulate normal angiogenic responses. These downstream pathways include the phospholipase Cγ (PLCγ)–ERK1/2 pathway, the PI3K–AKT–mTOR pathway and CDC42-p38 pathway (Figure 2). Although BMP9 is known to counter the proangiogenic effects of VEGF and act as a circulating vascular quiescence factor [12,67], it is not known how exactly this is achieved by crosstalk between BMP9/10 and VEGF signalling pathways. There may simply be increased circulating levels of VEGF in HHT patients [68], perhaps due to local tissue hypoxia (as discussed above) or to an altered balance of ALK5/ACVRL1 signalling [69] and it is this increased VEGF that disturbs the balance of VEGF signalling to generate AVMs. However, this systemic increase in VEGF would not in itself explain the localised nature of AVMs in HHT.

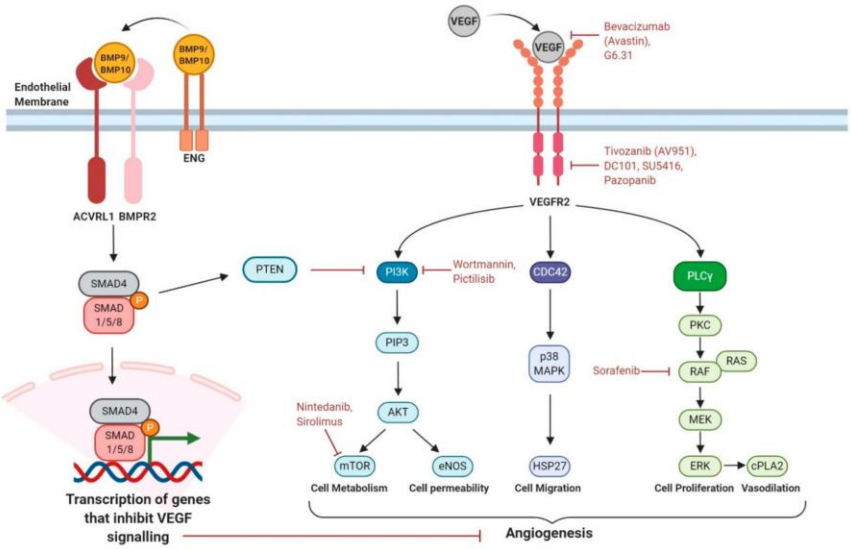

Figure 2. Schematic summary of crosstalk between BMP9/10 and VEGF signalling pathways in endothelial cells. Figure created with BioRender (https://biorender.com/).

EC-based studies in vitro have been used to interrogate the molecular interactions between BMP9/10 and VEGF signalling. BMP9 inhibits PI3K signalling by increasing activity of PTEN, a phosphatase that decreases PI3K activity [44]. In this way, localised loss of BMP9 signalling would drive a corresponding local increase in PI3K–AKT–mTOR signalling (Figure 2). Increased activation of PI3K is also seen when ACVRL1 levels are reduced either in HHT2 patients or mouse models of HHT2 and targeting PI3K can protect against AVM formation in the HHT2 neonatal mouse retina [17]. Important considerations limiting translatability of these findings are uncertainty over which PI3K isoforms are involved and clinically significant adverse effects of first generation PI3K inhibitors [70].

ECs lacking ENG protein show an increased rate of recycling of VEGFR2 to the plasma membrane which may contribute to enhanced downstream VEGF signalling [37]. Intriguingly, *ENG*-depleted ECs show reduced VEGFR2 expression compared with wild type cells, as well as reduced VEGFR2 phosphorylation in response to VEGF, yet still show increased ERK and AKT activation downstream of VEGF stimulation [43,71]. An added complexity is that a minimum of 2 h preincubation of cells with BMP9 can block VEGF stimulated cell responses, suggesting there are yet unidentified downstream factors involved in crosstalk between these two pathways [44]. These interactions are summarised in Figure 2.

As targeting VEGF with Bevacizumab requires intravenous delivery, some investigations have focussed on orally effective receptor tyrosine kinase inhibitors (TKI) used in oncology. These often target a broad range of growth factor receptors, and because HHT studies have recruited either few or single cases it is too early to conclude whether these provide a useful approach. The largest of these studies in seven HHT patients suggested that the TKI Pazopanib gave some benefit in reducing epistaxis [52]. Ongoing larger trials should provide firmer evidence in this area. In a preclinical model of HHT2, none of the 4 TKI drugs tested reduced wound-induced AVMs, but Sorafenib and a Pazopanib analogue (GW771806) did significantly improved gastrointestinal bleeding [56]. An interesting recent study has pointed to the power of a combination drug approach [54]. In mice with HHT (due to antibody blockade of BMP9/10) with the receptor TKI, nintedanib, together with the mTOR inhibitor, sirolimus, prevented as well as reversed retinal AVMs. This same drug combination reduced gastrointestinal bleeding and anaemia in an independent mouse model of HHT (inducible *Acvrl1*-deficient adult mice) [54].

In addition, VEGFR1 (also known as FLT1) acts as a natural decoy of VEGF signalling, trapping the VEGF ligand away from the VEGFR2 receptor. HHT2 mice show downregulation of VEGFR1 protein leading to enhanced VEGF signalling that will inevitably contribute to abnormal endothelial responses [46,72].

5.4. β-Blockers

Arteriovenous shunts are high flow abnormalities that deliver blood at high pressure into weak walled veins designed for low pressure flow. The small arteriovenous shunts in mucosal telangiectases are at high risk of rupture, likely on the venous side. Thus, blood pressure lowering medication may be beneficial. Propranolol, a nonselective β-blocker with antiangiogenic effects, has shown some benefit used topically on nasal telangiectases [73], although a double blind randomized placebo-controlled trial using topical application of the β-blocker Timolol showed no benefit on epistaxis [53].

5.5. Enhancing Pericyte–Endothelial Cell Interactions

Although Thalidomide was temporarily taken off the market following the tragic teratogenic outcomes when used to treat nausea in pregnant mothers in the 1960s, it has recently shown promise as a treatment for epistaxis in HHT [38,74]. Thalidomide has antiangiogenic effects by increasing EC–pericyte interactions. These cell–cell interactions are disrupted following endothelial loss of *ENG* or *ACVRL1* and Thalidomide appears to compensate for this to increase vessel stability. Mechanistic understanding of this effect is based on findings that loss of *Eng* in ECs leads to reduced crosstalk to adjacent muscle cells,

leading to reduced downstream paracrine TGFβ signalling [75]. The resultant reduction in vascular mural cell coverage in mouse models of HHT are rescued following increased *PdgfB* expression stimulated by thalidomide [38,57]. However, in addition to its teratogenic effects, thalidomide can induce irreversible neuropathy so less neurotoxic derivatives are now under investigation.

The angiopoietin–Tie2 pathway is also critical for maintaining vessel stability. Angiopoietin-1 (ANGPT1), produced by mural cells, activates the endothelial TIE2 receptor to maintain vascular smooth muscle cell (VSMC) coverage in mature blood vessels. Following an inflammatory stimulus, ANGPT2 is rapidly released by ECs and inhibits ANGPT1-mediated TIE2 activation, leading to destabilisation of the VSMC–endothelial interaction and pericyte detachment. Interestingly, endothelial loss of *Smad4* in mouse leads to increased *Angptl2* and downregulated *Tie2* expression. The endothelial-specific *Smad4* null mouse model of HHT has an increased EC footprint and retinal AVM formation that could be prevented by inhibiting ANGPT2 function with LC10 [58]. However, the link to HHT remains to be clarified as circulating levels of ANGPT2 have been reported as reduced in HHT patients [76].

6. Summary and Conclusions

Recent advances in understanding the biological basis of HHT and the development of a range of preclinical models for drug testing has led to a gear change in efforts to find effective treatments for HHT. Patient-specific therapies/personalised medicine options may be required depending on individual disease symptoms and mutations. If similar cellular and molecular changes cause both small telangiectases and larger AVMs, with just a difference in scale, it is also possible that treatments targeting epistaxis may be equally effective for attenuating AVM progression in major organs. Certainly, VEGF and its downstream pathways are a major focus of current investigations along these lines. Pharmaceutical treatment that could reverse the vessel remodelling in AVMs would be life changing for HHT patients with severe morbidities. Finally, with better understanding of the molecular and cellular defects in HHT lesions, there is real hope that effective therapies are on the horizon.

Author Contributions: R.O.S., T.J.A.C. and H.M.A. writing and editing. All authors have read and agreed to the published version of the manuscript.

Funding: R.O.S. is funded by an MRC DiMeN studentship; research in T.J.A.C. and H.M.A. laboratories is funded by the British Heart Foundation.

Institutional Review Board Statement: Not applicable.

Informed Consent Statement: Not applicable.

Data Availability Statement: Data sharing not applicable.

Conflicts of Interest: The authors declare no conflict of interest.

References

1. McDonald, J.; Wooderchak-Donahue, W.; VanSant Webb, C.; Whitehead, K.; Stevenson, D.A.; Bayrak-Toydemir, P. Hereditary hemorrhagic telangiectasia: Genetics and molecular diagnostics in a new era. *Front. Genet.* **2015**, *6*, 1. [CrossRef] [PubMed]
2. Gallione, C.J.; Repetto, G.M.; Legius, E.; Rustgi, A.K.; Schelley, S.L.; Tejpar, S.; Mitchell, G.; Drouin, E.; Westermann, C.J.; Marchuk, D.A. A combined syndrome of juvenile polyposis and hereditary haemorrhagic telangiectasia associated with mutations in MADH4 (SMAD4). *Lancet* **2004**, *363*, 852–859. [CrossRef]
3. Wooderchak-Donahue, W.L.; McDonald, J.; O'Fallon, B.; Upton, P.D.; Li, W.; Roman, B.L.; Young, S.; Plant, P.; Fulop, G.T.; et al. BMP9 mutations cause a vascular-anomaly syndrome with phenotypic overlap with hereditary hemorrhagic telangiectasia. *Am. J. Hum. Genet.* **2013**, *93*, 530–537. [CrossRef] [PubMed]
4. Bayrak-Toydemir, P.; McDonald, J.; Markewitz, B.; Lewin, S.; Miller, F.; Chou, L.S.; Gedge, F.; Tang, W.; Coon, H.; Mao, R. Genotype-phenotype correlation in hereditary hemorrhagic telangiectasia: Mutations and manifestations. *Am. J. Med. Genet. A* **2006**, *140*, 463–470. [CrossRef] [PubMed]

5. Lesca, G.; Olivieri, C.; Burnichon, N.; Pagella, F.; Carette, M.F.; Gilbert-Dussardier, B.; Goizet, C.; Roume, J.; Rabilloud, M.; Saurin, J.C.; et al. Genotype-phenotype correlations in hereditary hemorrhagic telangiectasia: Data from the French-Italian HHT network. *Genet. Med.* **2007**, *9*, 14–22. [CrossRef] [PubMed]
6. Tual-Chalot, S.; Oh, S.P.; Arthur, H.M. Mouse models of hereditary hemorrhagic telangiectasia: Recent advances and future challenges. *Front. Genet.* **2015**, *6*, 25. [CrossRef]
7. Bidart, M.; Ricard, N.; Levet, S.; Samson, M.; Mallet, C.; David, L.; Subileau, M.; Tillet, E.; Feige, J.J.; Bailly, S. BMP9 is produced by hepatocytes and circulates mainly in an active mature form complexed to its prodomain. *Cell. Mol. Life Sci.* **2012**, *69*, 313–324. [CrossRef]
8. Chen, H.; Shi, S.; Acosta, L.; Li, W.; Lu, J.; Bao, S.; Chen, Z.; Yang, Z.; Schneider, M.D.; Chien, K.R.; et al. BMP10 is essential for maintaining cardiac growth during murine cardiogenesis. *Development* **2004**, *131*, 2219–2231. [CrossRef]
9. Ricard, N.; Ciais, D.; Levet, S.; Subileau, M.; Mallet, C.; Zimmers, T.A.; Lee, S.J.; Bidart, M.; Feige, J.J.; Bailly, S. BMP9 and BMP10 are critical for postnatal retinal vascular remodeling. *Blood* **2012**, *119*, 6162–6171. [CrossRef]
10. Salmon, R.M.; Guo, J.; Wood, J.H.; Tong, Z.; Beech, J.S.; Lawera, A.; Yu, M.; Grainger, D.J.; Reckless, J.; Morrell, N.W.; et al. Molecular basis of ALK1-mediated signalling by BMP9/BMP10 and their prodomain-bound forms. *Nat. Commun.* **2020**, *11*, 1621. [CrossRef]
11. Castonguay, R.; Werner, E.D.; Matthews, R.G.; Presman, E.; Mulivor, A.W.; Solban, N.; Sako, D.; Pearsall, R.S.; Underwood, K.W.; Seehra, J.; et al. Soluble Endoglin Specifically Binds Bone Morphogenetic Proteins 9 and 10 via Its Orphan Domain, Inhibits Blood Vessel Formation, and Suppresses Tumor Growth. *J. Biol. Chem.* **2011**, *286*, 30034–30046. [CrossRef] [PubMed]
12. Scharpfenecker, M.; van Dinther, M.; Liu, Z.; van Bezooijen, R.L.; Zhao, Q.; Pukac, L.; Lowik, C.W.; ten Dijke, P. BMP-9 signals via ALK1 and inhibits bFGF-induced endothelial cell proliferation and VEGF-stimulated angiogenesis. *J. Cell Sci.* **2007**, *120*, 964–972. [CrossRef] [PubMed]
13. David, L.; Mallet, C.; Mazerbourg, S.; Feige, J.J.; Bailly, S. Identification of BMP9 and BMP10 as functional activators of the orphan activin receptor-like kinase 1 (ALK1) in endothelial cells. *Blood* **2007**, *109*, 1953–1961. [CrossRef] [PubMed]
14. Saito, T.; Bokhove, M.; Croci, R.; Zamora-Caballero, S.; Han, L.; Letarte, M.; de Sanctis, D.; Jovine, L. Structural Basis of the Human Endoglin-BMP9 Interaction: Insights into BMP Signaling and HHT1. *Cell Rep.* **2017**, *19*, 1917–1928. [CrossRef] [PubMed]
15. Lawera, A.; Tong, Z.; Thorikay, M.; Redgrave, R.E.; Cai, J.; van Dinther, M.; Morrell, N.W.; Afink, G.B.; Charnock-Jones, D.S.; Arthur, H.M.; et al. Role of soluble endoglin in BMP9 signaling. *Proc. Natl. Acad. Sci. USA* **2019**, *116*, 17800–17808. [CrossRef]
16. Tillet, E.; Ouarne, M.; Desroches-Castan, A.; Mallet, C.; Subileau, M.; Didier, R.; Lioutsko, A.; Belthier, G.; Feige, J.J.; Bailly, S. A heterodimer formed by bone morphogenetic protein 9 (BMP9) and BMP10 provides most BMP biological activity in plasma. *J. Biol. Chem.* **2018**, *293*, 10963–10974. [CrossRef]
17. Ola, R.; Dubrac, A.; Han, J.; Zhang, F.; Fang, J.S.; Larrivee, B.; Lee, M.; Urarte, A.A.; Kraehling, J.R.; Genet, G.; et al. PI3 kinase inhibition improves vascular malformations in mouse models of hereditary haemorrhagic telangiectasia. *Nat. Commun.* **2016**, *7*, 13650. [CrossRef]
18. Ruiz, S.; Zhao, H.; Chandakkar, P.; Chatterjee, P.K.; Papoin, J.; Blanc, L.; Metz, C.N.; Campagne, F.; Marambaud, P. A mouse model of hereditary hemorrhagic telangiectasia generated by transmammary-delivered immunoblocking of BMP9 and BMP10. *Sci. Rep.* **2016**, *5*, 37366. [CrossRef]
19. Laux, D.W.; Young, S.; Donovan, J.P.; Mansfield, C.J.; Upton, P.D.; Roman, B.L. Circulating Bmp10 acts through endothelial Alk1 to mediate flow-dependent arterial quiescence. *Development* **2013**, *140*, 3403–3412. [CrossRef]
20. Capasso, T.L.; Li, B.; Volek, H.J.; Khalid, W.; Rochon, E.R.; Anbalagan, A.; Herdman, C.; Yost, H.J.; Villanueva, F.S.; Kim, K.; et al. BMP10-mediated ALK1 signaling is continuously required for vascular development and maintenance. *Angiogenesis* **2020**, *23*, 203–220. [CrossRef]
21. Levet, S.; Ciais, D.; Merdzhanova, G.; Mallet, C.; Zimmers, T.A.; Lee, S.J.; Navarro, F.P.; Texier, I.; Feige, J.J.; Bailly, S.; et al. Bone morphogenetic protein 9 (BMP9) controls lymphatic vessel maturation and valve formation. *Blood* **2013**, *122*, 598–607. [CrossRef] [PubMed]
22. Chen, H.; Brady Ridgway, J.; Sai, T.; Lai, J.; Warming, S.; Chen, H.; Roose-Girma, M.; Zhang, G.; Shou, W.; Yan, M. Context-dependent signaling defines roles of BMP9 and BMP10 in embryonic and postnatal development. *Proc. Natl. Acad. Sci. USA* **2013**, *110*, 11887–11892. [CrossRef] [PubMed]
23. Townson, S.A.; Martinez-Hackert, E.; Greppi, C.; Lowden, P.; Sako, D.; Liu, J.; Ucran, J.A.; Liharska, K.; Underwood, K.W.; Seehra, J.; et al. Specificity and structure of a high affinity activin receptor-like kinase 1 (ALK1) signaling complex. *J. Biol. Chem.* **2012**, *287*, 27313–27325. [CrossRef] [PubMed]
24. Crist, A.M.; Lee, A.R.; Patel, N.R.; Westhoff, D.E.; Meadows, S.M. Vascular deficiency of Smad4 causes arteriovenous malformations: A mouse model of Hereditary Hemorrhagic Telangiectasia. *Angiogenesis* **2018**, *21*, 363–380. [CrossRef] [PubMed]
25. Benn, A.; Alonso, F.; Mangelschots, J.; Genot, E.; Lox, M.; Zwijsen, A. BMP-SMAD1/5 Signaling Regulates Retinal Vascular Development. *Biomolecules* **2020**, *10*, 488. [CrossRef] [PubMed]
26. Dupuis-Girod, S.; Bailly, S.; Plauchu, H. Hereditary hemorrhagic telangiectasia: From molecular biology to patient care. *J. Thromb. Haemost.* **2010**, *8*, 1447–1456. [CrossRef]
27. Shovlin, C.L. Hereditary haemorrhagic telangiectasia: Pathophysiology, diagnosis and treatment. *Blood Rev.* **2010**, *24*, 203–219. [CrossRef]

28. Snellings, D.A.; Gallione, C.J.; Clark, D.S.; Vozoris, N.T.; Faughnan, M.E.; Marchuk, D.A. Somatic Mutations in Vascular Malformations of Hereditary Hemorrhagic Telangiectasia Result in Bi-allelic Loss of ENG or ACVRL1. *Am. J. Hum. Genet.* **2019**, *105*, 894–906. [CrossRef]
29. Li, C.; Guo, B.; Ding, S.; Rius, C.; Langa, C.; Kumar, P.; Bernabeu, C.; Kumar, S. TNF α down-regulates CD105 expression in vascular endothelial cells: A comparative study with TGF β 1. *Anticancer Res.* **2003**, *23*, 1189–1196.
30. Fernandez, L.A.; Sanz-Rodriguez, F.; Zarrabeitia, R.; Perez-Molino, A.; Morales, C.; Restrepo, C.M.; Ramirez, J.R.; Coto, E.; Lenato, G.M.; Bernabeu, C.; et al. Mutation study of Spanish patients with hereditary hemorrhagic telangiectasia and expression analysis of Endoglin and ALK1. *Hum. Mutat.* **2006**, *27*, 295. [CrossRef]
31. Kawasaki, K.; Freimuth, J.; Meyer, D.S.; Lee, M.M.; Tochimoto-Okamoto, A.; Benzinou, M.; Clermont, F.F.; Wu, G.; Roy, R.; Letteboer, T.G.; et al. Genetic variants of Adam17 differentially regulate TGFbeta signaling to modify vascular pathology in mice and humans. *Proc. Natl. Acad. Sci. USA* **2014**, *111*, 7723–7728. [CrossRef] [PubMed]
32. Park, S.O.; Wankhede, M.; Lee, Y.J.; Choi, E.J.; Fliess, N.; Choe, S.W.; Oh, S.H.; Walter, G.; Raizada, M.K.; Sorg, B.S.; et al. Real-time imaging of de novo arteriovenous malformation in a mouse model of hereditary hemorrhagic telangiectasia. *J. Clin. Investig.* **2009**, *119*, 3487–3496. [CrossRef] [PubMed]
33. Robinson, M.W.; Harmon, C.; O'Farrelly, C. Liver immunology and its role in inflammation and homeostasis. *Cell Mol. Immunol.* **2016**, *13*, 267–276. [CrossRef] [PubMed]
34. Baeyens, N.; Larrivee, B.; Ola, R.; Hayward-Piatkowskyi, B.; Dubrac, A.; Huang, B.; Ross, T.D.; Coon, B.G.; Min, E.; Tsarfati, M.; et al. Defective fluid shear stress mechanotransduction mediates hereditary hemorrhagic telangiectasia. *J. Cell Biol.* **2016**, *214*, 807–816. [CrossRef] [PubMed]
35. Corti, P.; Young, S.; Chen, C.Y.; Patrick, M.J.; Rochon, E.R.; Pekkan, K.; Roman, B.L. Interaction between alk1 and blood flow in the development of arteriovenous malformations. *Development* **2011**, *138*, 1573–1582. [CrossRef]
36. Rochon, E.R.; Menon, P.G.; Roman, B.L. Alk1 controls arterial endothelial cell migration in lumenized vessels. *Development* **2016**, *143*, 2593–2602. [CrossRef]
37. Jin, Y.; Muhl, L.; Burmakin, M.; Wang, Y.; Duchez, A.C.; Betsholtz, C.; Arthur, H.M.; Jakobsson, L. Endoglin prevents vascular malformation by regulating flow-induced cell migration and specification through VEGFR2 signalling. *Nat. Cell Biol.* **2017**, *19*, 639–652. [CrossRef]
38. Lebrin, F.; Srun, S.; Raymond, K.; Martin, S.; van den Brink, S.; Freitas, C.; Breant, C.; Mathivet, T.; Larrivee, B.; Thomas, J.L.; et al. Thalidomide stimulates vessel maturation and reduces epistaxis in individuals with hereditary hemorrhagic telangiectasia. *Nat. Med.* **2010**, *16*, 420–428. [CrossRef]
39. Chen, W.; Guo, Y.; Walker, E.J.; Shen, F.; Jun, K.; Oh, S.P.; Degos, V.; Lawton, M.T.; Tihan, T.; Davalos, D.; et al. Reduced mural cell coverage and impaired vessel integrity after angiogenic stimulation in the Alk1-deficient brain. *Arterioscler. Thrombosis Vasc. Biol.* **2013**, *33*, 305–310. [CrossRef]
40. Winkler, E.A.; Birk, H.; Burkhardt, J.K.; Chen, X.; Yue, J.K.; Guo, D.; Rutledge, W.C.; Lasker, G.F.; Partow, C.; Tihan, T.; et al. Reductions in brain pericytes are associated with arteriovenous malformation vascular instability. *J. Neurosurg.* **2018**, *129*, 1464–1474. [CrossRef]
41. Nikolaev, S.I.; Vetiska, S.; Bonilla, X.; Boudreau, E.; Jauhiainen, S.; Rezai Jahromi, B.; Khyzha, N.; DiStefano, P.V.; Suutarinen, S.; Kiehl, T.R.; et al. Somatic activating KRAS mutations in arteriovenous malformations of the brain. *N. Eng. J. Med.* **2018**, *378*, 250–261. [CrossRef] [PubMed]
42. Fish, J.E.; Flores Suarez, C.P.; Boudreau, E.; Herman, A.M.; Gutierrez, M.C.; Gustafson, D.; DiStefano, P.V.; Cui, M.; Chen, Z.; De Ruiz, K.B.; et al. Somatic Gain of KRAS Function in the Endothelium Is Sufficient to Cause Vascular Malformations That Require MEK but Not PI3K Signaling. *Circ. Res.* **2020**, *127*, 727–743. [CrossRef] [PubMed]
43. Tual-Chalot, S.; Garcia-Collado, M.; Redgrave, R.E.; Singh, E.; Davison, B.; Park, C.; Lin, H.; Luli, S.; Jin, Y.; Wang, Y.; et al. Loss of Endothelial Endoglin Promotes High-Output Heart Failure Through Peripheral Arteriovenous Shunting Driven by VEGF Signaling. *Circ. Res.* **2020**, *126*, 243–257. [CrossRef] [PubMed]
44. Alsina-Sanchis, E.; Garcia-Ibanez, Y.; Figueiredo, A.M.; Riera-Domingo, C.; Figueras, A.; Matias-Guiu, X.; Casanovas, O.; Botella, L.M.; Pujana, M.A.; Riera-Mestre, A.; et al. ALK1 Loss Results in Vascular Hyperplasia in Mice and Humans Through PI3K Activation. *Arterioscler. Thrombosis Vasc. Biol.* **2018**, *38*, 1216–1229. [CrossRef]
45. Mahmoud, M.; Allinson, K.R.; Zhai, Z.; Oakenfull, R.; Ghandi, P.; Adams, R.H.; Fruttiger, M.; Arthur, H.M. Pathogenesis of arteriovenous malformations in the absence of endoglin. *Circ. Res.* **2010**, *106*, 1425–1433. [CrossRef]
46. Tual-Chalot, S.; Mahmoud, M.; Allinson, K.R.; Redgrave, R.E.; Zhai, Z.; Oh, S.P.; Fruttiger, M.; Arthur, H.M. Endothelial depletion of Acvrl1 in mice leads to arteriovenous malformations associated with reduced endoglin expression. *PLoS ONE* **2014**, *9*, e98646. [CrossRef]
47. Iriarte, A.; Figueras, A.; Cerda, P.; Mora, J.M.; Jucgla, A.; Penin, R.; Vinals, F.; Riera-Mestre, A. PI3K (Phosphatidylinositol 3-Kinase) Activation and Endothelial Cell Proliferation in Patients with Hemorrhagic Hereditary Telangiectasia Type 1. *Cells* **2019**, *8*, 971. [CrossRef]
48. Jakobsson, L.; Arthur, H.M. Oncogenes in Brain Arteriovenous Malformations. *Circ. Res.* **2020**, *127*, 744–746. [CrossRef]
49. Dupuis-Girod, S.; Ginon, I.; Saurin, J.C.; Marion, D.; Guillot, E.; Decullier, E.; Roux, A.; Carette, M.F.; Gilbert-Dussardier, B.; Hatron, P.Y.; et al. Bevacizumab in patients with hereditary hemorrhagic telangiectasia and severe hepatic vascular malformations and high cardiac output. *JAMA* **2012**, *307*, 948–955. [CrossRef]

50. Al-Samkari, H.; Kasthuri, R.S.; Parambil, J.G.; Albitar, H.A.; Almodallal, Y.A.; Vazquez, C.; Serra, M.M.; Dupuis-Girod, S.; Wilsen, C.B.; McWilliams, J.P.; et al. An international, multicenter study of intravenous bevacizumab for bleeding in hereditary hemorrhagic telangiectasia: The InHIBIT-Bleed study. *Haematologica* **3324**. [CrossRef]
51. Dupuis-Girod, S.; Fargeton, A.E.; Grobost, V.; Riviere, S.; Beaudoin, M.; Decullier, E.; Bernard, L.; Breant, V.; Colombet, B.; Philouze, P.; et al. Efficacy and Safety of a 0.1% Tacrolimus Nasal Ointment as a Treatment for Epistaxis in Hereditary Hemorrhagic Telangiectasia: A Double-Blind, Randomized, Placebo-Controlled, Multicenter Trial. *J. Clin. Med.* **2020**, *9*, 1262. [CrossRef] [PubMed]
52. Faughnan, M.E.; Gossage, J.R.; Chakinala, M.M.; Oh, S.P.; Kasthuri, R.; Hughes, C.C.W.; McWilliams, J.P.; Parambil, J.G.; Vozoris, N.; Donaldson, J.; et al. Pazopanib may reduce bleeding in hereditary hemorrhagic telangiectasia. *Angiogenesis* **2019**, *22*, 145–155. [CrossRef] [PubMed]
53. Dupuis-Girod, S.; Pitiot, V.; Bergerot, C.; Fargeton, A.E.; Beaudoin, M.; Decullier, E.; Breant, V.; Colombet, B.; Philouze, P.; Faure, F.; et al. Efficacy of TIMOLOL nasal spray as a treatment for epistaxis in hereditary hemorrhagic telangiectasia. A double-blind, randomized, placebo-controlled trial. *Sci Rep* **2019**, *9*, 11986. [CrossRef] [PubMed]
54. Ruiz, S.; Zhao, H.; Chandakkar, P.; Papoin, J.; Choi, H.; Nomura-Kitabayashi, A.; Patel, R.; Gillen, M.; Diao, L.; Chatterjee, P.K.; et al. Correcting Smad1/5/8, mTOR, and VEGFR2 treats pathology in hereditary hemorrhagic telangiectasia models. *J. Clin. Investig.* **2020**, *130*, 942–957. [CrossRef]
55. Han, C.; Choe, S.W.; Kim, Y.H.; Acharya, A.P.; Keselowsky, B.G.; Sorg, B.S.; Lee, Y.J.; Oh, S.P. VEGF neutralization can prevent and normalize arteriovenous malformations in an animal model for hereditary hemorrhagic telangiectasia 2. *Angiogenesis* **2014**, *17*, 823–830. [CrossRef]
56. Kim, Y.H.; Kim, M.J.; Choe, S.W.; Sprecher, D.; Lee, Y.J.; Oh, S.P. Selective effects of oral antiangiogenic tyrosine kinase inhibitors on an animal model of hereditary hemorrhagic telangiectasia. *J. Thromb. Haemost.* **2017**, *15*, 1095–1102. [CrossRef]
57. Zhu, W.; Chen, W.; Zou, D.; Wang, L.; Bao, C.; Zhan, L.; Saw, D.; Wang, S.; Winkler, E.; Li, Z.; et al. Thalidomide Reduces Hemorrhage of Brain Arteriovenous Malformations in a Mouse Model. *Stroke* **2018**, *49*, 1232–1240. [CrossRef]
58. Crist, A.M.; Zhou, X.; Garai, J.; Lee, A.R.; Thoele, J.; Ullmer, C.; Klein, C.; Zabaleta, J.; Meadows, S.M. Angiopoietin-2 Inhibition Rescues Arteriovenous Malformation in a Smad4 Hereditary Hemorrhagic Telangiectasia Mouse Model. *Circulation* **2019**, *139*, 2049–2063. [CrossRef]
59. Ruiz, S.; Chandakkar, P.; Zhao, H.; Papoin, J.; Chatterjee, P.K.; Christen, E.; Metz, C.N.; Blanc, L.; Campagne, F.; Marambaud, P. Tacrolimus rescues the signaling and gene expression signature of endothelial ALK1 loss-of-function and improves HHT vascular pathology. *Hum. Mol. Genet.* **2017**, *26*, 4786–4798. [CrossRef]
60. Albinana, V.; Sanz-Rodriguez, F.; Recio-Poveda, L.; Bernabeu, C.; Botella, L.M. Immunosuppressor FK506 increases endoglin and activin receptor-like kinase 1 expression and modulates transforming growth factor-beta1 signaling in endothelial cells. *Mol. Pharmacol.* **2011**, *79*, 833–843. [CrossRef]
61. Spiekerkoetter, E.; Sung, Y.K.; Sudheendra, D.; Bill, M.; Aldred, M.A.; van de Veerdonk, M.C.; Vonk Noordegraaf, A.; Long-Boyle, J.; Dash, R.; Yang, P.C.; et al. Low-Dose FK506 (Tacrolimus) in End-Stage Pulmonary Arterial Hypertension. *Am. J. Respir. Crit. Care Med.* **2015**, *192*, 254–257. [CrossRef]
62. Sommer, N.; Droege, F.; Gamen, K.E.; Geisthoff, U.; Gall, H.; Tello, K.; Richter, M.J.; Deubner, L.M.; Schmiedel, R.; Hecker, M.; et al. Treatment with low-dose tacrolimus inhibits bleeding complications in a patient with hereditary hemorrhagic telangiectasia and pulmonary arterial hypertension. *Pulm. Circ.* **2019**, *9*, 2045894018805406. [CrossRef] [PubMed]
63. Hwan Kim, Y.; Vu, P.N.; Choe, S.W.; Jeon, C.J.; Arthur, H.M.; Vary, C.P.H.; Lee, Y.J.; Oh, S.P. Overexpression of Activin Receptor-Like Kinase 1 in Endothelial Cells Suppresses Development of Arteriovenous Malformations in Mouse Models of Hereditary Hemorrhagic Telangiectasia. *Circ. Res.* **2020**, *127*, 1122–1137. [CrossRef] [PubMed]
64. Echevarria, L.; Aupy, P.; Goyenvalle, A. Exon-skipping advances for Duchenne muscular dystrophy. *Hum. Mol. Genet.* **2018**, *27*, R163–R172. [CrossRef] [PubMed]
65. Keeling, K.M.; Xue, X.; Gunn, G.; Bedwell, D.M. Therapeutics based on stop codon readthrough. *Annu. Rev. Genom. Hum. Genet.* **2014**, *15*, 371–394. [CrossRef] [PubMed]
66. Flieger, D.; Hainke, S.; Fischbach, W. Dramatic improvement in hereditary hemorrhagic telangiectasia after treatment with the vascular endothelial growth factor (VEGF) antagonist bevacizumab. *Ann. Hematol.* **2006**, *85*, 631–632. [CrossRef] [PubMed]
67. David, L.; Mallet, C.; Keramidas, M.; Lamande, N.; Gasc, J.M.; Dupuis-Girod, S.; Plauchu, H.; Feige, J.J.; Bailly, S. Bone morphogenetic protein-9 is a circulating vascular quiescence factor. *Circ. Res.* **2008**, *102*, 914–922. [CrossRef]
68. Sadick, H.; Riedel, F.; Naim, R.; Goessler, U.; Hormann, K.; Hafner, M.; Lux, A. Patients with hereditary hemorrhagic telangiectasia have increased plasma levels of vascular endothelial growth factor and transforming growth factor-beta1 as well as high ALK1 tissue expression. *Haematologica* **2005**, *90*, 818–828.
69. Shao, E.S.; Lin, L.; Yao, Y.; Bostrom, K.I. Expression of vascular endothelial growth factor is coordinately regulated by the activin-like kinase receptors 1 and 5 in endothelial cells. *Blood* **2009**, *114*, 2197–2206. [CrossRef]
70. Esposito, A.; Viale, G.; Curigliano, G. Safety, Tolerability, and Management of Toxic Effects of Phosphatidylinositol 3-Kinase Inhibitor Treatment in Patients With Cancer: A Review. *JAMA Oncol.* **2019**, *5*, 1347–1354. [CrossRef]
71. Tian, H.; Huang, J.J.; Golzio, C.; Gao, X.; Hector-Greene, M.; Katsanis, N.; Blobe, G.C. Endoglin interacts with VEGFR2 to promote angiogenesis. *FASEB J. Off. Publ. Fed. Am. Soc. Exp. Biol.* **2018**, *32*, 2934–2949. [CrossRef]

72. Thalgott, J.H.; Dos-Santos-Luis, D.; Hosman, A.E.; Martin, S.; Lamandé, N.; Bracquart, D.; Srun, S.; Galaris, G.; de Boer, H.C.; Tual-Chalot, S.; et al. Decreased expression of vascular endothelial growth factor receptor 1 contributes to the pathogenesis of hereditary hemorrhagic telangiectasia type 2. *Circulation* **2018**, *138*, 2698–2712. [CrossRef]
73. Mei-Zahav, M.; Gendler, Y.; Bruckheimer, E.; Prais, D.; Birk, E.; Watad, M.; Goldschmidt, N.; Soudry, E. Topical Propranolol Improves Epistaxis Control in Hereditary Hemorrhagic Telangiectasia (HHT): A Randomized Double-Blind Placebo-Controlled Trial. *J. Clin. Med.* **2020**, *9*, 3130. [CrossRef]
74. Harrison, L.; Kundra, A.; Jervis, P. The use of thalidomide therapy for refractory epistaxis in hereditary haemorrhagic telangiectasia: Systematic review. *J. Laryngol. Otol.* **2018**, *132*, 866–871. [CrossRef] [PubMed]
75. Carvalho, R.L.; Jonker, L.; Goumans, M.J.; Larsson, J.; Bouwman, P.; Karlsson, S.; Dijke, P.T.; Arthur, H.M.; Mummery, C.L. Defective paracrine signalling by TGFbeta in yolk sac vasculature of endoglin mutant mice: A paradigm for hereditary haemorrhagic telangiectasia. *Development* **2004**, *131*, 6237–6247. [CrossRef] [PubMed]
76. Ojeda-Fernandez, L.; Barrios, L.; Rodriguez-Barbero, A.; Recio-Poveda, L.; Bernabeu, C.; Botella, L.M. Reduced plasma levels of Ang-2 and sEng as novel biomarkers in hereditary hemorrhagic telangiectasia (HHT). *Clin. Chim. Acta* **2010**, *411*, 494–499. [CrossRef] [PubMed]

8. Bibliography

Al-Samkari, H., Kasthuri, R. S., Parambil, J. G., Albitar, H. A., Almodallal, Y. A., et al. (2021). "An international, multicenter study of intravenous bevacizumab for bleeding in hereditary hemorrhagic telangiectasia: the InHIBIT-Bleed study." Haematologica **106**(8): 2161-2169.

Alsina-Sanchís, E., García-Ibáñez, Y., Figueiredo, A. M., Riera-Domingo, C., Figueras, A., et al. (2018). "ALK1 Loss Results in Vascular Hyperplasia in Mice and Humans Through PI3K Activation." Arterioscler Thromb Vasc Biol **38**(5): 1216-1229.

Arthur, H. M., Ure, J., Smith, A. J., Renforth, G., Wilson, D. I., et al. (2000). "Endoglin, an ancillary TGFbeta receptor, is required for extraembryonic angiogenesis and plays a key role in heart development." Dev Biol **217**(1): 42-53.

Baeyens, N., Larrivée, B., Ola, R., Hayward-Piatkowskyi, B., Dubrac, A., et al. (2016). "Defective fluid shear stress mechanotransduction mediates hereditary hemorrhagic telangiectasia." J Cell Biol **214**(7): 807-816.

Belevich, I., Joensuu, M., Kumar, D., Vihinen, H. and Jokitalo, E. (2016). "Microscopy Image Browser: A Platform for Segmentation and Analysis of Multidimensional Datasets." PLoS Biol **14**(1): e1002340.

Bellón, T., Corbí, A., Lastres, P., Calés, C., Cebrián, M., et al. (1993). "Identification and expression of two forms of the human transforming growth factor-beta-binding protein endoglin with distinct cytoplasmic regions." Eur J Immunol **23**(9): 2340-2345.

Bierhaus, A., Fleming, T., Stoyanov, S., Leffler, A., Babes, A., et al. (2012). "Methylglyoxal modification of Nav1.8 facilitates nociceptive neuron firing and causes hyperalgesia in diabetic neuropathy." Nat Med **18**(6): 926-933.

Bise, T., Sallin, P., Pfefferli, C. and Jaźwińska, A. (2020). "Multiple cryoinjuries modulate the efficiency of zebrafish heart regeneration." Scientific Reports **10**(1): 11551.

Boselli, F., Freund, J. B. and Vermot, J. (2015). "Blood flow mechanics in cardiovascular development." Cell Mol Life Sci **72**(13): 2545-2559.

Bourdeau, A., Dumont, D. J. and Letarte, M. (1999). "A murine model of hereditary hemorrhagic telangiectasia." J Clin Invest **104**(10): 1343-1351.

Brown, M. A., Zhao, Q., Baker, K. A., Naik, C., Chen, C., et al. (2005). "Crystal structure of BMP-9 and functional interactions with pro-region and receptors." J Biol Chem **280**(26): 25111-25118.

Burns, C. G., Milan, D. J., Grande, E. J., Rottbauer, W., MacRae, C. A., et al. (2005). "High-throughput assay for small molecules that modulate zebrafish embryonic heart rate." Nat Chem Biol **1**(5): 263-264.

Burri, P. H., Hlushchuk, R. and Djonov, V. (2004). "Intussusceptive angiogenesis: its emergence, its characteristics, and its significance." Dev Dyn **231**(3): 474-488.

Capasso, T. L., Li, B., Volek, H. J., Khalid, W., Rochon, E. R., et al. (2020). "BMP10-mediated ALK1 signaling is continuously required for vascular development and maintenance." Angiogenesis **23**(2): 203-220.

Carmeliet, P., Ferreira, V., Breier, G., Pollefeyt, S., Kieckens, L., et al. (1996). "Abnormal blood vessel development and lethality in embryos lacking a single VEGF allele." Nature **380**(6573): 435-439.

Cassar, S., Adatto, I., Freeman, J. L., Gamse, J. T., Iturria, I., et al. (2020). "Use of Zebrafish in Drug Discovery Toxicology." Chem Res Toxicol **33**(1): 95-118.

Cermak, T., Doyle, E. L., Christian, M., Wang, L., Zhang, Y., et al. (2011). "Efficient design and assembly of custom TALEN and other TAL effector-based constructs for DNA targeting." Nucleic Acids Res **39**(12): e82.

Chablais, F. and Jazwinska, A. (2012). "The regenerative capacity of the zebrafish heart is dependent on TGFβ signaling." Development **139**(11): 1921-1930.

Cheifetz, S., Bellón, T., Calés, C., Vera, S., Bernabeu, C., et al. (1992). "Endoglin is a component of the transforming growth factor-beta receptor system in human endothelial cells." J Biol Chem **267**(27): 19027-19030.

Chen, H., Shi, S., Acosta, L., Li, W., Lu, J., et al. (2004). "BMP10 is essential for maintaining cardiac growth during murine cardiogenesis." Development **131**(9): 2219-2231.

Chen, H., et al. (2013). "Context-dependent signaling defines roles of BMP9 and BMP10 in embryonic and postnatal development." Proceedings of the National Academy of Sciences **110**(29): 11887-11892.

Chi, N. C., Shaw, R. M., De Val, S., Kang, G., Jan, L. Y., et al. (2008). "Foxn4 directly regulates tbx2b expression and atrioventricular canal formation." Genes Dev **22**(6): 734-739.

Cocks, E., Taggart, M., Rind, F. C. and White, K. (2018). "A guide to analysis and reconstruction of serial block face scanning electron microscopy data." J Microsc **270**(2): 217-234.

Corti, P., Young, S., Chen, C. Y., Patrick, M. J., Rochon, E. R., et al. (2011). "Interaction between alk1 and blood flow in the development of arteriovenous malformations." Development **138**(8): 1573-1582.

David, L., Mallet, C., Keramidas, M., Lamandé, N., Gasc, J. M., et al. (2008). "Bone morphogenetic protein-9 is a circulating vascular quiescence factor." Circ Res **102**(8): 914-922.

Diekmann, H., Kalbhen, P. and Fischer, D. (2015). "Active mechanistic target of rapamycin plays an ancillary rather than essential role in zebrafish CNS axon regeneration." Front Cell Neurosci **9**: 251.

Dupuis-Girod, S., Fargeton, A. E., Grobost, V., Rivière, S., Beaudoin, M., et al. (2020). "Efficacy and Safety of a 0.1% Tacrolimus Nasal Ointment as a Treatment for Epistaxis in Hereditary Hemorrhagic Telangiectasia: A Double-Blind, Randomized, Placebo-Controlled, Multicenter Trial." J Clin Med **9**(5).

Dupuis-Girod, S., Ginon, I., Saurin, J. C., Marion, D., Guillot, E., et al. (2012). "Bevacizumab in patients with hereditary hemorrhagic telangiectasia and severe hepatic vascular malformations and high cardiac output." JAMA **307**(9): 948-955.

El-Brolosy, M. A. and Stainier, D. Y. R. (2017). "Genetic compensation: A phenomenon in search of mechanisms." PLoS Genet **13**(7): e1006780.

Gallione, C. J., Repetto, G. M., Legius, E., Rustgi, A. K., Schelley, S. L., et al. (2004). "A combined syndrome of juvenile polyposis and hereditary haemorrhagic telangiectasia associated with mutations in MADH4 (SMAD4)." Lancet **363**(9412): 852-859.

Gao, C., Ren, S., Lee, J. H., Qiu, J., Chapski, D. J., et al. (2016). "RBFox1-mediated RNA splicing regulates cardiac hypertrophy and heart failure." J Clin Invest **126**(1): 195-206.

Gimbrone, M. A., Jr. and García-Cardeña, G. (2016). "Endothelial Cell Dysfunction and the Pathobiology of Atherosclerosis." Circ Res **118**(4): 620-636.

Girerd, B., Montani, D., Coulet, F., Sztrymf, B., Yaici, A., et al. (2010). "Clinical outcomes of pulmonary arterial hypertension in patients carrying an ACVRL1 (ALK1) mutation." Am J Respir Crit Care Med **181**(8): 851-861.

Gleeson, M., Connaughton, V. and Arneson, L. S. (2007). "Induction of hyperglycaemia in zebrafish (Danio rerio) leads to morphological changes in the retina." Acta Diabetol **44**(3): 157-163.

Goel, S., Duda, D. G., Xu, L., Munn, L. L., Boucher, Y., et al. (2011). "Normalization of the vasculature for treatment of cancer and other diseases." Physiol Rev **91**(3): 1071-1121.

González-Rosa, J. M. and Mercader, N. (2012). "Cryoinjury as a myocardial infarction model for the study of cardiac regeneration in the zebrafish." Nat Protoc **7**(4): 782-788.

Gordon, K. J. and Blobe, G. C. (2008). "Role of transforming growth factor-beta superfamily signaling pathways in human disease." Biochim Biophys Acta **1782**(4): 197-228.

Gougos, A. and Letarte, M. (1990). "Primary structure of endoglin, an RGD-containing glycoprotein of human endothelial cells." J Biol Chem **265**(15): 8361-8364.

Goumans, M. J., Valdimarsdottir, G., Itoh, S., Rosendahl, A., Sideras, P., et al. (2002). "Balancing the activation state of the endothelium via two distinct TGF-beta type I receptors." EMBO J **21**(7): 1743-1753.

Govani, F. S. and Shovlin, C. L. (2009). "Hereditary haemorrhagic telangiectasia: a clinical and scientific review." Eur J Hum Genet **17**(7): 860-871.

Han, C., Choe, S. W., Kim, Y. H., Acharya, A. P., Keselowsky, B. G., et al. (2014). "VEGF neutralization can prevent and normalize arteriovenous malformations in an animal model for hereditary hemorrhagic telangiectasia 2." Angiogenesis **17**(4): 823-830.

Harrison, M. R., Bussmann, J., Huang, Y., Zhao, L., Osorio, A., et al. (2015). "Chemokine-guided angiogenesis directs coronary vasculature formation in zebrafish." Dev Cell **33**(4): 442-454.

Howe, K., Clark, M. D., Torroja, C. F., Torrance, J., Berthelot, C., et al. (2013). "The zebrafish reference genome sequence and its relationship to the human genome." Nature **496**(7446): 498-503.

Huang, C. J., Tu, C. T., Hsiao, C. D., Hsieh, F. J. and Tsai, H. J. (2003). "Germ-line transmission of a myocardium-specific GFP transgene reveals critical regulatory elements in the cardiac myosin light chain 2 promoter of zebrafish." Dev Dyn **228**(1): 30-40.

Hwan Kim, Y., Vu, P. N., Choe, S. W., Jeon, C. J., Arthur, H. M., et al. (2020). "Overexpression of Activin Receptor-Like Kinase 1 in Endothelial Cells Suppresses Development of Arteriovenous Malformations in Mouse Models of Hereditary Hemorrhagic Telangiectasia." Circ Res **127**(9): 1122-1137.

Isogai, S., Horiguchi, M. and Weinstein, B. M. (2001). "The vascular anatomy of the developing zebrafish: an atlas of embryonic and early larval development." Dev Biol **230**(2): 278-301.

Jakobsson, L. and Arthur, H. M. (2020). "Oncogenes in Brain Arteriovenous Malformations." Circ Res **127**(6): 744-746.

Jin, Y., Muhl, L., Burmakin, M., Wang, Y., Duchez, A. C., et al. (2017). "Endoglin prevents vascular malformation by regulating flow-induced cell migration and specification through VEGFR2 signalling." Nat Cell Biol **19**(6): 639-652.

Jonker, L. and Arthur, H. M. (2002). "Endoglin expression in early development is associated with vasculogenesis and angiogenesis." Mech Dev **110**(1-2): 193-196.

Jörgens, K., Stoll, S. J., Pohl, J., Fleming, T. H., Sticht, C., et al. (2015). "High Tissue Glucose Alters Intersomitic Blood Vessels in Zebrafish via Methylglyoxal Targeting the VEGF Receptor Signaling Cascade." Diabetes **64**(1): 213-225.

Kim, J., Wu, Q., Zhang, Y., Wiens, K. M., Huang, Y., et al. (2010). "PDGF signaling is required for epicardial function and blood vessel formation in regenerating zebrafish hearts." Proc Natl Acad Sci U S A **107**(40): 17206-17210.

Kim, Y. G., Cha, J. and Chandrasegaran, S. (1996). "Hybrid restriction enzymes: zinc finger fusions to Fok I cleavage domain." Proc Natl Acad Sci U S A **93**(3): 1156-1160.

Koleva, R. I., Conley, B. A., Romero, D., Riley, K. S., Marto, J. A., et al. (2006). "Endoglin structure and function: Determinants of endoglin phosphorylation by transforming growth factor-beta receptors." J Biol Chem **281**(35): 25110-25123.

Koth, J., Maguire, M. L., McClymont, D., Diffley, L., Thornton, V. L., et al. (2017). "High-Resolution Magnetic Resonance Imaging of the Regenerating Adult Zebrafish Heart." Sci Rep **7**(1): 2917.

Kugler, E., Plant, K., Chico, T. and Armitage, P. (2019). "Enhancement and Segmentation Workflow for the Developing Zebrafish Vasculature." Journal of Imaging **5**(1): 14.

Kugler, E. C., Frost, J., Silva, V., Plant, K., Chhabria, K., et al. (2020). "3D quantification of zebrafish cerebrovascular architecture by automated image analysis of light sheet fluorescence microscopy datasets." bioRxiv: 2020.2008.2006.239905.

Kugler, E. C., van Lessen, M., Daetwyler, S., Chhabria, K., Savage, A. M., et al. (2019). "Cerebrovascular endothelial cells form transient Notch-dependent cystic structures in zebrafish." EMBO Rep **20**(8): e47047.

Laflamme, M. A. and Murry, C. E. (2011). "Heart regeneration." Nature **473**(7347): 326-335.

Lawera, A., Tong, Z., Thorikay, M., Redgrave, R. E., Cai, J., et al. (2019). "Role of soluble endoglin in BMP9 signaling." Proc Natl Acad Sci U S A **116**(36): 17800-17808.

Lawrence, C. (2016). "New frontiers for zebrafish management." Methods Cell Biol **135**: 483-508.

Lawson, N. D., Vogel, A. M. and Weinstein, B. M. (2002). "sonic hedgehog and vascular endothelial growth factor act upstream of the Notch pathway during arterial endothelial differentiation." Dev Cell **3**(1): 127-136.

Lawson, N. D. and Weinstein, B. M. (2002). "In vivo imaging of embryonic vascular development using transgenic zebrafish." Dev Biol **248**(2): 307-318.

Lebrin, F., Srun, S., Raymond, K., Martin, S., van den Brink, S., et al. (2010). "Thalidomide stimulates vessel maturation and reduces epistaxis in individuals with hereditary hemorrhagic telangiectasia." Nat Med **16**(4): 420-428.

Leaños-Miranda, A., et al. (2019). "Soluble Endoglin As a Marker for Preeclampsia, Its Severity, and the Occurrence of Adverse Outcomes." Hypertension 74(4): 991-997.

Levet, S., Ciais, D., Merdzhanova, G., Mallet, C., Zimmers, T. A., et al. (2013). "Bone morphogenetic protein 9 (BMP9) controls lymphatic vessel maturation and valve formation." Blood **122**(4): 598-607.

Levine, R. J., Lam, C., Qian, C., Yu, K. F., Maynard, S. E., et al. (2006). "Soluble endoglin and other circulating antiangiogenic factors in preeclampsia." N Engl J Med **355**(10): 992-1005.

Li, D. Y., Sorensen, L. K., Brooke, B. S., Urness, L. D., Davis, E. C., et al. (1999). "Defective angiogenesis in mice lacking endoglin." Science **284**(5419): 1534-1537.

Liu, Y., Asnani, A., Zou, L., Bentley, V. L., Yu, M., et al. (2014). "Visnagin protects against doxorubicin-induced cardiomyopathy through modulation of mitochondrial malate dehydrogenase." Sci Transl Med **6**(266): 266ra170.

Lupu, I. E., De Val, S. and Smart, N. (2020). "Coronary vessel formation in development and disease: mechanisms and insights for therapy." Nat Rev Cardiol **17**(12): 790-806.

Ma, H., Marti-Gutierrez, N., Park, S. W., Wu, J., Lee, Y., et al. (2017). "Correction of a pathogenic gene mutation in human embryos." Nature **548**(7668): 413-419.

MacRae, C. A. and Peterson, R. T. (2015). "Zebrafish as tools for drug discovery." Nat Rev Drug Discov **14**(10): 721-731.

Mahmoud, M., Allinson, K. R., Zhai, Z., Oakenfull, R., Ghandi, P., et al. (2010). "Pathogenesis of arteriovenous malformations in the absence of endoglin." Circ Res **106**(8): 1425-1433.

Margiotta-Casaluci, L., Owen, S. F., Rand-Weaver, M. and Winter, M. J. (2019). "Testing the Translational Power of the Zebrafish: An Interspecies Analysis of Responses to Cardiovascular Drugs." Front Pharmacol **10**: 893.

McAllister, K. A., Baldwin, M. A., Thukkani, A. K., Gallione, C. J., Berg, J. N., et al. (1995). "Six novel mutations in the endoglin gene in hereditary hemorrhagic telangiectasia type 1 suggest a dominant-negative effect of receptor function." Hum Mol Genet **4**(10): 1983-1985.

McAllister, K. A., Grogg, K. M., Johnson, D. W., Gallione, C. J., Baldwin, M. A., et al. (1994). "Endoglin, a TGF-beta binding protein of endothelial cells, is the gene for hereditary haemorrhagic telangiectasia type 1." Nat Genet **8**(4): 345-351.

McDonald, J., et al. (2015). "Hereditary hemorrhagic telangiectasia: genetics and molecular diagnostics in a new era." Front Genet 6: 1.

Murphy, S. P., Ibrahim, N. E. and Januzzi, J. L., Jr. (2020). "Heart Failure With Reduced Ejection Fraction: A Review." JAMA **324**(5): 488-504.

Murray, C. J., Barber, R. M., Foreman, K. J., Abbasoglu Ozgoren, A., Abd-Allah, F., et al. (2015). "Global, regional, and national disability-adjusted life years (DALYs) for 306 diseases and injuries and healthy life expectancy (HALE) for 188 countries, 1990-2013: quantifying the epidemiological transition." Lancet **386**(10009): 2145-2191.

Nagasawa-Masuda, A. and Terai, K. (2016). "ERK activation in endothelial cells is a novel marker during neovasculogenesis." Genes Cells **21**(11): 1164-1175.

Nasevicius, A. and Ekker, S. C. (2000). "Effective targeted gene 'knockdown' in zebrafish." Nat Genet **26**(2): 216-220.

Neal, A., Nornes, S., Payne, S., Wallace, M. D., Fritzsche, M., et al. (2019). "Venous identity requires BMP signalling through ALK3." Nat Commun **10**(1): 453.

Nikolaev, S. I., Vetiska, S., Bonilla, X., Boudreau, E., Jauhiainen, S., et al. (2018). "Somatic Activating KRAS Mutations in Arteriovenous Malformations of the Brain." N Engl J Med **378**(3): 250-261.

Ola, R., Dubrac, A., Han, J., Zhang, F., Fang, J. S., et al. (2016). "PI3 kinase inhibition improves vascular malformations in mouse models of hereditary haemorrhagic telangiectasia." Nat Commun **7**: 13650.

Paneni, F., Beckman, J. A., Creager, M. A. and Cosentino, F. (2013). "Diabetes and vascular disease: pathophysiology, clinical consequences, and medical therapy: part I." Eur Heart J **34**(31): 2436-2443.

Panzica-Kelly, J. M., Zhang, C. X. and Augustine-Rauch, K. A. (2015). "Optimization and Performance Assessment of the Chorion-Off [Dechorinated] Zebrafish Developmental Toxicity Assay." Toxicol Sci **146**(1): 127-134.

Patel-Hett, S. and D'Amore, P. A. (2011). "Signal transduction in vasculogenesis and developmental angiogenesis." Int J Dev Biol **55**(4-5): 353-363.

Payne, S., Gunadasa-Rohling, M., Neal, A., Redpath, A. N., Patel, J., et al. (2019). "Regulatory pathways governing murine coronary vessel formation are dysregulated in the injured adult heart." Nat Commun **10**(1): 3276.

Pérez-Gómez, E., Del Castillo, G., Juan Francisco, S., López-Novoa, J. M., Bernabéu, C., et al. (2010). "The role of the TGF-β coreceptor endoglin in cancer." ScientificWorldJournal **10**: 2367-2384.

Peterson, R. T., Shaw, S. Y., Peterson, T. A., Milan, D. J., Zhong, T. P., et al. (2004). "Chemical suppression of a genetic mutation in a zebrafish model of aortic coarctation." Nat Biotechnol **22**(5): 595-599.

Poss, K. D., Wilson, L. G. and Keating, M. T. (2002). "Heart regeneration in zebrafish." Science **298**(5601): 2188-2190.

Quackenbush, E. J. and Letarte, M. (1985). "Identification of several cell surface proteins of non-T, non-B acute lymphoblastic leukemia by using monoclonal antibodies." J Immunol **134**(2): 1276-1285.

Ran, F. A., Hsu, P. D., Wright, J., Agarwala, V., Scott, D. A., et al. (2013). "Genome engineering using the CRISPR-Cas9 system." Nat Protoc **8**(11): 2281-2308.

Ray, B. N., Lee, N. Y., How, T. and Blobe, G. C. (2010). "ALK5 phosphorylation of the endoglin cytoplasmic domain regulates Smad1/5/8 signaling and endothelial cell migration." Carcinogenesis **31**(3): 435-441.

Ricard, N., Ciais, D., Levet, S., Subileau, M., Mallet, C., et al. (2012). "BMP9 and BMP10 are critical for postnatal retinal vascular remodeling." Blood **119**(25): 6162-6171.

Risau, W. (1997). "Mechanisms of angiogenesis." Nature **386**(6626): 671-674.

Roman, B. L., Pham, V. N., Lawson, N. D., Kulik, M., Childs, S., et al. (2002). "Disruption of acvrl1 increases endothelial cell number in zebrafish cranial vessels." Development **129**(12): 3009-3019.

Rossi, A., Kontarakis, Z., Gerri, C., Nolte, H., Hölper, S., et al. (2015). "Genetic compensation induced by deleterious mutations but not gene knockdowns." Nature **524**(7564): 230-233.

Ruiz, S., Zhao, H., Chandakkar, P., Chatterjee, P. K., Papoin, J., et al. (2016). "A mouse model of hereditary hemorrhagic telangiectasia generated by transmammary-delivered immunoblocking of BMP9 and BMP10." Sci Rep **5**: 37366.

Ruiz, S., Zhao, H., Chandakkar, P., Papoin, J., Choi, H., et al. (2020). "Correcting Smad1/5/8, mTOR, and VEGFR2 treats pathology in hereditary hemorrhagic telangiectasia models." J Clin Invest **130**(2): 942-957.

Saito, T., Bokhove, M., Croci, R., Zamora-Caballero, S., Han, L., et al. (2017). "Structural Basis of the Human Endoglin-BMP9 Interaction: Insights into BMP Signaling and HHT1." Cell Rep **19**(9): 1917-1928.

Salehpour, A., Rezaei, M., Khoradmehr, A., Tahamtani, Y. and Tamadon, A. (2021). "Which Hyperglycemic Model of Zebrafish (Danio rerio) Suites My Type 2 Diabetes Mellitus Research? A Scoring System for Available Methods." Front Cell Dev Biol **9**: 652061.

Santoro, M. M., Beltrame, M., Panáková, D., Siekmann, A. F., Tiso, N., et al. (2019). "Advantages and Challenges of Cardiovascular and Lymphatic Studies in Zebrafish Research." Front Cell Dev Biol **7**: 89.

Schindelin, J., Arganda-Carreras, I., Frise, E., Kaynig, V., Longair, M., et al. (2012). "Fiji: an open-source platform for biological-image analysis." Nat Methods **9**(7): 676-682.

Schmierer, B. and Hill, C. S. (2007). "TGFbeta-SMAD signal transduction: molecular specificity and functional flexibility." Nat Rev Mol Cell Biol **8**(12): 970-982.

Sehnert, A. J., Huq, A., Weinstein, B. M., Walker, C., Fishman, M., et al. (2002). "Cardiac troponin T is essential in sarcomere assembly and cardiac contractility." Nat Genet **31**(1): 106-110.

Sehnert, A. J. and Stainier, D. Y. (2002). "A window to the heart: can zebrafish mutants help us understand heart disease in humans?" Trends Genet **18**(10): 491-494.

Serbanovic-Canic, J., de Luca, A., Warboys, C., Ferreira, P. F., Luong, L. A., et al. (2017). "Zebrafish Model for Functional Screening of Flow-Responsive Genes." Arterioscler Thromb Vasc Biol **37**(1): 130-143.

Shao, E. S., Lin, L., Yao, Y. and Boström, K. I. (2009). "Expression of vascular endothelial growth factor is coordinately regulated by the activin-like kinase receptors 1 and 5 in endothelial cells." Blood **114**(10): 2197-2206.

Shin, M., Beane, T. J., Quillien, A., Male, I., Zhu, L. J., et al. (2016). "Vegfa signals through ERK to promote angiogenesis, but not artery differentiation." Development **143**(20): 3796-3805.

Shovlin, C. L. (2010). "Hereditary haemorrhagic telangiectasia: pathophysiology, diagnosis and treatment." Blood Rev **24**(6): 203-219.

Siekmann, A. F. and Lawson, N. D. (2007). "Notch signalling limits angiogenic cell behaviour in developing zebrafish arteries." Nature **445**(7129): 781-784.

Singh, E., Redgrave, R. E., Phillips, H. M. and Arthur, H. M. (2020). "Arterial endoglin does not protect against arteriovenous malformations." Angiogenesis **23**(4): 559-566.

Snellings, D. A., Gallione, C. J., Clark, D. S., Vozoris, N. T., Faughnan, M. E., et al. (2019). "Somatic Mutations in Vascular Malformations of Hereditary Hemorrhagic Telangiectasia Result in Bi-allelic Loss of ENG or ACVRL1." Am J Hum Genet **105**(5): 894-906.

Snodgrass, R. O., Arthur, H. M. and Chico, T. J. A. (2021). "Synergistic TOR and ERK inhibition mitigates the hereditary haemorrhagic telangiectasia-like phenotype and excess kugel formation in endoglin mutant zebrafish." bioRxiv: 2021.2006.2016.448717.

Snodgrass, R. O., Chico, T. J. A. and Arthur, H. M. (2021). "Hereditary Haemorrhagic Telangiectasia, an Inherited Vascular Disorder in Need of Improved Evidence-Based Pharmaceutical Interventions." Genes **12**(2): 174.

Stelzer, E. H. K., Strobl, F., Chang, B.-J., Preusser, F., Preibisch, S., et al. (2021). "Light sheet fluorescence microscopy." Nature Reviews Methods Primers **1**(1): 73.

Sugden, W. W., Meissner, R., Aegerter-Wilmsen, T., Tsaryk, R., Leonard, E. V., et al. (2017). "Endoglin controls blood vessel diameter through endothelial cell shape changes in response to haemodynamic cues." Nat Cell Biol **19**(6): 653-665.

Suter, T. M. and Ewer, M. S. (2013). "Cancer drugs and the heart: importance and management." Eur Heart J **34**(15): 1102-1111.

Suzuki, Y., Ohga, N., Morishita, Y., Hida, K., Miyazono, K., et al. (2010). "BMP-9 induces proliferation of multiple types of endothelial cells in vitro and in vivo." J Cell Sci **123**(Pt 10): 1684-1692.

Tamplin, O. J., White, R. M., Jing, L., Kaufman, C. K., Lacadie, S. A., et al. (2012). "Small molecule screening in zebrafish: swimming in potential drug therapies." Wiley Interdiscip Rev Dev Biol **1**(3): 459-468.

Toporsian, M., Gros, R., Kabir, M. G., Vera, S., Govindaraju, K., et al. (2005). "A role for endoglin in coupling eNOS activity and regulating vascular tone revealed in hereditary hemorrhagic telangiectasia." Circ Res **96**(6): 684-692.

Torsney, E., Charlton, R., Diamond, A. G., Burn, J., Soames, J. V., et al. (2003). "Mouse model for hereditary hemorrhagic telangiectasia has a generalized vascular abnormality." Circulation **107**(12): 1653-1657.

Totzeck, M., Mincu, R. I. and Rassaf, T. (2017). "Cardiovascular Adverse Events in Patients With Cancer Treated With Bevacizumab: A Meta-Analysis of More Than 20 000 Patients." J Am Heart Assoc **6**(8).

Tual-Chalot, S., Garcia-Collado, M., Redgrave, R. E., Singh, E., Davison, B., et al. (2020). "Loss of Endothelial Endoglin Promotes High-Output Heart Failure Through Peripheral Arteriovenous Shunting Driven by VEGF Signaling." Circ Res **126**(2): 243-257.

Tual-Chalot, S., Mahmoud, M., Allinson, K. R., Redgrave, R. E., Zhai, Z., et al. (2014). "Endothelial depletion of Acvrl1 in mice leads to arteriovenous malformations associated with reduced endoglin expression." PLoS One **9**(6): e98646.

Tual-Chalot, S., Oh, S. P. and Arthur, H. M. (2015). "Mouse models of hereditary hemorrhagic telangiectasia: recent advances and future challenges." Front Genet **6**: 25.

Urness, L. D., Sorensen, L. K. and Li, D. Y. (2000). "Arteriovenous malformations in mice lacking activin receptor-like kinase-1." Nat Genet **26**(3): 328-331.

van Laake, L. W., van den Driesche, S., Post, S., Feijen, A., Jansen, M. A., et al. (2006). "Endoglin has a crucial role in blood cell-mediated vascular repair." Circulation **114**(21): 2288-2297.

Venkatesha, S., Toporsian, M., Lam, C., Hanai, J., Mammoto, T., et al. (2006). "Soluble endoglin contributes to the pathogenesis of preeclampsia." Nat Med **12**(6): 642-649.

Vorselaars, V., Velthuis, S., van Gent, M., Westermann, C., Snijder, R., et al. (2017). "Pulmonary Hypertension in a Large Cohort with Hereditary Hemorrhagic Telangiectasia." Respiration **94**(3): 242-250.

Wieser, R., Wrana, J. L. and Massagué, J. (1995). "GS domain mutations that constitutively activate T beta R-I, the downstream signaling component in the TGF-beta receptor complex." EMBO J **14**(10): 2199-2208.

Wiggenhauser, L. M., Kohl, K., Dietrich, N., Hammes, H. P. and Kroll, J. (2017). "Studying Diabetes Through the Eyes of a Fish: Microdissection, Visualization, and Analysis of the Adult tg(fli:EGFP) Zebrafish Retinal Vasculature." J Vis Exp(130).

Wooderchak-Donahue, W. L., McDonald, J., O'Fallon, B., Upton, P. D., Li, W., et al. (2013). "BMP9 mutations cause a vascular-anomaly syndrome with phenotypic overlap with hereditary hemorrhagic telangiectasia." Am J Hum Genet **93**(3): 530-537.

Yadav, L., Puri, N., Rastogi, V., Satpute, P. and Sharma, V. (2015). "Tumour Angiogenesis and Angiogenic Inhibitors: A Review." J Clin Diagn Res **9**(6): 01-05.

Youjin, S. and Jun, Y. (2009). "The treatment of hemophilia A: from protein replacement to AAV-mediated gene therapy." Biotechnol Lett **31**(3): 321-328.

Yu, P. B., Deng, D. Y., Lai, C. S., Hong, C. C., Cuny, G. D., et al. (2008). "BMP type I receptor inhibition reduces heterotopic [corrected] ossification." Nat Med **14**(12): 1363-1369.

Yu, P. B., Hong, C. C., Sachidanandan, C., Babitt, J. L., Deng, D. Y., et al. (2008). "Dorsomorphin inhibits BMP signals required for embryogenesis and iron metabolism." Nat Chem Biol **4**(1): 33-41.